12-2014

Flatness-Based Control Methodologies to Improve Frequency Regulation in Power Systems with High Penetration of Wind

Maryam Hassani Variani
University of Tennessee - Knoxville, mhassani@vols.utk.edu

To the Graduate Council:

I am submitting herewith a thesis written by Maryam Hassani Variani entitled "Flatness-Based Control Methodologies to Improve Frequency Regulation in Power Systems with High Penetration of Wind." I have examined the final electronic copy of this thesis for form and content and recommend that it be accepted in partial fulfillment of the requirements for the degree of Doctor of Philosophy, with a major in Electrical Engineering.

Kevin Tomsovic, Major Professor

We have read this thesis and recommend its acceptance:

Yilu Liu, Seddik M. Djouadi, Xiaopeng Zhao

Accepted for the Council:

Carolyn R. Hodges

Vice Provost and Dean of the Graduate School

(Original signatures are on file with official student records.)

Flatness-Based Control Methodologies to Improve Frequency Regulation in Power Systems with High Penetration of Wind

A Dissertation Presented for the

Doctor of Philosophy

Degree

The University of Tennessee, Knoxville

Maryam Hassani Variani

December 2014

This thesis is dedicated to my wonderful family.

My parents, Monir and Jafar, for their endless support in all aspect of my life. Their love embraces me everywhere regardless of the wide distance between us.

My husband, Benyamin, who gave me the most precious gift of life, Love, and supported me at each step of this dissertation with his encouragement.

My brother, Pejman, who gave me hope and taught me to never give up. Thanks to his kindness and generosity, I could concentrate on my PhD with piece of mind while I was far away from my parents.

Acknowledgements

I would like to express my deepest appreciation and gratitude to my advisor Dr. Kevin Tomsovic. His constant support and persistency to solve problems from a new perspective inspired me to work harder and to think out of box. Moreover, with his wonderful personality he always understood and supported me in my academic experience and personal life.

I would like to thank Dr. Yilu Liu for her support and precious comments, and Dr. Seddik M. Djouadi and Dr. Xiaopeng Zhao for their time and effort in serving as my thesis committee.

I am very thankful to CURENT for providing me an amazing atmosphere and facilities to conduct my research.

And last but not least, I would like to express my heartfelt thanks to my husband and colleague, Dr. Benyamin Moradzadeh, for all our valuable technical discussions and inspiration.

Abstract

To allow for high penetration of distributed generation and alternative energy units, it is critical to minimize the complexity of generator controls and to minimize the need for close coordination across regions. We propose that existing controls be replaced by a two-tier structure of local control operating within a global context of situational awareness. Flatness as an extension of controllability for non-linear systems is a key to enabling planning and optimization at various levels of the grid in this structure. In this study, flatness-based control for: one, Automatic Generation Control (AGC) of a multi-machine system including conventional generators; and two, Doubly fed Induction Machine (DFIG) is investigated. In the proposed approach applied to conventional generators, the local control tracks the reference phase, which is obtained through economic dispatch at the global control level. As a result of applying the flatness-based method, an n machine system is decoupled into n linear controllable systems in canonical form. The control strategy results in a distributed AGC formulation which is significantly easier to design and implement relative to conventional AGC. Practical constraints such as generator ramping rates can be considered in designing the local controllers. The proposed strategy demonstrates promising performance in mitigating frequency deviations and the overall structure facilitates operation of other non-traditional generators. For DFIG, the rotor flux and rotational speed are controlled to follow the desired values for active and reactive power control. Different control objectives, such as maximum power point tracking

(MPPT), voltage support or curtailing wind to contribute in secondary frequency regulation, can be achieved in this two-level control structure.

Table of Contents

List of Tables

List of Figures

Chapter 1

Introduction

1.1 Overview

The rapid introduction of wind and other alternative energy sources has begun to impact overall power system control, and particularly, frequency regulation. As a fundamental characteristic of electric power operations, frequency of the system deviates from its nominal value due to generation-demand imbalance. Conventional generators, in which the turbine rotational speed is nearly constant, provide inertia and governor response against frequency deviations; however, the speed of a wind turbine is not synchronous with the grid. Therefore, wind plant power production is not inherently coupled to the system frequency and does not provide inertial and governor response. On the other hand, wind plants have not been historically required to participate in frequency regulation and are usually controlled to maximize active power production. Still, modern wind plants offer limited ability to contribute in frequency regulation within a few seconds after loss of generation [1].

With increased penetration of wind energy, system operators have begun to study the performance of the primary frequency response. An investigation of US interconnections has shown that the frequency response has been declining during the last several years. The average decline of the Eastern Interconnection is about

$60 - 70MW/0.1HZ$ per year [2]. Due to the reduction in frequency response, North American Electric Reliability Corporation (NERC) proposed a new standard that would obligate each Balancing Authority (BA) to have a minimum frequency response [3]. A California ISO frequency response study shows that the reduced system inertia due to penetration of wind units has an impact on the initial rate of change of frequency but has little impact on the severity of the frequency excursion and settling frequency [4]. Inertia controls from wind generation can significantly improve the frequency nadir but they do relatively little to correct the shortage in the amount of available response. Unlike inertial response, wind plant governor like control will significantly improve frequency nadir and settling frequency. This control requires the wind plants to work below available power [4]. However, another study has suggested that for higher penetration of wind, a combination of inertia and primary frequency response would result in higher frequency nadir and settling frequency [5]. Another assessment of frequency control considered changing a fraction of the on-line turbine capacity that provides primary and secondary control. This study showed that adequate reserve to cover expected variations of wind power is not sufficient on its own. In fact, proper dynamic characteristics and control capabilities are as important as the level of reserves [6].

The amount of secondary control response capability required and the rate at which it must be delivered have historically been functions of the daily load forecast, allowance for error in the forecast, and provision for contingencies. The introduction of variable resources adds a new and potentially large component to the requirement for secondary response with respect to both amount and rate of delivery. The correct operation of the system for load frequency control (LFC) to handle as much as possible of the deviations results in minimizing the use of primary response capability [6]. Also if secondary control is exhausted due to wind, solar or load variability, the actions of primary frequency control will reduce primary frequency response capability for responding to the faults [4]. According to the investigation of wind generation penetration in the Electric Reliability Council of Texas (ERCOT)

market, the percentage increase in regulation requirements has been found to be equal to the percentage wind penetration on a capacity basis. The regulation needs to increase much more for certain times of the year. It is observed that the existing non-wind generation has the capability to provide regulation for up to 23% wind penetration for all times but down regulation for about 51 hours per year. Sub-Optimal commitment of conventional generators and dispatching wind generation are possible solutions for these hours and higher penetration of wind [7]. Secondary control action is based on the assumption that frequency error throughout a balancing authority is identical. This assumption may not be well suited for systems with high wind penetration because larger imbalances may occur at locations with high installed wind capacity [8].

Along with the high penetration of renewables and the related control challenges, power system sensor and measurement technologies have a great improvement during the last decade. The increased integration of Phasor Measurement Units (PMUs) and improvements in wide area measurements allow for use of more advanced control techniques based on wide-are measurement signals. PMUs differ significantly from traditional, SCADA, due to two important features: First, is the higher sampling rate and bandwidth where PMUs normally measures the signal at 30-60 times per seconds, relative to SCADA measurement which is performed once in few seconds. Also, a PMU has the capability to record synchronized measurements from widely geographically dispersed locations.

Issues related to communication latency, reliability, security and cost will of course influence the use of PMU-measured quantities in feedback design. However, the availability of PMU measurements makes the prospect of control utilizing multi-variable system outputs over a wide geographic area much more viable than in the past. The high sampling rate and time synchronization of PMU measurements, combined with improved algorithms and computational hardware, open the door to dynamic observation of system state in the power grid, which is required for state feedback optimal control designs [9].

As a result improvements in wide area measurements allow a more distributed secondary control. Thus, a high proportion of wind powered generation will require renewed attention to primary and secondary control capabilities in both conventional generators and wind plants. This research suggests the control needs to be replaced by a simpler, less hierarchical structure with a local control within a more global context for the system. The proposed structure consists of two levels at each scale:

- Local control in which individual components operate in a manner that tends to support the best interests of the overall system, for reliability, speed, and robustness of control actions.

- Contextual control in which larger-scale controllers select one of a finite number of system-level control goals, such as efficiency maximization, cost minimization, stabilization, network recovery, or other goals that best reflect needs based on overall system status at a given moment.

1.1.1 Frequency Regulation in Power Systems

Active power load-generation balance is vital in a power system in order to maintain the system frequency at the reference value. In energy markets, usually system reserve requirement is defined to keep a portion of generation capacity to meet the load variation and achieve demand-supply balance and maintain frequency at the reference value. This generation control which is used to keep up with system demand changes is usually referred to as frequency control. It is often called "regulation up" when the reserve capacity is used to increase the active power generation and compensate for system frequency drop. When system reserve capacity is used to manage the load-generation imbalance due to drop in demand, i.e., frequency raise, it is referred to as "regulation down". Frequency control is categorized into two main levels depending on the time frame: primary control and secondary control.

Primary control is traditionally used to automatically control local generators in response to frequency measurements. This control is designed to achieve demand-supply balance following a large generation/load disturbance. This is important from both steady sate and dynamic stability point of views. In a synchronous generator, the torque produced by magnetic field interactions is equal to the generated power divided by rotational speed. This implies that the rotational acceleration/deceleration is the result of difference between the applied mechanical shaft power produced by the prime mover and the electrical powered delivered to the grid. Only when the mechanical power and output electrical power are in balance does the machine operates at constant speed.

Droop control is a primary frequency control mechanism which consists of a simple proportional feedback to modify mechanical input with respect to the speed error. This mechanism responds to frequency deviation through controlling the output of local generator. Primary control has a fast operating time scale of seconds and is applied through turbine governors. Droop governor control contributes to both steady state and dynamic stability of the system by keeping transient response stable. Compared to primary control, secondary frequency control has a slower time scale and operates in a more centralized perspective. The centralized control procedure changes generators output, i.e., regulation up and regulation down, to restore frequency to the normal value. Another purpose of secondary control is to keep the flows on the interties between two areas to scheduled values. Without secondary control, power output of the generators are set based on their droop constants which may not lead to an economic operation point. Moreover, this excludes the generators not participating in the primary control [9].

Primary control should be an automated because of its fast time scale. This time scale is similar to the electromechanical dynamics of interconnected synchronous generators and therefore it significantly impacts the grid stability. Every BA, a geographically and electrically contiguous region consisting of a set of buses with intercommunicating measurements and telemetry, is responsible for controlling

its production to maintain its interchange schedule with adjacent areas while participating in frequency regulation. In multi-area systems, these two objectives are combined and form a single objective known as Area Control Error (ACE) [9].

The NERC has defined two standards, CPS1 and CPS2, to assess ACE in multi-area systems. These standards indicate whether generation in an area is sufficiently controlled to meet its interchange schedule and frequency support obligation. CPS1 measures ACE variability, which indicates short-term imbalance between load and generation, to compare the performance of a BA's ACE in conjunction with the frequency error of the interconnection. CPS2, on the other hand, includes ten-minute averages collected from ACE [10].

1.1.2 Frequency Regulation with Wind Integration

Wind generation capacity is rapidly increasing in the U.S. The increased penetration of this intermittent energy resource creates new challenges to the economic, reliable, and secure operation of power systems. Despite the conventional synchronous generators, most new wind generation units, e.g., Type-3 and Type-4 systems, are integrated to the grid via power electronic-based converters. These converters decouple wind units from the grid leading to a significantly different impact on electromechanical stability of the gird compared to conventional generators. The more conventional units are replaced by wind units, the less inertia the system has which makes the grid more vulnerable to disturbances. On the other hand, the easy to control switching operations of the converters offers more flexibility for the wind units to contribute to the stability.

DFIG wind units are gaining more utilization due to their higher efficiency compared to the conventional fixed speed wind turbine generators. The variable speed capability of the DFIG units, which is provided by controlling the back-to-back AC/DC/AC power electronic converters, enables these generators to operate near their optimal turbine efficiency in a wide range of wind speed. As mentioned before,

a major challenge associated with the high penetration of the power electronic-based wind generators is the reduced system inertia. In order to compensate the reduced inertia caused by increased utilization of DFIG wind units, new control designs need to be implemented to draw/feed active power from/to the grid in response to frequency deviation. This power control is provided via controlling either the wind turbine blade pitch or the rotor side converters [11–14].

1.2 Dissertation Outline

This dissertation is organized in following chapters:

In chapter 2, the literature related to development of AGC, standards and the effect of integration of renewable, specifically wind generation, is discussed. Then the recent efforts on contribution of wind generation on frequency regulation including the inertia, primary and secondary control is presented. The relevant and application of PMU, are presented.

In chapter 3, the flatness-based control approach is introduced. This chapter starts with an introduction on flat systems and their properties. The flatness-based control approach is presented. Application of this approach on trajectory generation and generation tracking is described.

Chapter 4 starts with a more detailed explanation of primary and secondary frequency control and afterwards the proposed flatness-based AGC is presented. The approach is implemented on a 39 bus, 10 generators and 3 area system. Large scale and hardware test beds at CURENT are used to asses the performance of the proposed flatness based AGC.

Flatness-based DFIG for active and reactive power control, is presented in chapter 5. Wind generation using DFIG is described. The two level control of wind farms including supervisory and turbine level controls is presented. A two-level control for wind farms using flatness-based control is described.

1.3 Summary of Contributions

The contribution of this work is summarized as follows:

- It is shown that the fourth order model of synchronous machine, with rotor angle, rotational speed, governor power and mechanical power as state variables, has the flatness property with rotor angle as a flat output. As an important feature of this formulation, a multi-machine with n machines is decoupled into n linear controllable subsystems.

- Flatness-based control including trajectory generation and trajectory tracking is used to implement AGC for multi area systems. The reference active power generation values for generators participating in secondary control are found by economic dispatch or other methods in global control level. At the local control level, trajectory generation determines the reference for the flat output and tracking the reference is guaranteed through trajectory tracking. In contrast to conventional AGC, where an integral controller is applied to ACE at BA control level, the trajectory tracking is performed at generator level with proportional controllers. The ACE signal is generated from tie line measurements and is updated every 2-4 seconds (SCADA scan rate), while trajectory tracking is based on local PMU measurements.

- The active power generation set points for generators contributing to AGC are updated every 5 minutes using economic dispatch. The hard to predict changes in load or generation can change the optimum operating point of the system. For this purpose, an algorithm based on PMU measurements and deploying system shift factors is developed to update the references more frequently. An optimization problem is formulated to minimize the tie-line flow deviations from the nominal value and find the active power generation set points for generators contributing in AGC.

- To enable the application of flatness-based AGC to large scale power systems, a User Defined Model (UDM) is developed in DSA tools and the approach is implemented on Northeast Power Coordinating Council (NPCC) system.
- The approach is successfully implemented on Hardware Test Bed (HTB) at Center for Ultra-Wide-Area Resilient Electric Energy Transmission Networks (CURENT), in the presence of wind variation and considering practical system constrains.
- It is shown that a DFIG 3rd order model is a flat system considering electrical torque, T_e, and θ, argument of rotor flux, as flat outputs. This formulation allows interpreting the active and reactive power generation of DFIG machine as an algebraic function of flat outputs.
- The two level PI controllers in DFIG vector control method are replaced with two levels of a flatness-based control approach. At the trajectory generation level, the references for active and reactive powers, sent from supervisory wind farm control, are converted to references for flat outputs using algebraic equations. This level is a replacement for the first set of PI controllers in vector control. At the trajectory tracking level, proportional controllers are used to track the flat outputs references generated in upper level, which replaces the second set of PI controllers in vector control approach.
- The flatness-based structure for AGC and DFIG control built a comprehensive frequency control framework. The global control determines the schedules for conventional generators and wind farms considering the system status. In normal operation, the schedules are found through economic dispatch. For synchronous machines, the references are followed by local controllers. At the two-level wind farm control, the supervisory control sends the appropriate schedule to each DFIG machine based on available wind power at each turbine. Tracking the references by each DFIG results in the scheduled power for the wind farm.

Chapter 2

Literature Review

2.1 AGC

AGC, secondary frequency control, has been conventionally performed by integrating the ACE, which acts on the load reference settings of the governors. The basics of AGC and the fundamental considerations affecting AGC is described in the task force paper [15]. According to NERC standards the AGC performance used to be evaluated using A1-A2 control performance policy, implemented in 1973. A1 required the balancing authority's ACE to return to zero within 10 minutes of previous zero. A2 required that the balancing authority's averaged ACE for each 10-minute period must be within limit. Considering A1-A2 criteria, small and large ACE were treated the same. Also, frequency deviation did not impact A1-A2. Therefore, in 1996, a new NERC policy, based on CPS1 and CPS2, was approved. CPS1 measures the statistical variation of ACE in combination with interconnection frequency error. Due to CPS2, similar to A2, each balancing authority must operate within the limit for at least 90% of 10-minutes periods in a month [16]. These control performances are discussed in [17]. Moreover, NERC proposed a new standard in 2008 that requires each BA to provide sufficient frequency response to maintain interconnection frequency within the balanced range [3].

Many methods to implement AGC have been proposed in literature. The integral of square error (ISE) is used in [18] to find the optimum gain for the controller. Performance of other classical control methods such as Proportional-Integral (PI), Integral-Derivative (ID), Proportional-Integral-Derivative (PID) and Integral-Double Derivative (IDD) controllers is investigated in [19]. It is shown that integral (I), PI, ID, and PID controllers provide more or less same response while IDD controller leads to a much better response.

Artificial intelligence methods have also been applied to AGC at different control levels. The calculation of ACE is done using Fuzzy logic controller in [20]. However, the main body of the AGC system is controlled by the conventional controllers. An adaptive fuzzy gain scheduling scheme for conventional PI and optimal load frequency controllers is proposed in [21]. Optimal parameters of PID control are computed by genetic algorithm (GA) and hybrid genetic algorithm-simulated annealing (GA-SA) techniques in [22]. Stochastic optimal relaxed control methodology based on reinforcement learning (RL) for solving the AGC is proposed in [23], where the moving averages of CPS1/ACE are adopted as the state feedback input, and the CPS control and relaxed control objectives are formulated as multi-criteria reward function. The application of artificial neural network (ANN) controller is proposed in [24]. Communication models for third party LFC and their requirements are introduced in [25]. The effect of signal delays on load following is investigated in study. It is shown that delays could slow down the system response and, in the worst case, can result in unstable or other unacceptable behavior.

All the mentioned algorithms are based on ACE calculation and methods to diminish the steady state error. However the new structures for tie line and frequency control are established in other works. The distributed Model Predictive Control (MPC) strategy is proposed in [26]. The concept of Enhanced ACE (E-ACE) and Smart Balancing Authority (SBA) are introduced in [27]. The E-ACE allows SBAs to provide service to other SBAs to reduce the cost of frequency regulation. RL is deployed in designing two algorithm for AGC in [28]. In the first algorithm limiting the

ACE is used as the objective while the second algorithm is only based on monitoring the tie-line flow deviations and system frequency without calculating the ACE.

It is proposed in [29] that the ACE deviations should be compensated through specific assets based on frequency of load change. In this structure, fluctuations caused by intermittent, non-dispatchable distributed energy resources are mostly compensated using distributed community storage and load dynamic response. Also, a cyber architecture is proposed to accommodate non-dispatchable and intermittent resources. In [30], AGC is assumed to be a multi-objective control problem and is studied in a restructured power system. A robust decentralized AGC using a mixed H_2/H_∞ is proposed based on bilateral contracts.

A new design is implemented in [31] relying on the use of PMUs, which for the given number of PMUs computes the best locations of PMUs and the control design gains based on these measurements in order to ensure that the flow deviations remain within the pre-specified limits.

In the present study, a flatness-based approach is applied to multi-machine AGC. The performance of the proposed control system is investigated under the penetration of wind generation. Flat systems were first introduced by Fliess [32] using the formalism of differential algebra. In differential algebra, a system is viewed as a differential field generated by a set of variables. The system is said to be flat if one can find a set of variables, called the flat outputs, such that the system is algebraic over the differential field generated by the set of flat outputs. The flatness-based approach is well adopted to control systems in two levels of planning, trajectory generation, and tracking the desired trajectories.

In the proposed structure, the n-machine system is split into n linear controllable systems. Consequently, the control strategy is significantly easier to implement relative to conventional AGC. The flatness property of synchronous machines is introduced in [33] and applied to a single machine connected to infinite bus. The approach is extended in this work to establish a two-tier structure in a multi-machine system to control the frequency and tie-line power flow considering the overall

system reliability, speed, and robustness. In local control, individual components and individual loads operate in a manner to follow some desired trajectory based on local observations. The global control, on the other hand, refers to the desired trajectory which is determined by the context of the overall system needs.

2.2 DFIG

Several efforts have been directed at improving primary frequency response of wind power plants in recent years, e.g., GE wind turbines include an optional feature for inertia control. A new method is proposed in [34] to enhance the participation of variable-speed wind energy conversion systems (WECS) in existing frequency regulation mechanisms. The proposed approach, based on a modified inertial control scheme, takes advantage of the fast response capability associated with electronically-controlled WECS, allowing the kinetic energy stored by rotational masses to be partly and transiently released in order to provide earlier frequency support. An additional improvement is achieved by communicating the WECS response to conventional generators so that these can eventually assume the full load imbalance.

However, the ability of wind plants to contribute to secondary frequency control has not been thoroughly investigated. Wind plants would need to lower their generation from maximum power point to be able to participate in regulation. This reduction in generation may not be an economic choice (depending on how they are compensated in the market) due to the fact that wind plants do not use fuel. The analysis of required regulation and the energy price in [35] shows that it may be both technically and economically feasible for wind plants to supply minute-to-minute regulation under some circumstances. AGC for a wind farm with variable speed wind turbines is proposed in [36]. The proposed control method consists of two levels: a supervisory control level which includes two control loops for active and reactive power control. The active power loop receives a power reference from the grid operator. The controller then sends the reference active power to each machine based

on availability of wind power. In the reactive power control loop, first the desired reactive power and voltage level reference are determined, usually based on unity power factor. Then the wind farm voltage controller calculates the reactive power reference for each wind machine. On the other hand, the wind turbine control system also consists of two control loops, one for machine active power control and the other one for reactive power control. For the active power control, when the power reference is available from the supervisory control system and wind speed is high enough, the wind power is curtailed through pitch blades and speed control to follow the desired value. But if the wind speed is not high enough the turbine operates at maximum power output. If the reference is not available from the supervisory level, the wind turbine generates the maximum available power. The reactive power control ensures following the reference reactive power and that the voltage limits are not violated. Different options to perform secondary control are suggested in [37]. In delta control, the wind farm is ordered to operate with a certain constant reserve capacity in relation to its momentary available power production capacity. The advantage of such control is that the reserve power is available and can be used in the next control which is power balance. In the latter control, the wind farm production can be adjusted downwards or upwards, in steps at constant levels. The power gradient limiter sets how fast the wind farm power production, can be adjusted upwards and downwards that helps to keep the production balance between wind farms and the conventional power plants.

All the suggested secondary control methods are implemented in the supervisory control level of wind farms, in which the appropriate set points for both active and reactive powers are determined and sent to the wind turbine control level. The control of wind turbines to generate less power than the available wind power and hold the rest in reserve to contribute in governor response is also proposed in [38]. The wind turbine control level addresses the local control system of each single wind turbine and ensures that the references sent from the wind farm control level are tracked. Each local wind turbine control system also has a hierarchical structure. It contains

a slow dynamic control level (control of speed and power) and a fast dynamic control level (electrical control of the generator currents). This latter addresses the electrical control of the frequency converter. The slow dynamic control level provides reference signals to the pitch system of the wind turbine [37].

Electrical control is typically performed with PI controllers based on the decoupled control of torque and rotor excitation current presented in [39] using stator flux orientation. Nonlinear control methods have been proposed in literature. An adaptive nonlinear controller for a doubly fed induction generator (DFIG) based on the feedback linearization technique is introduced in [40]. The proposed controller includes a disturbance observer for estimation of parameter uncertainties and the uncertainties values are injected in order to construct the control law. Exact feedback linearization of DFIG is presented in [41]. It contains a direct decoupling between active and reactive power. It is shown that this method improves the system performance during grid faults. A cascaded nonlinear sliding mode controller is proposed in [42] for power production optimization of DFIG. The inner loop controller ensures a robust tracking of both generator torque and rotor flux, while the outer loop controller achieves a robust tracking of the optimal blade rotor to optimize energy capture. The state feedback-PI controller jointly with an estimator is used in [43]. Exact linearization of a DFIG 3rd order model is implemented in [44] to improve the transient stability of the power system and enhance system damping. The stator voltage and rotor slip are the output variables used to linearize the system.

2.3 PMU Measurements

The use Synchronous Phasor Measurements is widely growing in power system for variety of applications. They use Global Positioning System (GPS) and the sampled data processing algorithms to provide promising and synchronized measurements of positive-sequence voltage and current measurements. Furthermore, they have the capability to quantify local frequency and frequency rate of change. The

positive-sequence measurements makes the power system states directly available at each measurement sample (typically 30 times per seconds) which has resulted in development of advanced control techniques in power system. The first prototypes of PMUs using GPS were developed at Virginia Tech in the 1980s. These prototype PMUs built at Virginia Tech were placed at certain substations of the Bonneville Power Administration (BPA), the New York Power Authority (NYPA), and the American Electric Power Service Corporation (AEPSC) [45]. The importance of positive-sequence voltage and current phasor measurements and some of the applications were first introduced in [46]. Since then, several studies have been performed to develop the application of PMUs in power system including: monitoring and control of system in real time, state estimation, power system protection, overload and dynamic rating monitoring, power system restoration and so on. Theory and implementation of state estimation is explained in [47]. An online voltage stability using PMU measurement, using a decision tree-based algorithm, to prevent a large scale blackout is presented in [48]. Early detection of voltage instability from the system states, before abnormally low voltages are observed, using synchronized phasor measurement is presented in [49] [50]. In [51], the authors investigated the possibility of estimating the rotor angle of synchronous generators from the measurements of terminal voltage, active power output, and field voltage of the generator.

Chapter 3

Flatness-Based Control

3.1 Introduction

Feedback control has been widely used to control systems ranging from simple room temperature thermostats to flight control systems for high performance aircraft. In many modern systems, the control input is derived by inverting the dynamics of system. The input is found to steer a control system from an initial to final state through a desired trajectory for some or all of the states. The optimal control input for such trajectories is computed by a compromise between performance and cost of the control.

The benefit of control systems with feedback control is in the presence of noise and uncertainty, where the dynamics of the system change due to the disturbances. The uncertainty usually exists in practice and must be considered in control design. Feedback is often used to improve the stability and accuracy of a system by correcting the errors and unwanted changes.

Finding the mathematical model of the system is the first step in designing control. Often, the system can be linearized and linear control techniques are applied to find the system input. Linearization must be applied to different operating points to find the appropriate gains for the system over a range of operating conditions. As

systems become more complex, the use of linear structure alone is often not sufficient to solve the control problems that are arise in applications. This is especially true of the inverse dynamics problems, where the desired task may span multiple operating regions and hence the use of a single linear system is inappropriate.

These harder problems have been addressed with various control methods such as feedback linearization, flatness-based control, backsteppting and sliding mode control. In this study, flatness-based control related to a specific class of systems, called "flat systems", is investigated. These systems are linearizable by a special type of feedback called endogenous and also trajectories for such systems are generated without solving differential equations. Flatness is particularly well suited for allowing one to solve the inverse dynamics problems and one builds off of that fundamental solution in using the structure of flatness to solve more general control problems [52].

Flatness was first defined by Fliess [32] using the formalism of differential algebra. In differential algebra, a system is viewed as a differential field generated by a set of variables, states and inputs. The system is said to be flat if one can find a set of variables, called the flat outputs, such that the system is algebraic over the differential field generated by the set of flat outputs. In the other words, a system is flat if a set of outputs can be found, equal in number to the number of inputs, such that all states and inputs can be determined from these outputs without integration.

Many classes of systems commonly used in nonlinear control theory are flat. Also all controllable linear systems can be shown to be flat. Indeed, any system that can be transformed into a linear system by change of coordinates, static feedback transformations, or dynamic feedback transformation is also flat [52].

3.2 Flat Systems

When a system is flat, it is an indication that the nonlinear structure of the system is well characterized and one can exploit that structure in designing control algorithms for motion planning, trajectory generation, and stabilization. One major property of

differential flatness is that the state and input variables can be directly expressed in terms of the flat output and a finite number of its derivatives. [52].

Consider

$$\dot{x} = f(x, u) \qquad (x \in R^n,\ u \in R^m) \tag{3.1}$$

The dynamic feedback linearizability of (3.1) means the existence of a regular dynamic compensator

$$\dot{z} = a(x, z, v) \tag{3.2a}$$

$$u = b(x, z, v) \quad (z \in R^{\alpha-1}, v \in R^m) \tag{3.2b}$$

and a diffeomorphism

$$\xi = \Xi(x, z) \qquad (\xi \in R^{n+\alpha-1}) \tag{3.3}$$

such that (3.1) and (3.2), whose $(n + \alpha - 1)$ dimensional dynamics is given by

$$\dot{x} = f(x, b(x, z, v)) \tag{3.4a}$$

$$\dot{z} = a(x, z, v) \tag{3.4b}$$

becomes, according to (3.3), a constant linear controllable system $\dot{\xi} = F\xi + Gv$.

Up to a static state feedback and a linear invertible change of coordinates, this linear system may be written in Brunovsky canonical form,

$$\begin{aligned} y_1^{(\alpha_1)} &= v_1 \\ &\cdot \\ &\cdot \\ &\cdot \\ y_m^{(\alpha_m)} &= v_m \end{aligned} \tag{3.5}$$

Then it can be deduced that

$$x = (y, \dot{y}, ..., y^{\alpha-1}) \tag{3.6}$$

$$u = (y, \dot{y}, ..., y^{(\alpha)}) \tag{3.7}$$

where $(y, \dot{y}, ..., y^{(\alpha-1)})$ corresponds symbolically to $(y_1, ..., y_1^{(\alpha_1-1)}, ..., y_m, ..., y_m^{(\alpha_m-1)})$ and the same for $(y, \dot{y}, ..., y^{(\alpha)})$ [32, 53].

The dynamic feedback (3.2) is said to be endogenous if and only if, the converse holds, i.e., if and only if, any component of y can be expressed as a real-analytic function of x and u and a finite number of its derivatives

$$y = h(x, u, \dot{u}, ..., u^{(\gamma)}) \tag{3.8}$$

A dynamics (3.1) which is linearizable via such an endogenous feedback is said to be (differentially) flat and y is called flat output. The flatness property may be very useful when dealing with trajectories: from the y trajectories, x and u trajectories are immediately deduced. These properties permit a straightforward open loop path tracking. On the other hand, equivalence of the flat system with a controllable linear system via an endogenous feedback yields a feedback stabilization of the desired trajectory. According to the flat output properties, system trajectories joining a collection of points with given velocities, acceleration, jerks, etc., are easily generated. This replaces difficult dynamical computations by statistical interpolation techniques [54].

In nonlinear SISO systems, if a system is not linearizable by means of static state feedback and state coordinates transformation, then the system is also not linearizable by means of dynamic state feedback. This result, limits the class of flat systems to that of feedback linearizable systems in nonlinear SISO systems. In multivariable nonlinear systems, a system which is not linearizable by means of static state feedback may still be linearizable by means of dynamic state feedback. An important feature of flatness

is that when we know that the system is flat, the differential parametrization of the control inputs immediately point to which one of the outputs needs to be dynamically extended, and to what order, in order to have the possibilities of locally inverting the relation linking higher order derivatives of the flat outputs to suitable auxiliary control inputs represented by a sufficient number of derivatives of the original inputs [53].

3.3 Trajectory Generation

Trajectory generation or motion planning corresponds to preparing a path or a motion plan in advance. This path is supposed to relate a prescribed initial point to a prescribed final point, in open-loop, i.e., based on the knowledge of the system model only and without taking account of errors in the measurements of the system state and disturbances. Such a trajectory is often called reference or nominal trajectory. [52].

Considering the nonlinear system $\dot{x} = f(x, u)$. Given the initial time t_i, the initial conditions

$$x(t_i) = x_i, \quad u(t_i) = u_i \tag{3.9}$$

the final time t_f and the final conditions

$$x(t_f) = x_f, \quad u(t_f) = u_f \tag{3.10}$$

The motion planning problem consists in finding a trajectory $t \mapsto (x(t_i), u(t_i))$ for $t \in [t_i, t_f]$ that satisfies $\dot{x} = f(x, u)$ and the initial and final conditions (3.9), (3.10). System constraints also can be considered in trajectory generation [55].

This problem, in the general case, is quite difficult since it may require an iterative solution by numerical methods to find a control input u such that conditions (3.9), (3.10) are satisfied: starting with an input $t \mapsto u_0(t)$, the system equations are integrated from the initial conditions, and the solution is evaluated at final time t_f, and then the input is modified, say $t \mapsto u_1(t)$, to get closer to the final conditions, and so on. In this class, a typical method for the determination of u is the optimal

control approach, e.g., find the control that minimizes the square deviation to a given trajectory. For nonlinear systems, it may pose problems that are still open. In the case of flat systems, this problem is easily solved without approximation and without integrating the system differential equations [55].

For flat systems, generating a desired trajectory reduced to the existence of a flat output such that all the system variables can be expressed as functions of this flat output and a finite number of its successive derivatives. This parameterization is such that the system differential equations are identically satisfied.

Considering the problem of steering from an initial state to a final state and parameterizing the components of the flat output y_j for $j = 1, ..., m$ by

$$y_j(t) = \sum_{k=0}^{2\alpha+1} A_{jk}\lambda^k(t), \quad j = 1, ..., m. \tag{3.11}$$

where $T = t_f - t_i$ and $\lambda(t) = \frac{t-t_i}{T}$,then, it suffices to find a set of parameters, A_{jk} in following steps [52, 55]:

- Assuming the initial state x_i at time t_i and a final state x_f at time t_f.
- Calculating the values of the flat output and its derivatives from the desired initial and final points in state space.

$$y_1(t_i), ..., y_1^{(\alpha)}(t_i), ..., y_m(t_i), ..., y_m^{(\alpha)}(t_i) \tag{3.12}$$

$$y_1(t_f), ..., y_f^{(\alpha)}(t_f), ..., y_m(t_f), ..., y_m^{(\alpha)}(t_f) \tag{3.13}$$

- Solving for the A_{jk} coefficients by equating the successive derivatives of y_j at the initial and final times

$$y_j^k(t) = \frac{1}{T^k} \sum_{l=k}^{2\alpha+1} \frac{l!}{(l-k)} A_{jl}\lambda^{l-k}(t), \quad k = 1, ..., \alpha, j = 1, ..., m. \tag{3.14}$$

or, at $\lambda = 0$ which corresponds to $t = t_i$,

$$y_j^k(t_i) = \frac{k!}{T^k} A_{jl}(t), \quad k = 1, ..., \alpha, j = 1, ..., m. \tag{3.15}$$

and at $\lambda = 1$, or $t = t_f$,

$$y_j^k(t_f) = \frac{1}{T^k} \sum_{l=k}^{2\alpha+1} \frac{l!}{(l-k)} A_{jl} \lambda^{l-k}(t), \quad k = 1, ..., \alpha, j = 1, ..., m. \tag{3.16}$$

which makes a total of 2α linear equations in the 2α coefficient $A_{j,0}, ..., A_{j,\alpha+1}$, for every $j = 1, ..., m$. This system can in fact be reduced to $\alpha + 1$ linear equations in the $\alpha + 1$ unknown coefficient $A_{j,\alpha+1}, ..., A_{j,2\alpha+1}$, since the $\alpha + 1$ first equations related to initial conditions are solved in $A_{j,0}, ..., A_{j,\alpha}$

$$A_{j,k} = \frac{T^k}{k!} y_j^k(t_j), \quad k = 1, ..., \alpha. \tag{3.17}$$

The remaining $\alpha + 1$ coefficients are given by

$$\begin{aligned} \begin{pmatrix} 1 & 1 & \dots & 1 \\ \alpha+1 & \alpha+2 & & 2\alpha+1 \\ \alpha(\alpha+1) & (\alpha+1)(\alpha+2) & & 2\alpha(2\alpha+1) \\ \vdots & & & \vdots \\ (\alpha+1)! & \frac{(\alpha+2)!}{2} & \dots & \frac{(2\alpha+1)!}{(\alpha+1)!} \end{pmatrix} \begin{pmatrix} A_{j,\alpha+1} \\ \vdots \\ A_{j,2\alpha+1} \end{pmatrix} \\ = \begin{pmatrix} y_j(t_f) - \sum_{t=0}^{\alpha} \frac{T^l}{l!} y_j^{(l)}(t_i) \\ \vdots \\ T^k \left(y_j^{(k)}(t_f) - \sum_{t=k}^{\alpha} \frac{T^{l-k}}{(l-k)!} y_j^{(l)}(t_i) \right) \\ \vdots \\ T^\alpha (y_j^{(\alpha)}(t_f) - y_j^{(\alpha)}(t_i)) \end{pmatrix} \end{aligned} \tag{3.18}$$

If the starting point $(x(t_i), u(t_i))$ and ending point $(x(t_f), u(t_f))$ are equilibrium points, it can be said that $\dot{x}(t_i) = 0$, $\dot{u}(t_i) = 0$ and $\dot{x}(t_f) = 0$, $\dot{u}(t_f) = 0$. According to (3.6)-(3.7) $y(t_i) = 0$ and $y(t_f) = 0$ are equilibrium points too for the associated trivial system [55]. It can be proved that the polynomial rest-to-rest trajectories are of the form

$$y_j(t) = y_j(t_i) + (y_j(t_f) - y_j(t_i)) \left(\frac{t - t_i}{t_f - t_i}\right)^{\alpha+1} \left(\sum_{k=0}^{\alpha} A_{j,k} \left(\frac{t - t_i}{t_f - t_i}\right)^k\right), j = 1, \ldots, m \tag{3.19}$$

with $A_{j,0}, \ldots, A_{j,\alpha}$ solution of

$$\begin{pmatrix} 1 & 1 & \ldots & 1 \\ \alpha+1 & \alpha+2 & & 2\alpha+1 \\ \alpha(\alpha+1) & (\alpha+1)(\alpha+2) & & 2\alpha(2\alpha+1) \\ \vdots & & & \vdots \\ (\alpha+1)! & \frac{(\alpha+2)!}{2} & \ldots & \frac{(2\alpha+1)!}{(\alpha+1)!} \end{pmatrix} \begin{pmatrix} A_{j,0} \\ \vdots \\ A_{j,\alpha} \end{pmatrix} = \begin{pmatrix} 1 \\ 0 \\ \vdots \\ 0 \end{pmatrix} \tag{3.20}$$

3.4 Trajectory Tracking

For the solution of the motion planning problem, that is all required is the knowledge of a dynamical model and the time. This type of design is called open-loop. If the system dynamics are precisely known and if the disturbances don't produce significant deviations from the predicted trajectories, the open-loop design may be sufficient. If measurements of the system are available, they may be used to compensate for such disturbances. On the other hand, if disturbances create significant deviations from predictions the loop may closed by using the measurements to compute at every time the deviation with respect to desired trajectory and deduce some correction term in the control to decrease this deviation.

For a flat system, if there are enough sensors to measure all the system states, the trajectory tracking may be designed by establishing the equivalence to a trivial

system of endogenous dynamic feedback. If y is a flat output of the system whose state is x and input u, assumed to be measured, and if y^* is the reference trajectory of the at output, denote by $e_i = y_i - y_i^*$, $i = 1, ..., m$, the components of the error. An endogenous dynamic feedback can be computed such that the system reads $y^{(r+1)} = v$. If we set $v^* = (y^*)^\alpha$, the error equation reads

$$e^\alpha = v - v^* + w \tag{3.21}$$

where w is an unmeasured disturbance term. It suffices then to set, componentwise

$$v_i = v_i^* - \sum_{j=0}^{\alpha-1} k_{i,j} e_i^{(j)}, \quad i = 1, \ldots, m \tag{3.22}$$

The gains $k_{i,j}$ are chosen such that the m polynomials $s^\alpha + \sum_{j=0}^{\alpha-1} k_{i,j} s^{(j)} = 0$ have their roots with strictly negative real part, $i = 1, \ldots, m$. Thus, if, e.g., $w(t)$ converges to 0 as $t \to \infty$, the error e exponentially converges to 0

$$e_i^\alpha = -\sum_{j=0}^{\alpha-1} + w_j, \quad i = 1, \ldots, m \tag{3.23}$$

and y and all its derivatives up to order α converge to their reference $y^*, \ldots, (y^*)^\alpha$ and it can be concluded that the set of variables x and u of the original system locally exponentially converge to their references [55].

Chapter 4

Flatness-Based AGC

4.1 Introduction

System frequency deviates from the nominal setting whenever there is imbalance between generation and load. The imbalance will be drawn from the kinetic energy stored in the rotating masses of the generators. As frequency is a common factor throughout the system, a change in active power demand at one point is reflected throughout the system by a change in frequency. Because there are many generators supplying power into the system, some means must be provided to allocate change in demand to the generators. A speed governor on each generating unit provides the primary speed control function, while supplementary control originating at the control center allocates generation. In an interconnected system with two or more independently controlled areas, in addition to control of frequency, the generation within each area has to be controlled so as to maintain scheduled power interchange. The control of generation and frequency is implemented by AGC [56]. The reference power position, P_i^{ref}, is conventionally calculated through integration of ACE, which is a combination of frequency and tie line flow deviations. The main challenge in this method is the design of the integral controller and the coordination across areas. This becomes more challenging in the presence of wind farms in the system as the energy

generated by these units varies rapidly, which may result in misleading ACE signals. The remainder of this chapter is organized as follows. First the fundamentals of frequency control in an interconnected system and the required models are presented. Then, the AGC based on proposed flatness approach is introduced and finally simulation results and comparisons between the conventional and proposed method are provided.

4.2 Primary Speed Governing

When there is a load change, it is reflected instantaneously as change in the electrical torque output T_e of the generator. This causes a mismatch between the mechanical torque T_m and the electrical torque T_e which in turn results in speed variation as determined by equation of motion. For load-frequency studies, it is preferable to express this relationship in terms of mechanical and electrical power given by (4.1) rather than torque [57].

$$\triangle P_m - \triangle P_e = 2H\frac{d}{dt}(\triangle\omega_r) \tag{4.1}$$

Also since some of the loads in the system change with frequency, there is a need to model the effect of a change in frequency on the net load drawn by the system. This characteristic may be expressed as (4.2).

$$\triangle P_e = \triangle P_L + D \triangle \omega_r \tag{4.2}$$

where the damping constant, D, is expressed as a percent change in load for one percent change in frequency. Typical values of D are 1 to 2 percent.

To overcome the deviation in ω_r, a governing mechanism that senses the machine speed, and adjusts the input valve to change the mechanical power is added to the generating system. For power load sharing between generators connected to the

system, speed regulation through a droop characteristic is provided in governing system. The parameter R is referred to as droop and is equal to the ratio of speed deviation ($\triangle\omega_r$) to change in power output ($\triangle P$). The model for prime mover used in this study is a simple model of non-reheat steam turbines. The block diagram of a governor-prime-mover-rotating mass/load model is shown in Figure 4.1.

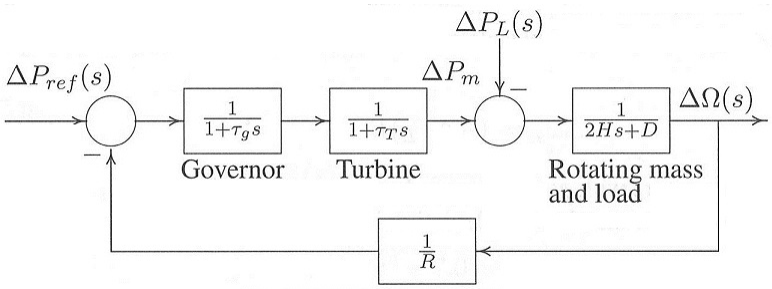

Figure 4.1: Governor-Prime Mover- Turbine Model

4.3 Automatic Generation Control

With primary speed control action, a change in system load will result in steady-state frequency deviation, depending on the governor droop characteristic and frequency sensitivity of the load. Also governor control does not adequately consider the cost of power production and control may not result in the most economical alternative. Supplemental control or AGC, on the other hand serves several functions, including restoration of the nominal frequency and maintenance of the scheduled interchanges between authority areas. These functions are primary objectives of AGC and are commonly referred to as load-frequency control (LFC). A secondary objective is to distribute change in generation among units to minimize operating cost. AGC in a given area should ideally correct only for changes in that area. The coordination among areas is achieved by defining the so-called ACE. A frequency bias setting, 10β, is multiplied by the frequency deviation, Δf, which is subtracted from the deviation

of tie flows to obtain ACE. ACE is integrated over time and this signal is used to determine the generator set points. The control center gathers the relevant frequency and power flow information, calculates the ACE and sends the appropriate set point adjustments for each of the units on AGC. A suitable bias factor for an area is its frequency response characteristic β given in (4.3).

$$\beta = \frac{1}{R} + D \tag{4.3}$$

ACE represents the required change in area generation, and its unit is MW. However, bias factor is usually expressed in $\frac{MW}{0.1Hz}$. The area frequency-response characteristic $(\frac{1}{R} + D)$ required for establishing the bias factors can be estimated by examination of chart records following a significant disturbance such as a sudden loss of a large unit.

Figure 4.2 illustrate how supplementary control is implemented in one area of an interconnected power system.

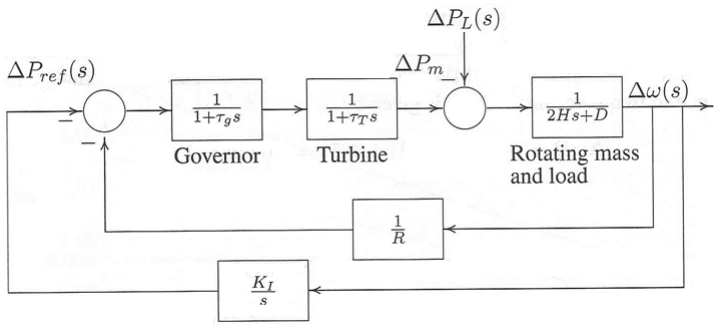

Figure 4.2: Supplementary Control

For control of tie line power and frequency, it is necessary to send signals to generating plants to control generation. It is possible to use these signals to control generation to satisfy economic dispatch criteria. Thus, the requirement for Economic

Dispatch (ED) can be handled as part of the AGC function. Since system load is continually changing, economic dispatch calculations have to be made at frequent intervals. The allocation of individual generation output is accomplished by using base points and participation factor (PF). The base point, P_{base}, represents the schedule for each generating unit, and the participation factor is the rate of change of the unit output with respect to a change in total generation, P_{tot}. The desired output for the i^{th} generator is calculated as (4.4). Economic dispatch is performed once every 5 minutes in many regions of North America, e.g, ERCOT, CAISO, PJM, MISO , NYISO and ISO-NE to follow changes in load and lessens the variability of the wind resources from one dispatch interval to the next [58].

$$P_{des_i} = P_{base_i} + PF(\triangle P_{tot}) \tag{4.4}$$

where

$$\triangle P_{tot} = P_{tot} - \sum_{i=1}^{n} P_{base_i} \tag{4.5}$$

In order to implement AGC, it is important to consider the fuel cost, avoid sustained operation of the generating of units in undesirable ranges and to minimize equipment wear and tear by limiting unnecessary maneuvering of generating units. Practical AGC systems achieve these objectives by keeping the control strategies simple, robust and reliable. The stability of an AGC system and its ability to react to changing inputs are influenced by phase lags in the input system quantities and in the transmission of it its control signal. With digitally based systems, experience has shown that the execution of AGC once every 2 to 4 seconds results in good performance. This means that ACE is computed and the raise/lower control signals are transmitted to the generating plant once every 2 to 4 seconds. Limitations of the prime mover also needs to be considered in AGC design, since the generation can be increased only to the limits of available spinning reserve and the load that can be picked up by a thermal unit is limited due to thermal stress in turbine. Initially, about 10% of turbine rated output can be picked up quickly without causing damage

by too rapid heating. This is followed by a slow increase of about 2% per minute. Also, speed governors have a time delay of 3 to 5 seconds [59].

Conventionally, each control area of an interconnected system is controlled in a similar manner, but independently of the other control areas. That is, the control of generation in the interconnected system is "area-wise decentralized" [59].

4.4 Modeling

In order to analyze the performance of AGC in a multi-machine system, it is necessary to provide appropriate models for the generators and the transmission network. Considering the governor-prime-mover-rotating mass/load model block diagram in Figure 4.1, a synchronous machine in a multi-machine system can be described by a fourth-order model in ((4.6)-(4.9)). Since the focus of this study is only on frequency response, it is appropriate to assume that the voltage regulator and other dynamics within the machine are fast compared to the phenomena of interest [60].

$$\dot{\delta}_i = \omega_i - \omega_s \tag{4.6}$$

$$\dot{\omega}_i = \frac{1}{2H_i}\left[P_{mi} - \frac{E_i V_i}{x'_{di}} sin(\delta_i - \theta_i) - D_i(\omega_i - \omega_s)\right] \tag{4.7}$$

$$\dot{P}_{gvi} = \frac{1}{\tau_{g_i}}(P_i^{ref} - \frac{\omega_i - \omega_s}{R_i \omega_s} - P_{gvi}) \tag{4.8}$$

$$\dot{P}_{mi} = \frac{1}{\tau_{T_i}}(P_{gvi} - P_{mi}) \tag{4.9}$$

In this model, the active power output at the generator internal nodes is stated as a function of terminal voltage, the voltage behind the reactance and x'_d [61]. Terminal voltage magnitude and angle depend on the network equations. Since the flux decay dynamics are neglected, terminal voltage can be calculated from the algebraic equations.

The internal-node model is used to simulate the network [61]. In this model, the dynamic circuit of the machines is modeled with constant voltages behind the reactance. Machines are added to the network at the generator buses $1, ..., n$ where n is the number of synchronous machines. The generator internal nodes are denoted as $m+1, ..., m+n$, where m is the number of network buses. Machines can be added to network equations using augmented Y matrix which is obtained by including the admittance corresponding to the transient reactances of the machines

$$\bar{y} = Diag\left(\frac{1}{jX'_{di}}\right) \qquad i = 1, ..., n \tag{4.10}$$

Loads are assumed to be constant impedances and converted to admittances in a m bus system as (4.2). There is a negative sign for $\bar{y}_{Li}$, since loads are assumed as injected quantities.

$$\bar{y}_{Li} = \frac{-(P_{Li} - jQ_{Li})}{V_i^2} \qquad i = 1, ..., m \tag{4.11}$$

If we neglect transmission line resistances, then the network admittance matrix is $\bar{Y}_N = [jB_{ij}]$ and the augmented admittance matrix can be defined as

$$
Y_{aug} = \begin{array}{c} \\ \text{m+1} \\ \vdots \\ \text{m+n} \\ \\ 1 \\ \vdots \\ \text{n} \\ \\ \text{n+1} \\ \vdots \\ \text{m} \end{array}
\begin{array}{c}
\begin{array}{ccccccccccccc} m+1 & \dots & m+n & & 1 & ... & n & & n+1 & \dots & m & & \end{array} \\
\begin{pmatrix}
 & & & \vdots & & & & \vdots & & & & & \\
 & \bar{y} & & \vdots & & -\bar{y} & & \vdots & & 0 & & & \\
 & & & \vdots & & & & \vdots & & & & & \\
\dots & \dots & \dots & \dots & \dots & \dots & \dots & \dots & \dots & \dots & \dots & \dots & \\
 & & & \vdots & & & & & & & & & \\
 & -\bar{y} & & \vdots & & & & & & & & & \\
 & & & \vdots & & & & & & & & & \\
\dots & \dots & \dots & \vdots & & & & \bar{Y}_{N2} & & & & & \\
 & & & \vdots & & & & & & & & & \\
 & 0 & & \vdots & & & & & & & & & \\
 & & & \vdots & & & & & & & & &
\end{pmatrix}
\end{array}
\tag{4.12}
$$

where

$$\bar{Y}_{N2} = \bar{Y}_{N1} + Diag(\bar{y}_{Li}) \tag{4.13}$$

$$\bar{Y}_{N1} = \bar{Y}_{N1} + \begin{bmatrix} \bar{y} & 0 \\ 0 & 0 \end{bmatrix} \tag{4.14}$$

The network equations for the new augmented network can be written as

$$
\begin{bmatrix} \bar{I}_A \\ 0 \end{bmatrix} = \begin{array}{c} \\ n \\ m \end{array}
\begin{array}{c}
\begin{array}{cc} n & m \end{array} \\
\begin{pmatrix} \bar{Y}_A & \bar{Y}_B \\ \bar{Y}_C & \bar{Y}_D \end{pmatrix}
\end{array}
\begin{bmatrix} \bar{E}_A \\ \bar{V}_B \end{bmatrix}
\tag{4.15}
$$

where $\bar{Y}_A = \bar{y}$, $\bar{Y}_B = \left[\begin{array}{c|c} -\bar{y} & 0 \end{array} \right]$, $\bar{Y}_C = \left[\begin{array}{c} -\bar{y} \\ \hline 0 \end{array} \right]$, and $\bar{Y}_D = \bar{Y}_{N2}$. The m network buses can be eliminated, since there is no current injection at these buses. Thus

$$\begin{aligned} \bar{I}_A &= (\bar{Y}_A - \bar{Y}_B \bar{Y}_D^{-1} \bar{Y}_C) \bar{E}_A \\ &= \bar{Y}_{int} \bar{E}_A \end{aligned} \tag{4.16}$$

where the elements of $\bar{I}_A$ and $\bar{E}_A$ are, respectively, $\bar{I}_i = (I_{di} + jI_{qi}) e^{j(\delta_i - \frac{\pi}{2})} = I_{Di} + jI_{Qi}$ and $\bar{E}_i = E_i \angle \delta_i$. The elements of $\bar{Y}_{int}$ are $\bar{Y}_{ij} = G_{ij} + jB_{ij}$. Since the network buses have been eliminated, we may renumber the internal nodes as $1, \ldots, m$ for ease of notation.

$$\bar{I}_i = \sum_{j=1}^{n} \bar{Y}_{ij} \bar{E}_j \qquad i = 1, .., n \tag{4.17}$$

Real electrical power out of the internal node i is given by

$$\begin{aligned} P_{ei} &= Re\left[\bar{E}_i \bar{I}_i^{\star}\right] \\ &= Re\left[E_i e^{j\delta_i} \sum_{j=1}^{n} \bar{Y}_{ij}^{\star} \bar{E}_j^{\star}\right] \\ &= Re\left[E_i e^{j\delta_i} \sum_{j=1}^{n} (G_{ij} - jB_{ij}) E_j e^{-j\delta_j}\right] \\ &= Re\left[\sum_{j=1}^{n} (G_{ij} - jB_{ij}) E_i E_j \left[\cos(\delta_i - \delta_j) + j \sin(\delta_i - \delta_j)\right]\right] \end{aligned} \tag{4.18}$$

Then

$$\begin{aligned} P_{ei} &= \sum_{j=1}^{n} E_i E_j (G_{ij} cos(\delta_i - \delta_j) + B_{ij} sin(\delta_i - \delta_j)) \\ &= E_i^2 G_{ii} + \sum_{j=1, j \neq i}^{n} (C_{ij} sin(\delta_i - \delta_j) + D_{ij} cos(\delta_i - \delta_j)) \end{aligned} \tag{4.19}$$

where

$$\begin{aligned} C_{ij} &= E_i E_j B_{ij} \\ D_{ij} &= E_i E_j G_{ij} \end{aligned} \tag{4.20}$$

Replacing (4.19) in (4.7) results in elimination of V_i and θ_i terms.

$$\dot{\omega}_i = \frac{1}{2H_i}\left[P_{mi} - E_i^2 G_{ii} - \sum_{j=1,j\neq i}^{n}(C_{ij}sin(\delta_i - \delta_j) + D_{ij}cos(\delta_i - \delta_j)) - D_i(\omega_i - \omega_s)\right] \tag{4.21}$$

Therefore, the dynamic equations of the systems will be solved without explicitly representing the algebraic equations, e.g., power flow equations.

4.5 Flatness-Based Control

Based on (4.6)-(4.9) and considering $\delta = [\delta_1, ..., \delta_i, ..., \delta_n]'$ as the flat output set, the flat outputs and their derivative up to degree four for a multi-machine system can be derived as follows

$$\dot{\delta}_i = \omega_i - \omega_s \tag{4.22}$$

$$\ddot{\delta}_i = \frac{1}{2H_i}\left[\ P_{mi} - \frac{E_i V_i}{x'_{di}} sin(\delta_i - \theta_i) - D_i\left(\omega_i - \omega_s\right)\ \right] \tag{4.23}$$

$$\delta_i^{(3)} = \frac{1}{2H_i}\left[\frac{1}{\tau_{Ti}}(P_{gvi} - P_{mi}) - D_i\ddot{\delta}_i - \frac{E_i V_i}{x'_{di}}\dot{\delta}_i cos(\delta_i - \theta_i)\right] \tag{4.24}$$

$$\delta_i^{(4)} = \frac{1}{2H_i}\begin{bmatrix} \frac{1}{\tau_{Ti}\tau_{gi}}(P_i^{ref} - \frac{\dot{\delta}_i}{R\omega_s} - P_{gv}) - \frac{1}{\tau_{Ti}^2}(P_{gvi} - P_{mi}) \\ -\frac{E_i V_i}{x'_{di}}(\ddot{\delta}_i cos(\delta_i - \theta_i) - (\dot{\delta}_i)^2 sin(\delta_i - \theta_i)) \\ -D_i\delta_i^{(3)} \end{bmatrix} \tag{4.25}$$

The algebraic relations between the state variables, input, flat outputs and their derivatives, verify that δ is the flat output in this system as stated in (4.22)-(4.25). The algebraic functions A, B and C can be defined as follows

$$\begin{aligned} x_i &= A(\delta_i, \dot{\delta}_i, \ddot{\delta}_i, \delta_i^{(3)}) \\ u_i &= B(\delta_i, \dot{\delta}_i, ..., \delta_i^{(4)}) \end{aligned} \tag{4.26}$$

$$\delta_i = C\left(x_i, u_i\right) \tag{4.27}$$

where $x_i = [\delta_i, \omega_i, P_{gvi}, P_{mi}]'$ $u_i = P_i^{ref}$. Therefore, this system is equivalent to the trivial system of

$$\begin{aligned} \dot{z}_{i1} &= z_{i2} \\ \dot{z}_{i2} &= z_{i3} \\ \dot{z}_{i3} &= z_{i4} \\ \dot{z}_{i4} &= v_i \end{aligned} \tag{4.28}$$

where $z_{i1} = \delta_i$ and $\delta_i^{(4)} = v_i$. According to (4.28), one sees that the dynamics of a multi-machine system can be split into n linear controllable subsystems. The trajectory generation and the asymptotic tracking of the desired trajectory, rotor angle, is studied in the following to find the control input, v_i, for each subsystem.

4.5.1 Trajectory generation for multi-machine AGC system

An important role of AGC is to allocate generation so that each power source is loaded most economically [59]. In this study, economic dispatch is performed to find the desired operating points. Note that this can be replaced by other methods depending on the system's overall needs. The desired operating point has to be updated at frequent intervals in order to follow load changes and wind generation variations. Here, intervals of five minutes are considered for economic dispatch as modern markets are moving to 5 minute schedules using security constrained economic dispatch. The reference points and participation factors are sent to generators every 5 minutes and a smooth trajectory is then planned locally. The planning method described in section 3.3 is deployed to generate the optimum path to be followed by trajectory tracking control. Within the five minute intervals, the reference values for rotor angle are updated such that each generator contributes in frequency regulation based on its participation factor. The desired operating point determines the participation factors.

Although the operating points in the system are updated every 5 minutes through economic dispatch, unpredicted significant wind power deviations, load changes or

generation trip may occur in the interval. In this situation, the trajectory needs to be updated to avoid significant changes in the tie-line flows. In the conventional AGC method, this action is performed using tie line flow measurements sent from SCADA every $2-4$ seconds. In this section, a novel method based on PMU measurements and an Injection Shift Factor (ISF) concept is proposed. The value of the ISF of a line with respect to bus i is defined to be: the change (or sensitivity) of active (MW) power flow in a reference direction on the line with respect to a change in injection at bus i and a corresponding change in withdrawal at the reference bus. In an AC network, ISFs could be calculated using power flow around a given generation and load pattern. However the ISF will change when the operating point, topology and/or line characteristics change. A method to estimate ISFs through linear least-squares estimation (LSE) is presented in [62], using PMU measurements collected in real-time. This approach does not rely on the system power flow model and can adapt to unexpected system topology and operating point changes. In a DC power flow model, on the other hand, the ISF does not change by operating point and only depends on the topology of the system and line impedance changes. Also, due to system linearity, the superposition applies and the effect of injection at a bus i and withdrawal from bus j could be found with summation of related shift factors.

Equation 4.29 shows the linearized relation between the ΔP_{line} that represents the transmission line flows, S_{inj} which is the ISF matrix and P_{inj}, the power injection at each bus except for the reference bus.

$$\Delta P_{line} = S_{in} \Delta P_{inj} \tag{4.29}$$

The P_{inj} vector consists of PV buses with generators contributing to AGC, PV buses with generators not contributing to AGC and all PQ buses. Reordering P_{inj} with PV buses contributing in AGC at the first rows and reordering S_inj matrix accordingly results in

$$\Delta P_{line} = S_{in}^{Dist} \Delta P_{inj}^{Dist} + S_{in}^{AGC} \Delta P_{inj}^{AGC} \tag{4.30}$$

The P_{line} vectors includes all transmission lines, however, we are interested to minimize the deviation in tie line flows between BAs. This problem can be formulated as the objective function below

$$min \sum_{i \in tie} | \sum_{j \in Dist} S_{in}^{Dist}(i,j) \Delta P_{inj}^{Dist}(j) + \sum_{j \in Dist} S_{in}^{AGC}(i,j) \Delta P_{inj}^{AGC}(j)| \tag{4.31}$$

s.t.

$$\sum_{j \in Dist} \Delta P_{inj}^{Dist}(j) = \sum_{j \in Dist} DeltaP_{inj}^{AGC}(j) \tag{4.32}$$

$$|P_{line}(i) + \sum_{j \in Dist} S_{in}^{Dist}(i,j) \Delta P_{inj}^{Dist}(j) + \sum_{j \in Dist} S_{in}^{AGC}(i,j) \Delta P_{inj}^{AGC}(j)| \leq P_{max}(i) \quad i \in line \tag{4.33}$$

$$P_{inj}^{AGC,min}(i) \leq P_{inj}^{AGC} + \Delta P_{inj}^{AGC}(i) \leq P_{inj}^{AGC,max}(i) \qquad i \in AGC \tag{4.34}$$

The constraints are the balance between changes in generation and load as shown in 4.32, the maximum line flow limits for all lines as stated in 4.33 and the generation limits for generators contributed in AGC shown in 4.34. ΔP_{inj}^{AGC} is unknown while ΔP_{inj}^{Dist} can be find from the PMU measurements and state estimation through formulation for fast decoupled power flow 4.35.

$$\Delta P_{inj} = J_1 \Delta \delta \tag{4.35}$$

where J_1 is the part of the Jacobian matrix in decoupled power flow. Quadratic programming is deployed to solve this optimization problem.

4.5.2 Trajectory tracking for multi-machine AGC system

The gains, $k_{i,j}$, in (3.22) should be designed to restore the nominal frequency and track the scheduled net interchange with desired performance characteristics. Individual units tracking the desired trajectory generated in section 4.5.1 will guarantee overall system performance. The trivial system of (4.28) for each area is the key to achieve tracking of the desired trajectory. In general, any simple linear control method can be applied to find the gain. In this work, the LQR method is employed which allows consideration of practical constraints related to AGC [63].

The obtained $k_{i,j}$ leads to asymptotic tracking of the desired trajectory. The practical constraints considered in this study are:

- Generator ramping rate constraint (GRC) which limits the rate of generation increase/decrease. In LQR method, this constraint can be considered by choosing a large value for R, which is representative of cost of the control.

- Raise/lower signals are sent to the governor every 2 seconds. Therefore, continuous optimal control may not be optimal for the system in practice. In order to design the digital control law for this continuous time systems, the flat system is discretized using 2 second samples. The discretization process assumes that the control input $v(t)$ to the continuous plant is switched only at times $2k$ and it is held constant between switchings [63]. In North America, AGC is typically executed once every 2 to 4 seconds. Note the control action in flatness approach is based on local measurements and due to a large sampling rate of modern units, measurement does not restrict the frequency of sending controller signal. In the other words, the control signal can be sent to governor as frequent as the governor limits allow.

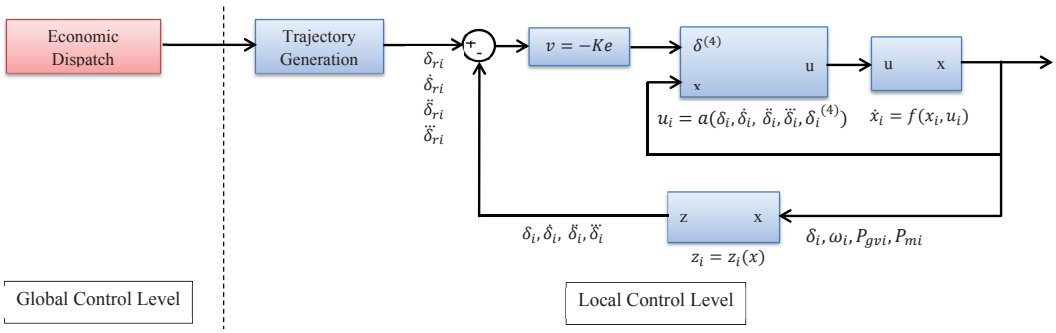

Figure 4.3: Flatness-Based Control Block Diagram

4.5.3 Summary of Approach

Figure 4.3 shows the schematic control diagram of the proposed approach. Desired operating points are determined at the global level control using the economic dispatch or other methods, while the trajectory is generated at the local control level. Rotor angle and frequency are the quantities requiring monitoring in this scheme. Due to the lack of a direct measurement of rotor angle, this parameter is assumed estimated using the measurements of a PMU [64]. In this study, rotor angle is estimated based on the terminal voltage angle and generator active and reactive powers as shown in (4.36) and (4.37).

$$I_i = I_{Di} + jI_{Qi} = (P_{Gi} - jQ_{Gi})/V_i e^{-j\theta_i} \tag{4.36}$$

$$\delta_i = \angle(V_i e^{j\theta_i} + jx'_{di}(I_{Di} + jI_{Qi})) \tag{4.37}$$

The measured and estimated quantities are compared with the reference values and the control signal is generated through a trajectory tracking approach at the generator level. In summary, the planning is performed at the global level and the trajectory is generated and tracked locally using closed loop control.

4.6 Simulation Results: 39-Bus System

In this section, the proposed flatness-based AGC is evaluated on a 3 area, 10-machine and 39-bus system shown in Figure 4.4 and is compared with conventional AGC [64]. The total load in this system is assumed to be 5.483 GW and economic dispatch is performed to find the scheduled active power generation. In order to evaluate the performance of the controller in the presence of wind units, the wind power profile shown in Figure 4.5 is applied to the test system. The wind power has an average value of 500 MW and the fluctuations are about $\pm 5\%$ of the average power. Frequency deviation in the frequency domain, considering spatial filtering of geographically dispersed wind turbines in a wind farm, is used to generate this wind power profile [65]. Two scenarios are studied:

- Scenario 1: 10% penetration of wind power generation in area 2.
- Scenario 2: 20% penetration of wind power generation in areas 1 and 2.

Based on the Western Wind and Solar Integration Study (WWSIS) results, the addition of every 3 MW of wind generation was accomplished with a 2 MW de-commitment and a 1 MW reduction in other generation. Therefore for 500 MW additional wind production, the 2/3 de-commitment objective is 333 MW and the 1/3 re-dispatch objective is 167 MW. De-commitment of the thermal units reduces the contribution of these units in frequency regulation, while dispatching down gives more headroom for secondary control [1]. The original dispatch and the updated dispatch related to scenarios 1 and 2 and generator data are shown in Table 4.1.

Note in the flatness approach the control areas would not necessarily be the same as today's balancing areas. Smaller balancing areas can be selected to improve the controller performance in presence of large scale wind generation at no additional cost of monitoring. The changes in the planning and trajectory generation are investigated in section 4.6.3.

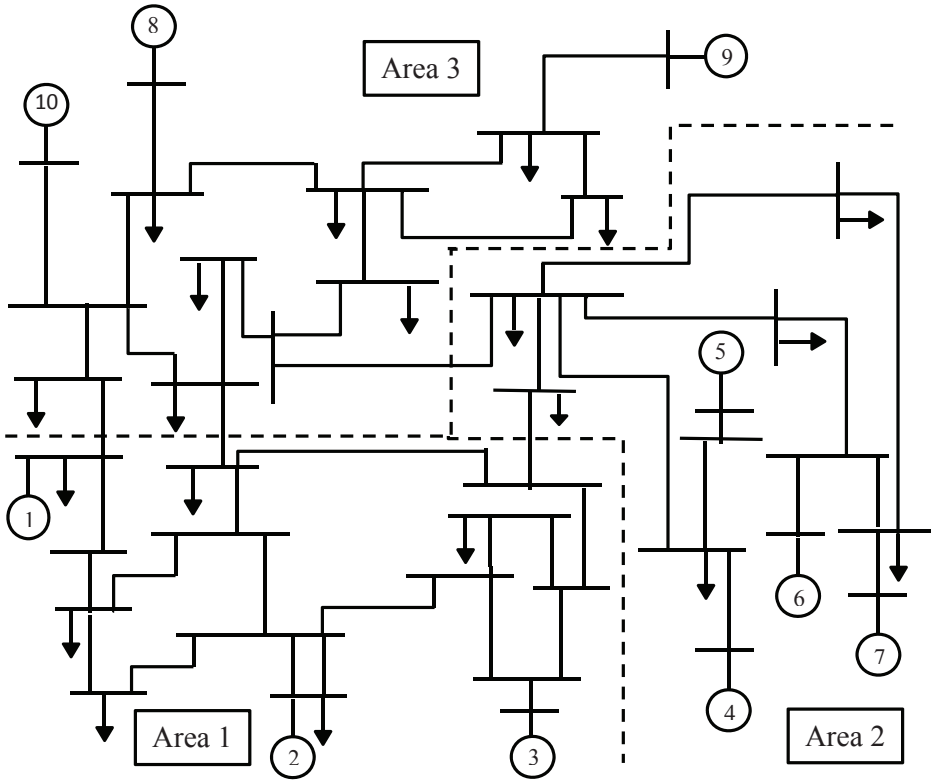

Figure 4.4: 10 Generator, 39 Bus Test System

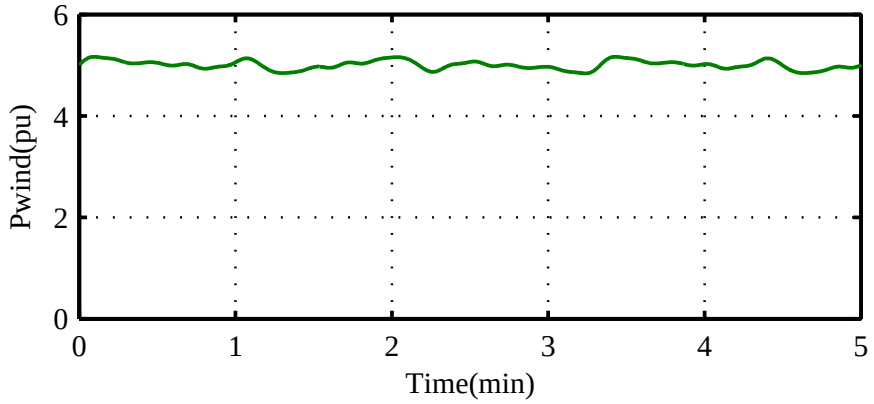

Figure 4.5: Wind Power (pu) - Base is 100 MVA

Table 4.1: Generator Dispatch in pu (base is 100MVA)

Area	Gen	Original Dispatch	Scenario 1 Dispatch	Scenario 2 Dispatch	Inertia $H(sec)$	x'_d (pu)
1	1	5.620	5.620	5.620	70.0	0.020
	2	3.727	3.727	2.454	30.3	0.070
	3	3.727	3.727	0	35.8	0.053
2	4	7.481	7.481	7.481	28.6	0.044
	5	7.796	7.796	7.796	26.0	0.132
	6	5.796	5.092	5.092	34.8	0.050
	7	4.296	0	0	26.4	0.049
3	8	4.296	4.296	4.296	24.3	0.057
	9	4.296	4.296	4.296	34.5	0.057
	10	7.797	7.797	7.797	20.0	0.044

4.6.1 Scenario 1

In this scenario, the wind power profile is added in area 2, which is about 10% of the total load. Figure 4.6 displays the average frequency deviations in each area. The total mechanical power values in each area are shown in Figure 4.7. Tie line flow deviations from the scheduled values are displayed in Figure 4.8. As observed, the flatness approach results in improved performance in mitigating both the frequency and tie flow deviations while the mechanical power changes do not exceed the ramping rate limits of the generators. Comparison of frequency deviations and tie flow deviations in three areas shows that, with the flatness-based approach the control actions occur primarily in the area where the wind farm is located. In other words, the wind power fluctuations are absorbed locally. It is worth mentioning that in the flatness-based approach, the average of the frequency in areas is only calculated for clarity of presentation. As stated in section 4.5.3, the frequency is measured locally and compared with a reference value for each generator.

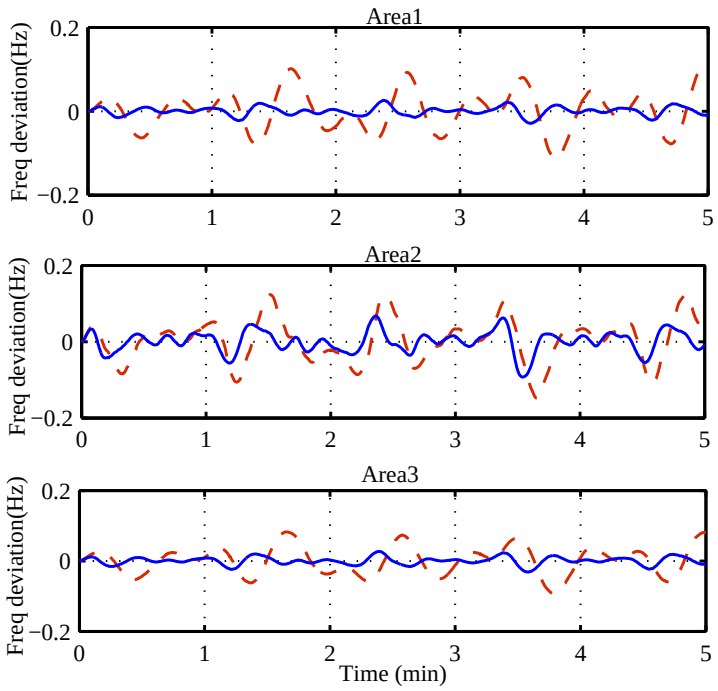

Figure 4.6: Frequency Deviation with Conventional (dash line) and Flatness-Based (solid line) with 10% Penetration

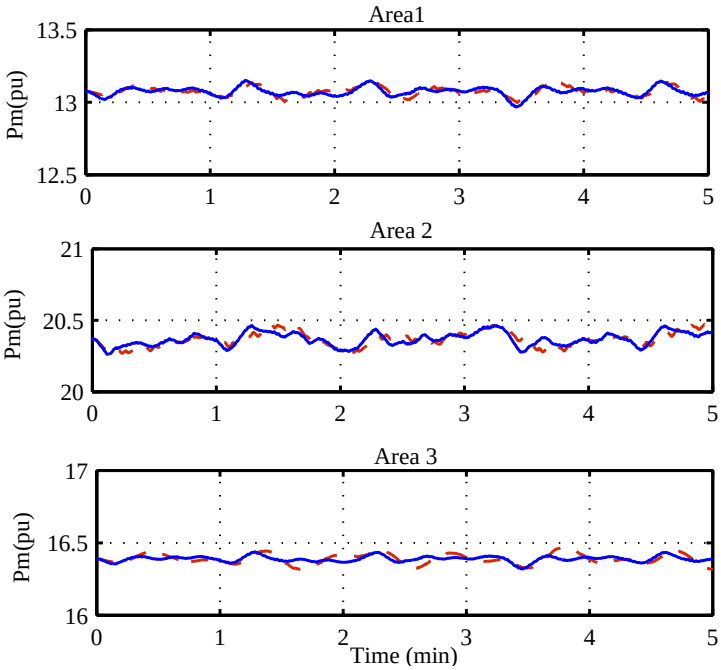

Figure 4.7: Mechanical Power with Conventional (dash line) and Flatness-Based (solid line) with 10% Penetration

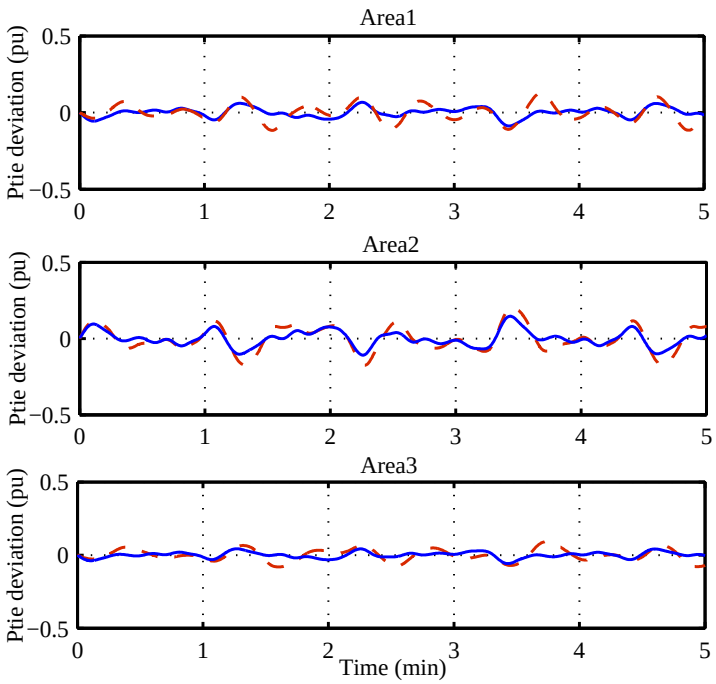

Figure 4.8: Tie Flow with Conventional (dash line) and Flatness-Based (solid line) with 10% Penetration

4.6.2 Scenario 2

In this scenario, a wind farm is in both areas 1 and 2. The average frequency deviations in each area, total mechanical power values in each area and tie flow fluctuations are shown in Figure 4.9, Figure 4.10 and Figure 4.11. The first observation is that higher penetration of wind power results in greater frequency and tie flow deviations in the system. Also, comparison of the two scenarios shows that the effectiveness of the flatness-based approach increases with the higher penetration of the wind power.

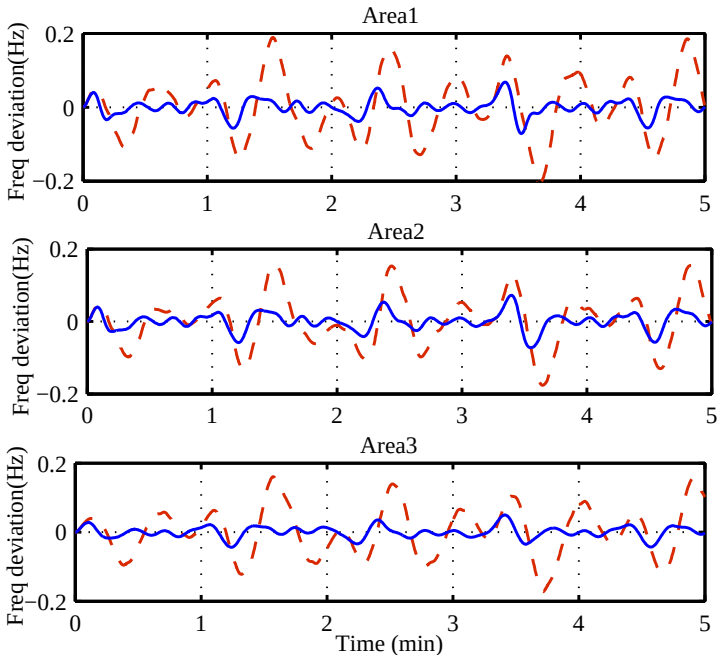

Figure 4.9: Frequency Deviation with Conventional (dash line) and Flatness-Based (solid line) with 20% Penetration

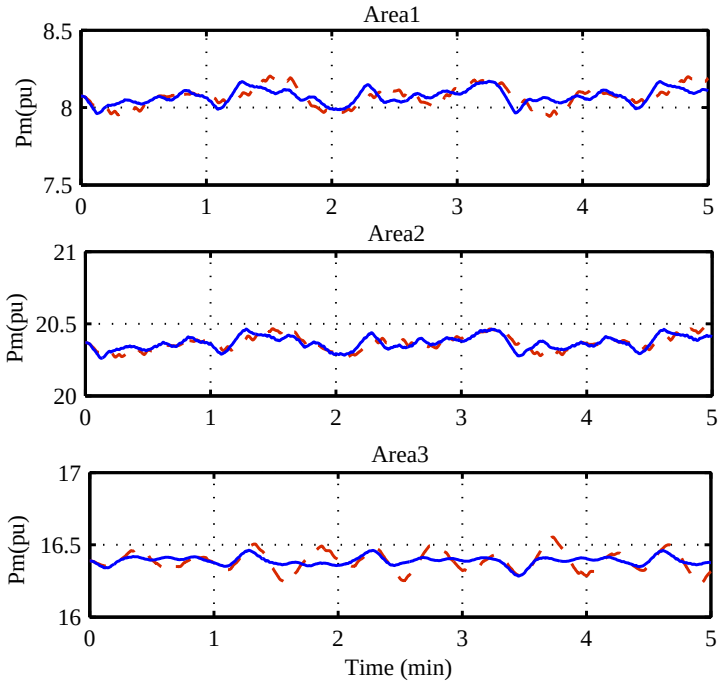

Figure 4.10: Mechanical Power with Conventional (dash line) and Flatness-Based (solid line) with 20% Penetration

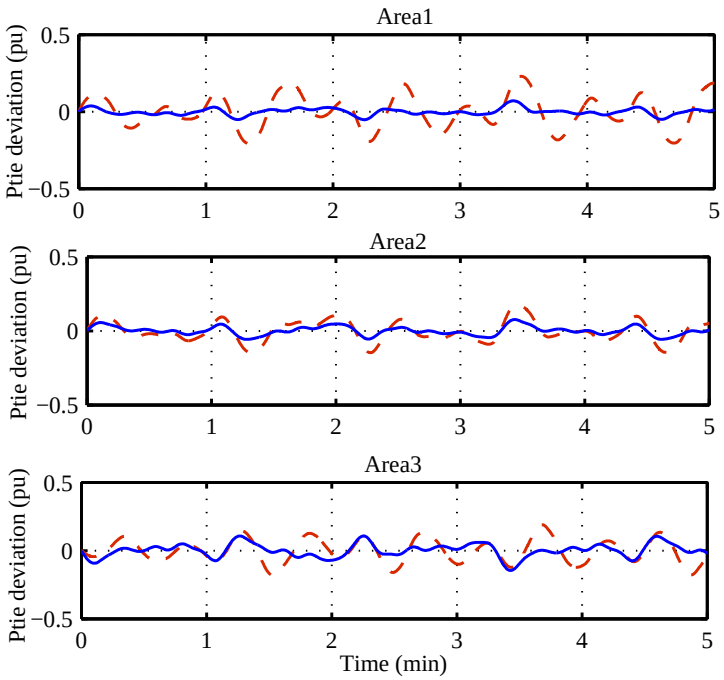

Figure 4.11: Tie Flow with Conventional (dash line) and Flatness-Based (solid line) with 20% Penetration

4.6.3 Planning

Simulation results shown in sections 4.6.1 and 4.6.2 are assumed to be performed in 5 minutes intervals with a constant desired operating point. In this section, the concept of trajectory generation that reflects the system needs is demonstrated. Two generators in area 2 are re-dispatched so that the scheduled value for generator 5 is decreased by 0.2 pu and the scheduled value for generator 7 is increased by the same amount. Figure 4.12 shows two different trajectories, one with a step change in the rotor angle trajectory and the other one based on generating a smooth trajectory. The actual rotor angles are also shown in the same figure. Figure 4.14 displays the frequency deviations in two generators related to two trajectories. It is observed that the smooth trajectories result in improved frequency and rotor angle deviations and the controller tracks the desired trajectories well. The lower deviations decrease the control effort required to keep the system at the desired operating point.

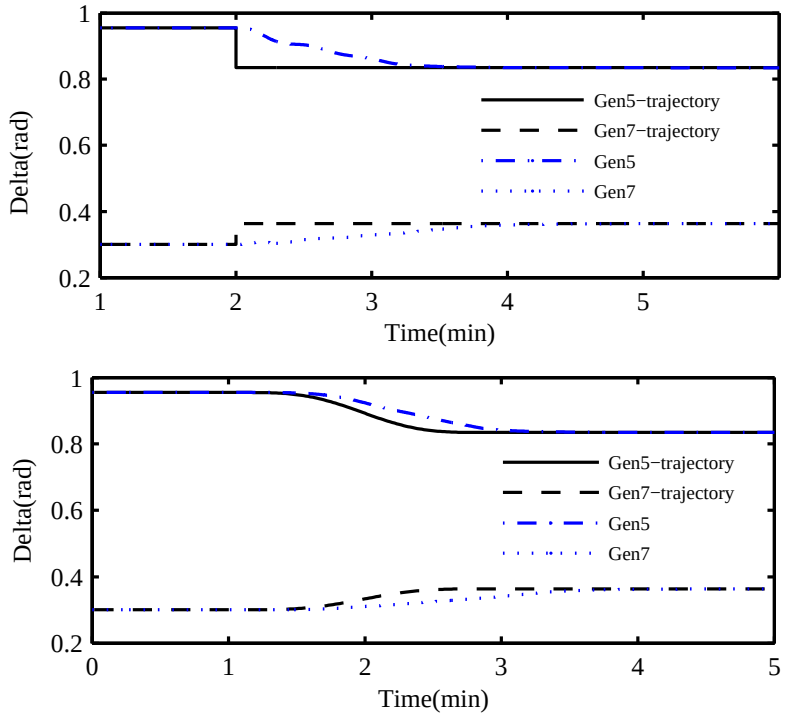

Figure 4.12: Rotor Angles and Trajectories in Area 2

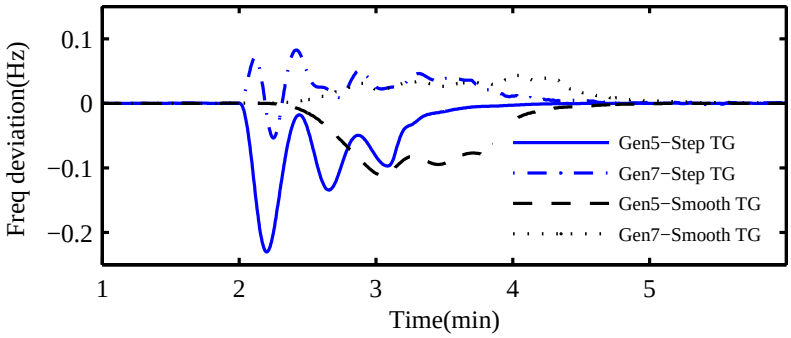

Figure 4.13: Frequency Deviation in Area2

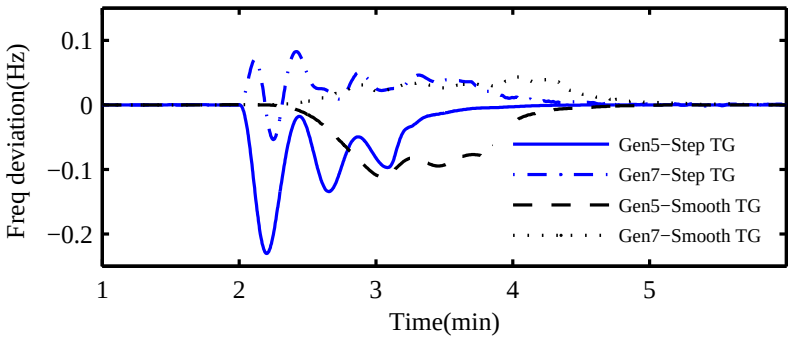

Figure 4.14: Frequency Deviation in Area2

4.7 Large Scale Test Bed Results

In this section, NPCC region system is studied. NPCC is one of the nine regional electric reliability councils under NERC authority. This system lies within the U.S. Eastern Interconnection (EI) and occupies the greater New England region of North America, covering the States of Maine, Vermont, New Hampshire, Massachusetts, New York, Connecticut, Rhode Island, and the Provinces of Ontario, Quebec, New Brunswick, Nova Scotia and Prince Edward Island. NPCC also has ties to non-NERC systems in Northern Canada. In terms of percentage of load served, NPCC provides 20% of the Eastern interconnection's total load demand. Figure 4.15 shows the one-line diagram of this system which includes five BAs: MISO, IESO, PJM, NYSO and NEPOOL.

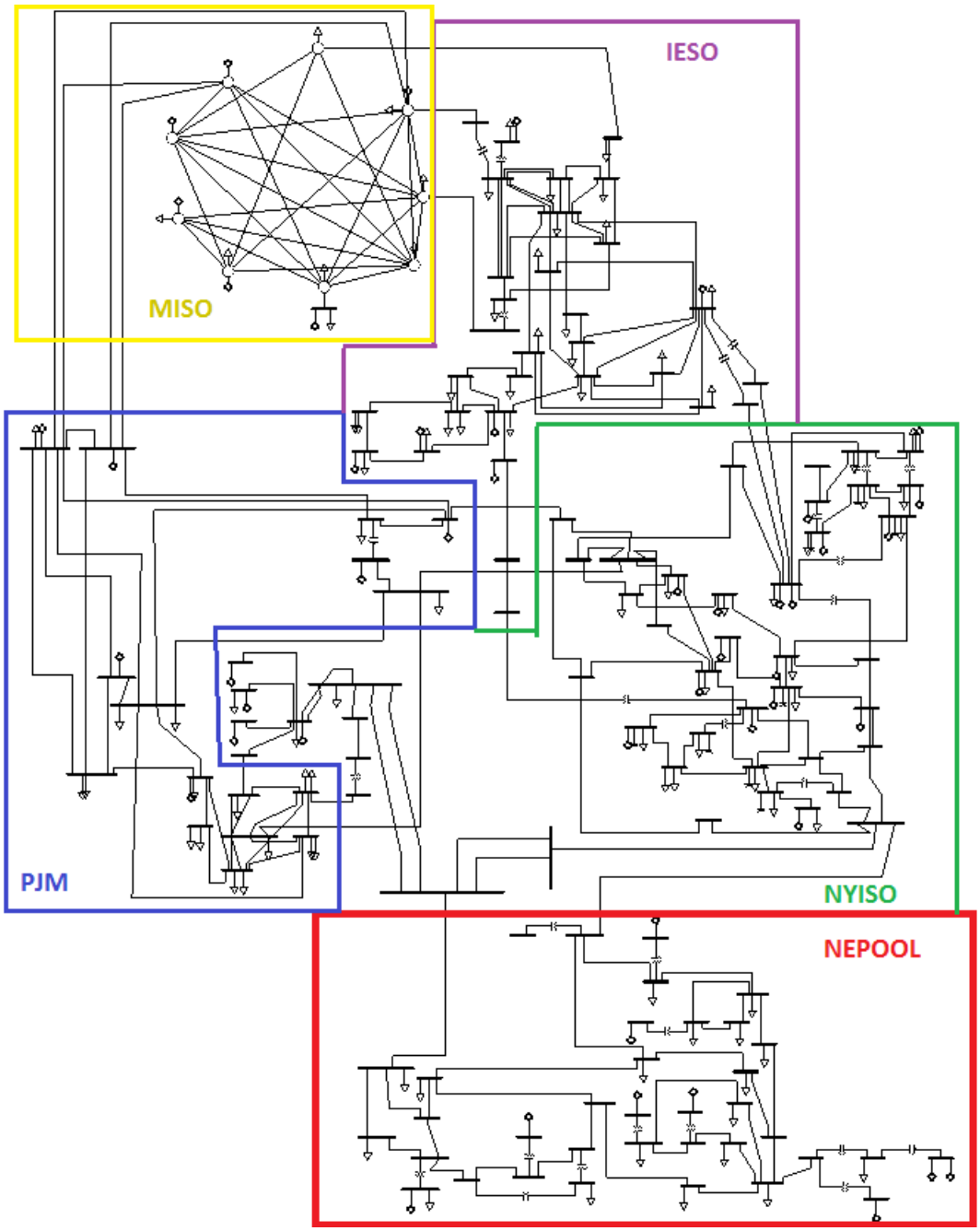

Figure 4.15: NPCC system one-line diagram

The model used in this study is a reduced model with 140 buses, and 48 machines. The total capacity of NPCC system is about 28 GW. The complete dynamic model of this system serves as a part of the CURENT large-scale testbed. The model was first converted to PSS/E format from the system data available in the MATLAB

Power System Toolbox. Power flow data were formatted into PSS/E raw file directly. However, the dynamic data were modified to meet the requirement of GENROU type generators. The PSS/E power flow raw file and the built dynamic file are then imported into DSA Tools to enable a variety of dynamic simulations with user defined models. In order to study frequency response of the system in presence of disturbances, governor models are added to the selected generators contributing in frequency regulation in the TSAT model. The user defined model (UDM) editor tool provides the opportunity to add customized models for AGC. In this study, it is assumed that one generator in each BA participates in secondary frequency control and the user-defined AGC models are added to these generators.

The first UDM added to the system is the conventional or ACE-based AGC. In this model, the tie line flows of each area and the frequency signals are added to the UDM assigned to generators contributing to AGC. Then ACE is calculated using tie line flow, frequency error and the bias factor. Before applying AGC, a generator trip is simulated to find the bias factor (β) or frequency response of this system. Frequency response is the metric used to describe how an interconnection performs in stabilizing frequency after loss of generation and it is calculated using

$$\beta = \frac{\Delta P}{\Delta f} \tag{4.38}$$

where ΔP is the change of power by all resources in response to generator trip and Δf is the change in frequency before applying AGC [14]. The change in power is mostly due to the governor response of synchronous generators. Responsive loads and storage units could also contribute to primary frequency response [66].

The second method for AGC implementation is the flatness-based AGC as described in 4.5. In this case, local signals for voltage magnitude and angle, active and reactive power and frequency are added to the UDM and rotor angle is estimated using these measurements. AGC signal is found using the rotor angle, frequency and acceleration errors, and applying appropriate gains.

To asses the performance of AGC, a load shedding contingency occurs at $t = 100(s)$ and load in the PJM area drops by 450 MW. The simulation results for frequency response and tie lines flowing out of each area, after adding AGC, are shown in Figures 4.16 and 4.17. It can be seen that AGC is successfully implemented and both frequency and tie line flows are returned to the original values. Figure 4.18 shows the power generation changes for the selected generators contributing in secondary regulation. During the first few seconds after load drop, all generators respond to the contingency through inertial and governor response. However, after a few minutes, AGC shares the amount of shed load among the generators so that the tie line flows are maintained at scheduled values. Each BA is responsible to compensate for the changes in generation/load within the area. In this scenario, the generation in PJM is decreased to maintain the balance in the BA.

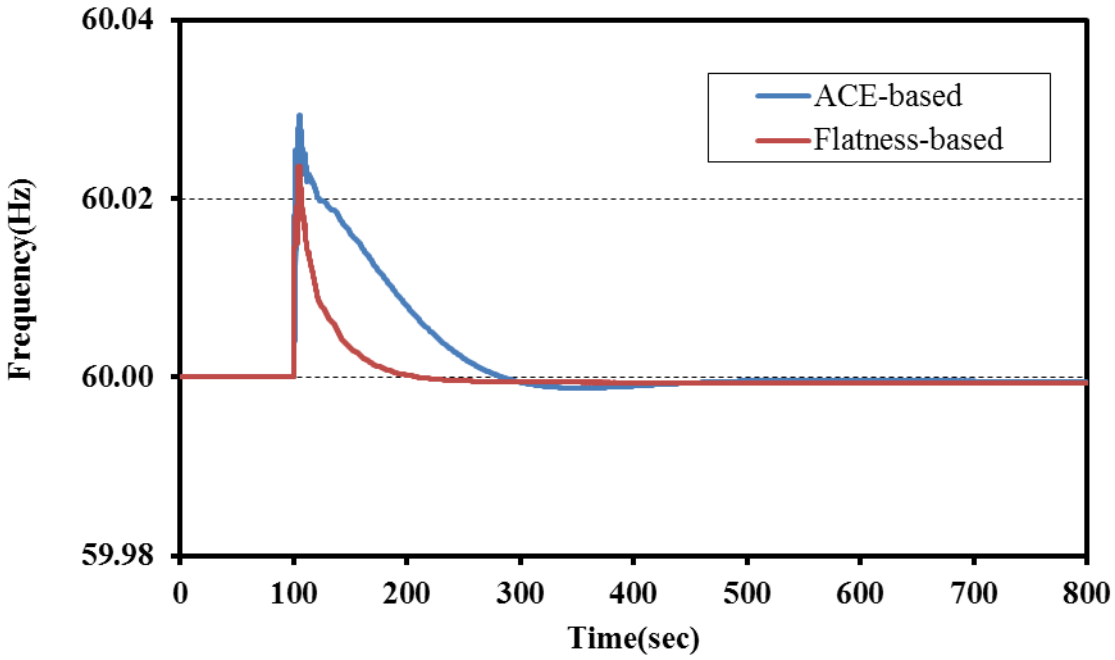

Figure 4.16: Frequency for load shedding scenario

Another purpose of this work is performing frequency regulation in presence of wind generation variations. The UDM editor is used to add built-in Type-3 wind generators to the system. Five wind farms with total capacity of about 4 GW replace

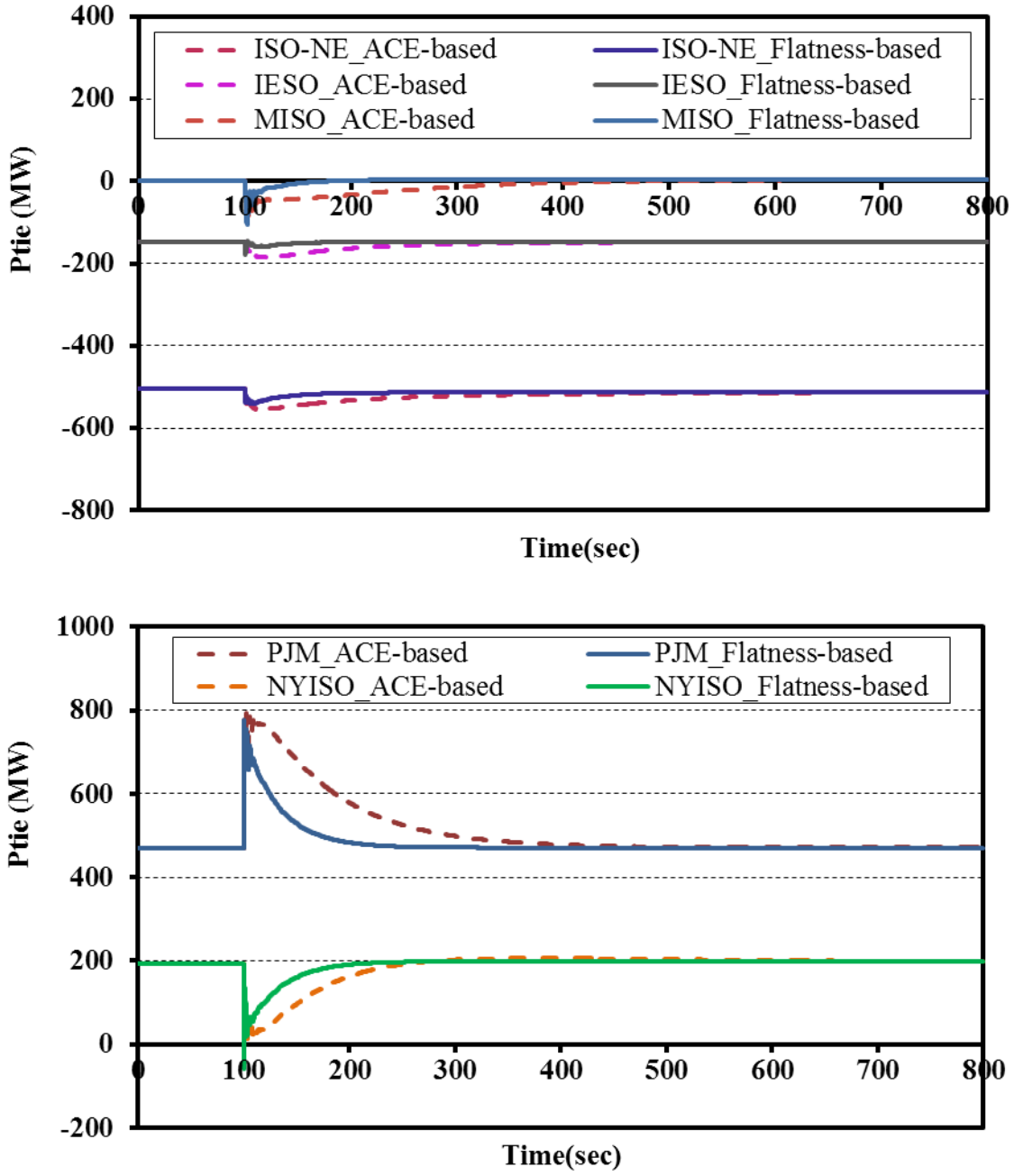

Figure 4.17: Tie-line flow for load shedding scenario

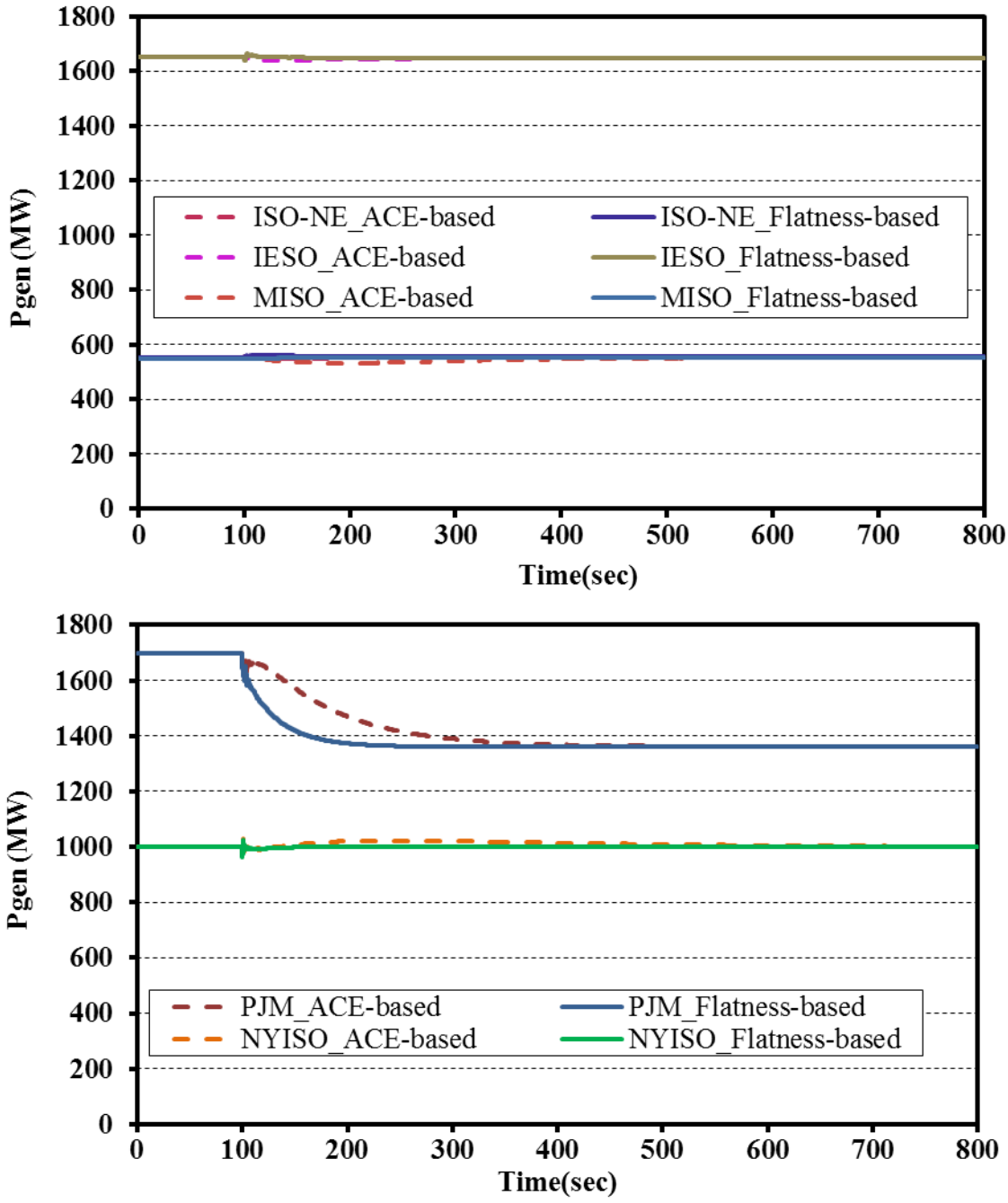

Figure 4.18: Active power generation for load shedding scenario

the conventional generators in the NYSO and NEPOOL areas. Since the Type-3 wind generator does not contribute to system inertia, replacing the conventional generators will reduce the inertia support from the network. Moreover, these wind generators do not provide governor response. The wind variations added to wind farms is shown in Figure 4.19. The active power generation of wind farms are shown in Figure 4.20. The simulation results shown in Figure 4.21 demonstrate the frequency deviations of the system in response to changes in wind power. The results show the improved performance of flatness-based method, specially when there is a significant drop in wind speed between $t = 100(s)$ and $t = 200(s)$. Tie line flow changes of the five BAs are shown in Figure 4.22. For the flatness-based method, tie line flows are closer to the nominal value in most of the time periods compared to the ACE-based ones.

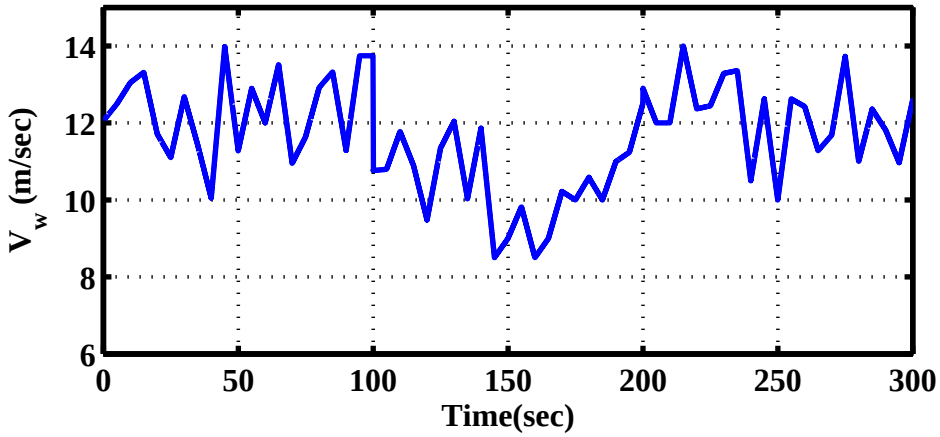

Figure 4.19: Wind speed

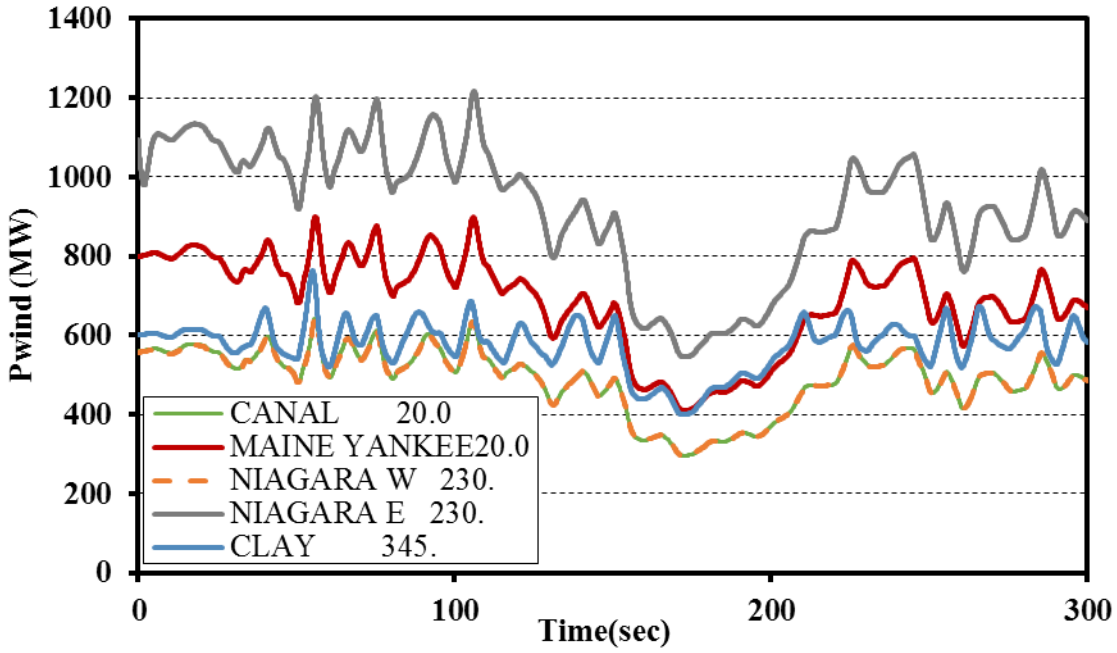

Figure 4.20: Wind power output

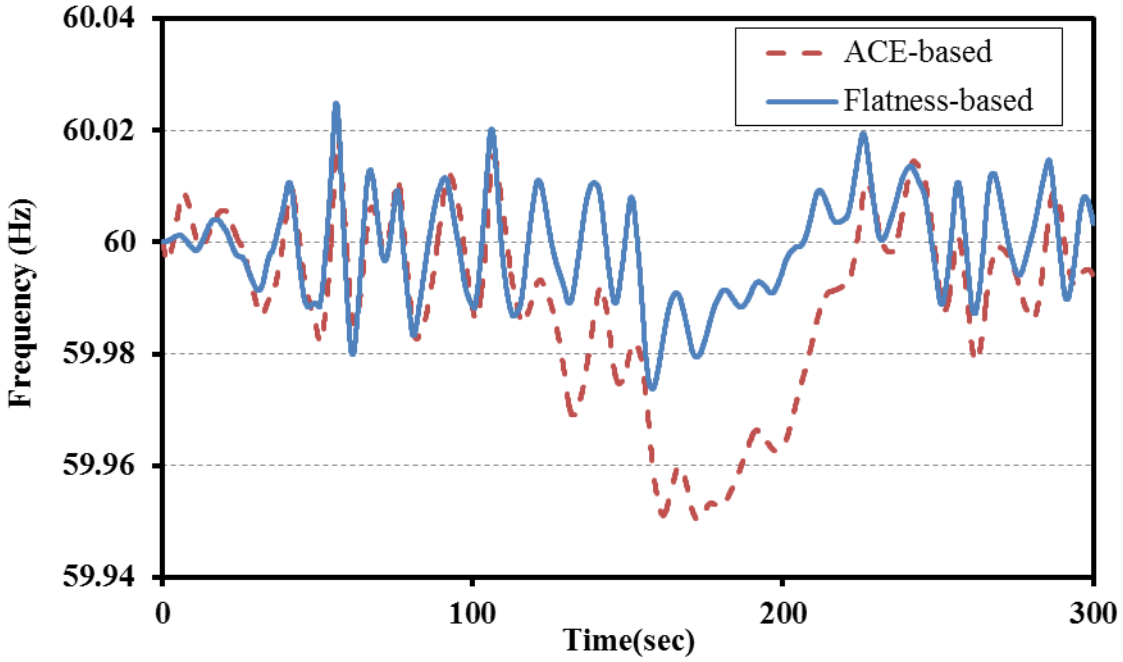

Figure 4.21: Frequency in presence of wind power variation

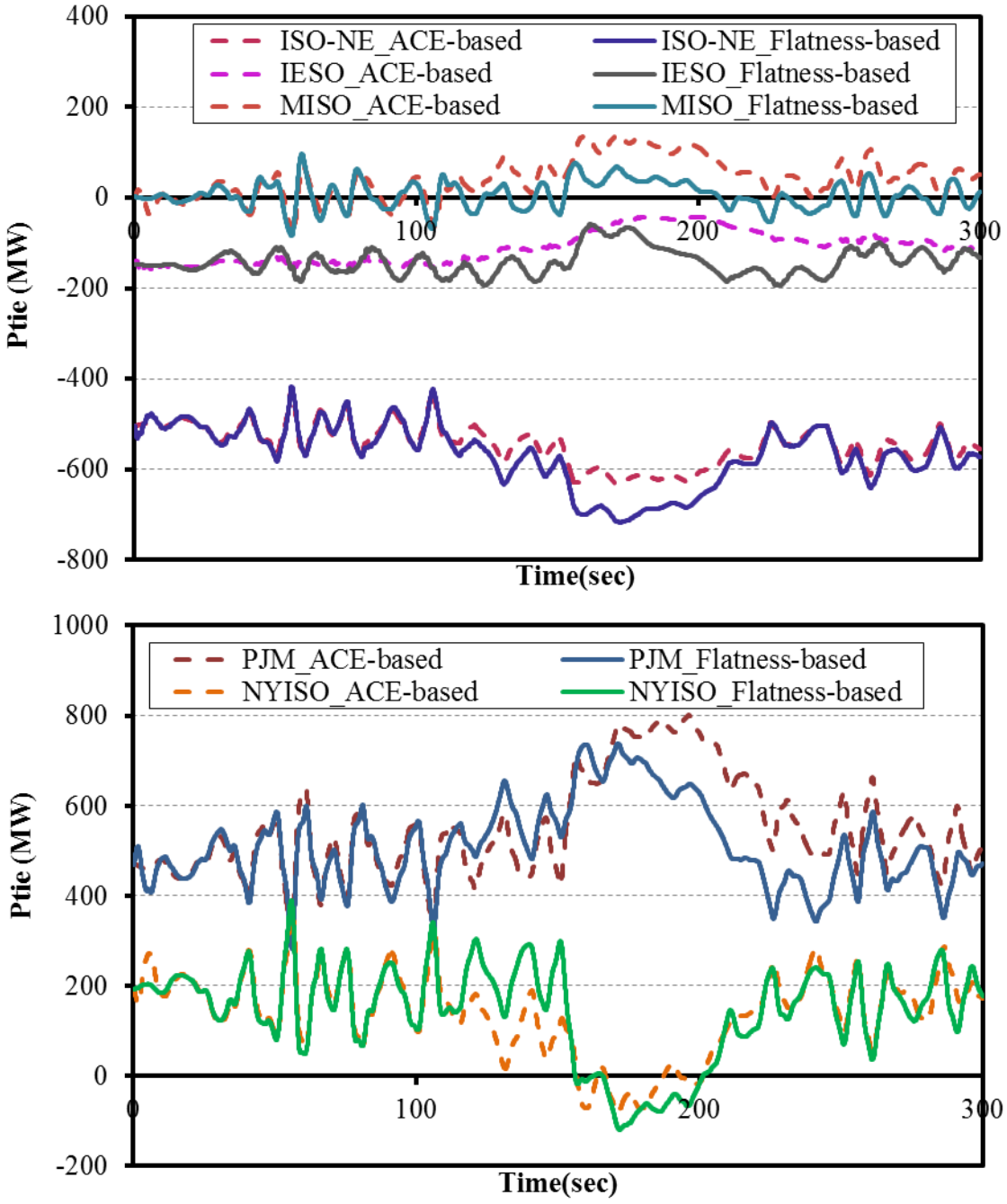

Figure 4.22: Tie-line flow in presence of wind power variation

4.8 Hardware Test Bed Results

In this section, assessment of flatness-based AGC method using HTB is presented. The HTB is a scaled hardware emulator, built in CURENT, that represents the electrical grid with sufficient details. Integration of new measurement technologies, sensors and communication has provided a platform for demonstrating and testing the studies performed in the center. The test bed consists of several emulators including a synchronous generator emulator [67], induction motor emulator [68, 69], wind turbine emulator [70], and solar power emulator [71,72]. The HTB contains three cabinets, two for generator and load emulators and one for HVDC or a long-distance transmission line. Communication and supervisory control is realized in LabVIEW to efficiently control the emulators and mimic power system management. The LabVIEW gathers data from monitoring devices such as a PMU and frequency data recorder (FDR) and sends supervisory control commands, such as power dispatch, wind speed, and irradiance level, to emulators. The HTB can be controlled remotely from a visualization and control room, where live data are displayed on 15 TV screens. The cabinets, visualization and control room of HTB are shown in Figures 4.23 and 4.24.

Using the three cabinets in HTB, the two-area power system shown in Figure 4.25 can be emulated [59]. This system is used to demonstrate flatness-based AGC and other system studies. The system parameters and operating point are shown in Appendix for simplicity. The same wind power profile as shown in 4.26 is added to bus 9 of the two area system while generators 1 and 3 are contributing to frequency regulation. The simulation results for Area 2 of the system, as they are demonstrated in visualization room, are shown in Figure 4.27. The top left figure shows the active power changes for generators 3 and 4 (blue and red, respectively) and the injection at bus 9 (green), considering wind generation and load. The top right figure shows reactive power changes which are not of interest in frequency regulation. The figures

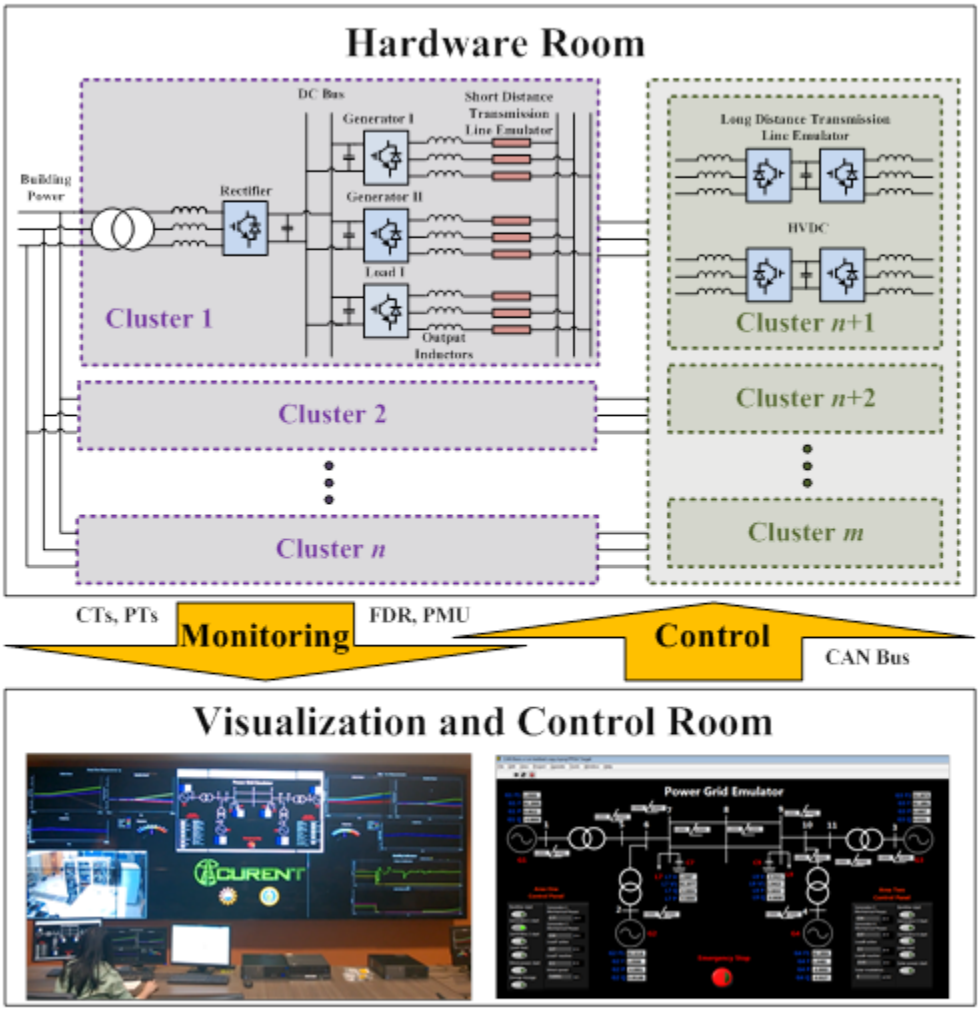

Figure 4.23: System configuration of hardware test-bed

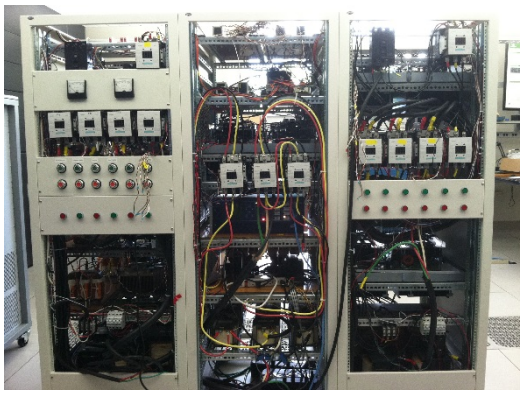

Figure 4.24: Cabinets in the HTB

in the bottom demonstrate the frequency variation which are compensated using AGC.

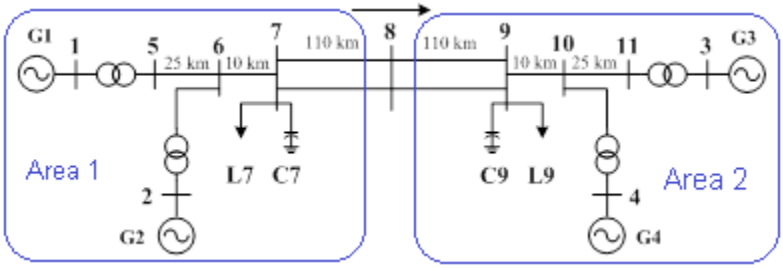

Figure 4.25: Two-area system

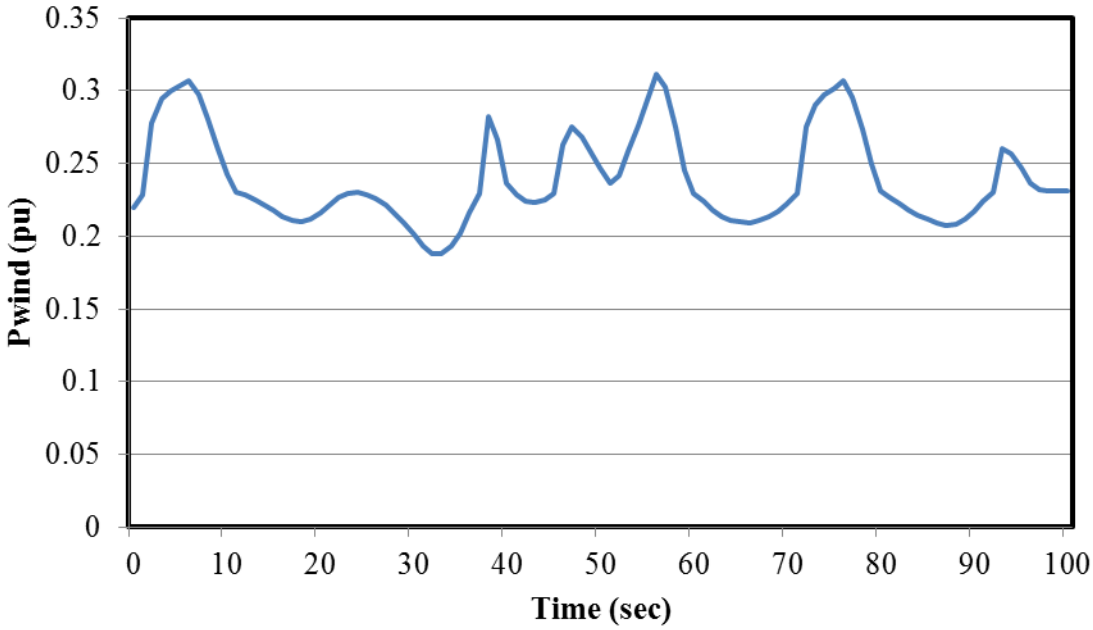

Figure 4.26: Wind power applied to HTB

4.9 Conclusions

This chapter presents a flatness-based method to control frequency and power flow for multi-area power systems. The two level control consisting of trajectory generation and trajectory tracking replaces conventional AGC. This approach can also replace

Figure 4.27: Simulation Results for Area 2

conventional area based frequency control. As an important feature of the proposed approach, the set of nonlinear equations corresponding to a n-machine system is decoupled into n linear controllable sub-systems. Therefore, the proposed AGC is easy to design and implement. Local linear controllers are designed for each sub-system to maintain the frequency at nominal value and to keep power flows near scheduled values. The main requirement is the availability of PMU measurements. The flatness-based control method demonstrates promising performance in mitigating frequency and tie-line flow deviation. This approach also provides a platform for non-conventional units to contribute to load following and frequency control as presented in Chapter 5.

Chapter 5

Flatness-Based DFIG

5.1 Introduction

Most wind farms built today use asynchronous generators. The dynamics of these asynchronous machines are very different from those of traditional synchronous units. With the large penetration of wind power, the dynamic performance of the grid will necessarily change in terms of angular stability, voltage stability and frequency response. While the WTGs in a wind farm are distributed, the total output of the farm normally connects to the bulk power system at a single substation, in a fashion similar to conventional central-station generation [11].

Increased variable wind generation will have many impacts on the primary frequency control actions of the power system. The lower system inertia will increase the need for primary frequency control reserves to arrest frequency decline following the sudden loss of generation. The combined inertial response of a wind power plant will depend on the electrical characteristics of its individual wind turbines. Constant-speed wind turbines have different inertial response than synchronous generators; however, they do not intrinsically decrease the power system inertia because of their

electromechanical characteristics. On the other hand, the rotating mass of variable-speed wind turbines is decoupled from the grid frequency and does not inherently exhibit an inertial response unless controlled for that specific purpose.

There are many different generator types for wind-power applications in use today. The differences among turbine types are mostly based on the electrical generation components consisting of generator, power converter and control algorithm. The strategies used to control the prime mover are generally similar. Mechanical brakes and blade pitch control are commonly used to avoid runaway conditions and keep stresses on the mechanical components of the wind turbine generator (WTG) within the design tolerance. The pitch angle of the blades is usually controlled during high wind speeds to restrict aerodynamic forces; thus, the output power and rotor speed can be kept within limits [73]. Generally there are four types of WTGs:

- Type 1: Induction generator operating at fixed speed
- Type 2: Wound-rotor induction generator with variable slip and adjustable external rotor resistance
- Type 3: Doubly-fed induction generators with variable speed
- Type 4: Permanent magnet synchronous generator with variable speed, direct drive and full converter

Types 1 through 3 are based on an induction generator and they require a gearbox to match the generator speed, high-speed shaft, to the turbine speed, low- speed shaft. Type 4 may or may not have a gearbox depending on the design.

Many modern wind plants have the ability to control active power output in response to grid frequency in ways that are important to overall grid performance. A performance similar to inertial response of synchronous generators can be achieved with a wind power plant by utilizing a controlled inertial response. Among those, variable speed wind turbines utilizing DFIGs are more popular in the power industry.

The DFIG is able to control its active and reactive power outputs as required by system operators within limits dependent on the wind speed.

In many restructured power systems throughout the world, ancillary service markets have been developed to incentivize ancillary services that support power system reliability. However, few ancillary service markets include a mechanism that explicitly incentivizes the provision of primary frequency response (PFR). Wind power may be an economic choice for providing inertial and PFR services in the presence of such markets [73]. Also, it may be both technically and economically feasible for wind plants to supply minute-to-minute regulation under some circumstances. For this reason, wind plants can provide regulation by curtailing energy production to create head room for up regulation. The plants also need to be operating above zero so that they can regulate down. It has been demonstrated that with pitch control, large state-of-the art wind turbines have very quick relative response rates and therefore entire wind farms should be capable of very fast and accurate response when providing regulation service. A study of West Texas energy prices for 2008 shows that a wind plant was producing at least a small amount of power during about 2800 of the 3282 hours when regulation was more profitable than energy for wind. The wind plant would have earned an additional $3.5 million in 2008 if it had sold regulation whenever the price of regulation exceeded the price of energy (including the lost energy revenue). That is an additional $9.96/MWh spread over the plant's entire production [35].

The amount of active power depends on the energy transferred from the wind, however it can be controlled in a transient manner by using the mechanical system kinetic energy to provide inertial response. In addition, DFIG machines can work at asynchronous speeds, increasing the wind energy transfer efficiency for a given wind speed while the mechanical stress is relieved to a certain extent [40]. Making full use of the capability of DFIG equipped wind turbines in providing fast active and reactive power injection and contributing to active power regulation requires replacing the existing linear controls with a nonlinear control. Feedback linearization has shown

promising results in [40], [41] and [43]. This control can be fulfilled by adding the trajectory generation which yields a two-level control structure. The flatness property for DFIG will be facilitate design of such control.

In the next sections, the DFIG dynamical model is described with the conventional controls and then the flatness-based control approach is developed.

5.2 Wind Turbine Generation (WTG) model

The focus of this study is on new control approaches for WTG type 3 turbines which are variable speed machines. The main components of this are turbine, DFIG, converters, and the DC-link. The converters make it possible to transform energy in both directions. When the machine operates at sub-synchronous speed, the power flows from grid or stator to rotor and at over-synchronous speed, the power flows from the rotor to the grid. The converters are partially scaled, requiring a rated power of about 30% of the generator rating. Usually, the generator slip varies between 40% at sub-synchronous speed and -30% at over-synchronous speed. Controlling the rotor current, with the rotor-side converter, makes it possible to change the machine slip and achieve the optimal power extraction from wind and a specified reactive power transferred to the grid [74, 75].

Assuming that the converters and DC-link are lossless, the net power injected by the generator to the grid is

$$P_{gen} = P_s - P_r \tag{5.1a}$$

$$Q_{gen} = Q_s \tag{5.1b}$$

where P_s and Q_s are the machine active and reactive power flowing out of the stator. P_r is the active power flowing from the rotor-side converter to the rotor circuit [74].

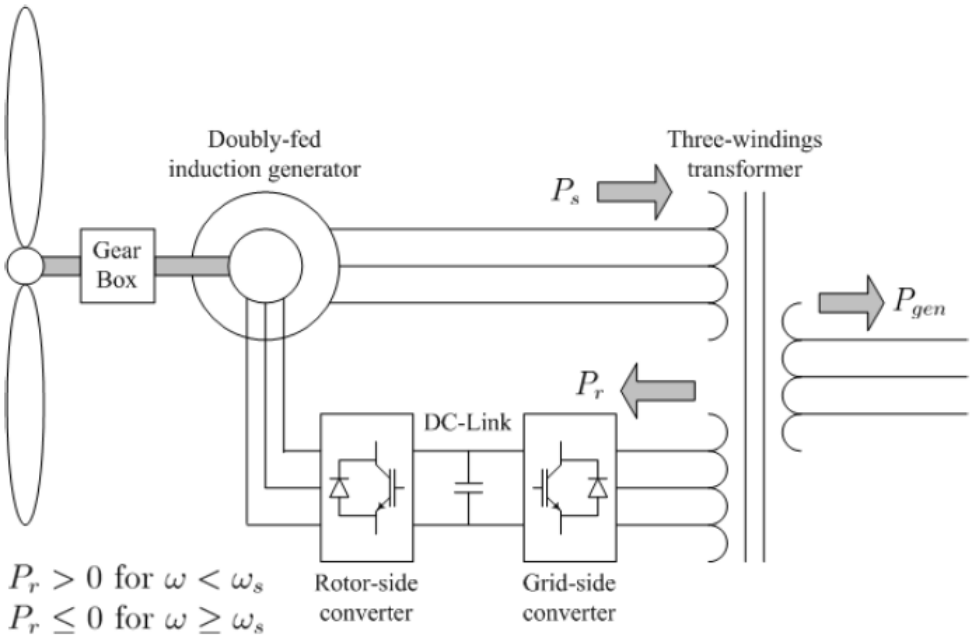

Figure 5.1: Wind Power Generator Scheme

5.2.1 Wind Turbine Model

In order to understand power extraction from wind, it is required to define the tip speed ratio, λ, which is the ratio between the speed of a blade tip, $v_{tip}[m/s]$, and the wind speed, $v_{wind}[m/s]$. Thus, $\lambda = \frac{v_{tip}}{v_{wind}} = \frac{\omega_{turbine} R_t}{v_{wind}}$, where R_t is the turbine radius. Then, the mechanical power extracted from a wind turbine can be estimated by

$$P_M = C_p(\lambda, \theta) P_{wind}\,(v_{wind}) = C_p(\lambda, \theta)\frac{1}{2}\rho A_{wt} v_{wind}^3 \quad [W] \tag{5.2}$$

where ρ is the air density $[kg/m^3]$, $A_{wt} = \pi R_t^2$ is the wind turbine swept area $[m^2]$ and v_{wind} is the wind speed $[m/s]$. $P_{wind}(v_{wind}) = \frac{1}{2}\rho A_{wt} v_{wind}^3$ is the theoretical potential power contained in an air mass at v_{wind}. C_p is the power coefficient, which is dimensionless and depends on both the tip speed ratio, λ, and the pitch angle, $\theta[degrees]$ angle of incidence of a turbine's blade and the wind direction. This coefficient takes into account the turbine's aerodynamic and establishes the fraction

of the potential power that can be extracted. Note that C_p is less than Betz's limit, i.e., $\forall\lambda, \theta, C_p(\lambda, \theta) < 0.593$. At every wind speed there is an optimum turbine speed at which the power extraction from the wind is maximized.

The power coefficient is estimated by

$$C_p(\lambda_i, \theta) = 0.22\left(\frac{116}{\lambda_i} - 0.4\theta - 5\right)e^{-\frac{12.5}{\lambda_i}} \tag{5.3}$$

where

$$\lambda_i = \left(\frac{1}{\lambda + 0.08\theta} - \frac{0.035}{\theta^3 + 1}\right)^{-1} \tag{5.4}$$

The gearbox model depends on its stiffness. If the gearbox has some degree of flexibility, a two-mass model is typically used which separately considers the mass of the turbine and the low speed side of the gearbox, and the mass of the generator and the high speed side of the gearbox. In this research, the gearbox is assumed to be stiff and the masses of the turbine, gearbox and generator are considered as a whole, single mass model [74].

5.2.2 Machine Model

Due to the fact that DFIG model is similar to a wound rotor induction machine (see for example [76]), only with both stator and rotor circuits energized, the same wound rotor equations can be used to model DFIG. However, the generation convention is used to indicate that the currents flowing out of stator and rotor have positive sign. Similarly, a positive sign is considered for active and reactive power feed into the grid [77]. The model is converted to synchronous rotating reference frame, with the q-axis leading the d-axis by 90°, in order to eliminate the off-diagonal elements of the

inductance matrix. The stator and rotor voltage equations are

$$v_{qs} = r_s i_{qs} + \frac{\omega}{\omega_s}\psi_{ds} + \frac{1}{\omega_s}\frac{d}{dt}\psi_{qs} \tag{5.5a}$$

$$v_{ds} = r_s i_{ds} - \frac{\omega}{\omega_s}\psi_{qs} + \frac{1}{\omega_s}\frac{d}{dt}\psi_{ds} \tag{5.5b}$$

$$v_{qr} = r_r i_{qr} + \frac{\omega - \omega_r}{\omega_s}\psi_{dr} + \frac{1}{\omega_s}\frac{d}{dt}\psi_{qr} \tag{5.5c}$$

$$v_{dr} = r_r i_{dr} - \frac{\omega - \omega_r}{\omega_s}\psi_{qr} + \frac{1}{\omega_s}\frac{d}{dt}\psi_{dr} \tag{5.5d}$$

and the flux equations are given by

$$\psi_{qs} = X_{ls} i_{qs} + X_M(i_{qs} + i_{qr}) \tag{5.6a}$$

$$\psi_{ds} = X_{ls} i_{ds} + X_M(i_{ds} + i_{dr}) \tag{5.6b}$$

$$\psi_{qr} = X_{lr} i_{qr} + X_M(i_{qs} + i_{qr}) \tag{5.6c}$$

$$\psi_{dr} = X_{lr} i_{dr} + X_M(i_{ds} + i_{dr}) \tag{5.6d}$$

where v, i, r, X and Ψ correspond to the voltages, currents, resistances, reactances and flux linkages, respectively. Also, X_m is the mutual reactance between the stator and the rotor, $X_s = X_{ls} + X_m$ is the stator reactance and $X_r = X_{lr} + X_m$ is the rotor reactance. X_{ls} and X_{lr} are the stator and rotor leakage-reactance, respectively. All variables and parameters are in per unit (p.u.), except ω_r and ω_s [74, 76] .

The electrical torque can be expressed as

$$T_e = \frac{X_M}{D}\left(\psi_{qr}\psi_{dr} - \psi_{dr}\psi_{qr}\right) \tag{5.7}$$

where

$$D = X_s X_r - {X_m}^2 \tag{5.8}$$

$X_s = X_{ls} + X_m$ is the stator reactance and $X_r = X_{lr} + X_m$ is the rotor reactance [74,76]. Considering the drive-train model as a lumped model including the total inertia of the wind wheel, generator, gearbox and rotor shaft, the drive-train can be described

by:

$$2H\frac{1}{\omega_s}\frac{d\omega_r}{dt} = T_m - T_e \tag{5.9}$$

Dynamic equations (5.5) and (5.9) form the DFIG 5^{th} order model.

5.3 Control System

A wind plant is controlled at two levels of the wind farm (supervisory) control and wind turbine level. Wind farm control is a centralize control and determines the required generation of each wind turbine. Wind turbines are controlled locally to regulate their outputs through speed control and generator control at wind turbine control level. A WTG Type C is a fully controlled system utilizing the turbine and generator controllers. The turbine controller acts on the blade pitch angle to vary the power generated from wind. The generator controller, on the other hand, acts on the generator rotor voltage through the converters, located between the induction machine terminal and rotor, and generates the rotor voltages v_{qr}, v_{dr} in the dq-rotating frame [75]. These controls are investigated in the next sections.

5.3.1 Supervisory Control

The wind farm control level behaves as a single central unit. It controls the power production of the wind farm by sending out active and reactive power references to the wind turbines. These power references are prepared in the wind farm control level based on several measurements at the point of common coupling (PCC) and on the available power of each individual wind turbine [37]. Wind farms with variable speed DFIGs must be able to provide advanced grid support, such as, functions for both active power control and reactive power control. For wind power units to participate in frequency control, a balance margin on the momentary production is required. In the case of traditional energy optimizing wind turbine operation known as MPPT, it is only possible to reduce power output, as there is no additional available power to

extract from the wind to perform any momentary power output increase. Frequency control schemes of wind turbines therefore deploy some kind of reduced output control often referred to as either balance or delta control. The idea behind both types of control is to keep a certain power reserve to be able to respond and alter production quickly both with positive and negative power ramps [78].

The possible active power control functions required by the system operators are as follows:

- Balance control: the wind farm production can be adjusted downwards or upwards, in steps at constant levels.
- Delta control: the wind farm is ordered to operate with a certain constant reserve capacity in relation to its momentary possible power production capacity. The advantage of such control is that the reserve power is available and it can be used in a frequency control action.
- Power gradient limiter: sets how fast the wind farm power production, can be adjusted upwards and downwards. Such a limiter helps to keep the production balance between wind farms and the conventional power plants.
- Automatic frequency control: the frequency measured at the wind farm point of common coupling (PCC) is controlled. The wind farm must be able to produce more or less active power in order to compensate for frequency deviations.

The reactive power control functions required by the system operators are:

- Reactive power control: the wind farm is required to produce or absorb a constant specific amount of reactive power.
- Automatic voltage control: the voltage at the wind farm PCC is controlled.

This implies that the wind farm can be asked to produce or absorb an amount of reactive power to the grid in order to compensate for the voltage deviations on the grid [37].

5.3.2 Speed Control

The active power controller is designed to extract maximum power from the wind. When the pitch angle is constant, power extraction depends on both v_{wind} (uncontrollable) and λ (controllable) which is defined in terms of ω_r. By controlling ω_r, we can move along the so called power curve for a given wind speed to maximize the power. Tracing a curve through the maximum power points for every given wind speed, a one-to-one correspondence between optimal power and rotor speed is obtained. This correspondence and the minimum speed, typically 0.7 rated, and maximum speed, 1.2 rated, due to converter ratings, is used to define a power reference (tracking curve). If the wind speed exceeds its maximum, pitch-angle control must be performed [74].

In medium wind speeds, the generator and power converter control the wind turbine to capture maximum energy from the wind. In the high wind speed region, the wind turbine is controlled to limit the aerodynamic power produced by the wind turbine. Variable pitch control can be used to shed the aerodynamic power generated by the wind turbine. With pitch control, the power captured from the wind power P_{wind} can be controlled by a pitch actuator through changing the power coefficient as expressed in (5.2) [79]. The speed control is achieved by closing the loop through a PI controller.

5.3.3 Generator Control

The machine converter control system consists of a set of controllers that allow control of real power/speed and the reactive power. The doubly-fed asynchronous machine controllers usually use the concept of separation of the real and reactive power controls by transformation of the machine parameters into dq-reference frame and by separation of the voltages v_{dr}, v_{qr} using field oriented control. Then, the real power (and speed) can be controlled by influencing the d-axis component of the rotor current i_{dr} while the reactive power can be controlled by influencing the q-axis

component of the rotor current i_{qr} [75]. Assuming that the d-axis is oriented along the stator flux axis, i.e., $v_s = v_{ds}$ with $v_{qs} = 0$, and neglecting R_s and using (5.5) in steady state to get $v_{ds} = \Psi_{qs} = 0$ and $v_{qs} = \Psi_{ds} = v_D$ with (5.6) yields

$$i_{qs} = \frac{X_m}{X_s} i_{qr} \qquad i_{ds} = \frac{X_m}{X_s} i_{dr} - \frac{v_D}{X_s} \tag{5.10}$$

Then, the complex power leaving the generator's stator is

$$\begin{aligned} P_s + jQ_s &= (v_{ds} i_{ds} + v_{qs} i_{qs}) + j(v_{qs} i_{ds} - v_{ds} i_{qs}) \\ &= \left(\frac{X_m}{X_s} v_D i_{qr} \right) + j \left(v_D \frac{X_m i_{dr} - v_D}{X_s} \right) \end{aligned} \tag{5.11}$$

It turns out that the control of active and reactive power can be performed independently by varying i_{qr} and i_{dr}, respectively. As a result, the reference values for i_{qr} and i_{dr} are obtained through a PI controller from active and reactive power errors. Then i_{qr} and i_{dr} are processed by another PI controller to give v_{qr} and v_{dr}. The alignment of the d- axis and stator flux axis is obtained by using the field-oriented control. The wind turbine control structure at different levels is shown in Figure 5.2.

5.4 Flatness-Based DFIG Control

5.4.1 Derivation of Flat Outputs

The first step in designing the control based on the flatness-based concept is to find the appropriate set of outputs. Unfortunately, there is no straightforward method to check for flatness. In addition, there is no implicit mathematical tools to find the map, f, and set of flat outputs. Physical intuition, careful inspection, and educated guesses are more typically the approaches that can be used to determine the appropriate outputs for a given nonlinear multi-variable system [53].

In [80], it is shown that for an induction motor system, where the stator voltages are the control inputs, the angle of rotor position and the rotor flux argument form

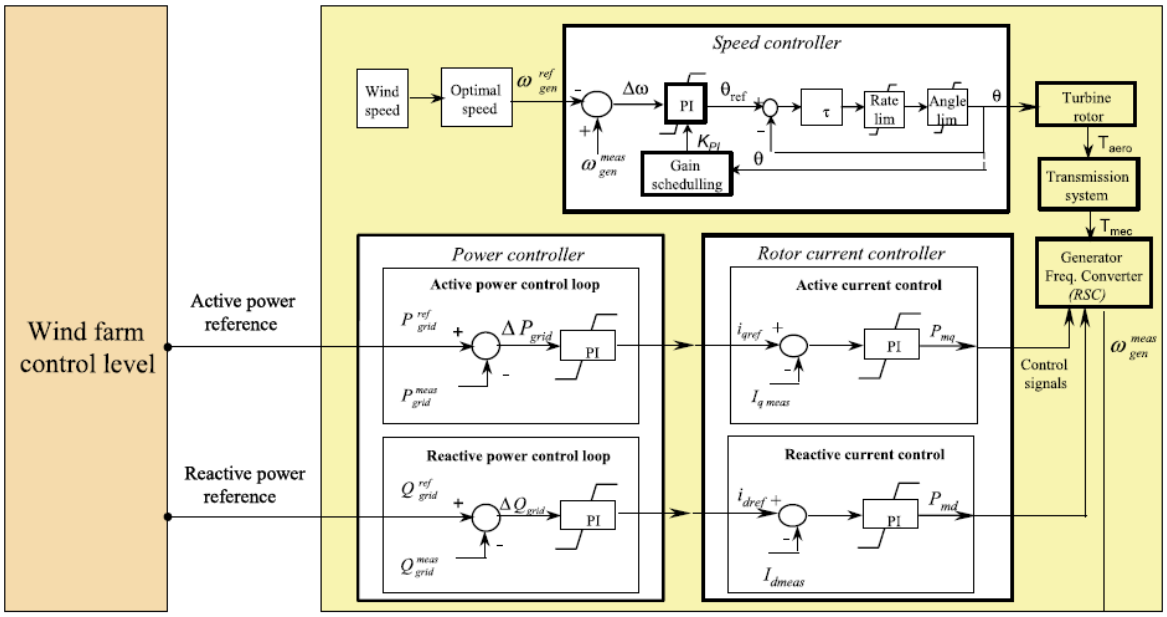

Figure 5.2: Wind Turbine Control Level

flat outputs. The authors in [81] followed the same approach for loss minimization objective and considered the argument of stator flux and rotor speed as flat outputs for the rotor converter side in DFIG, where the rotor voltages are the control inputs. The losses are expressed in terms of the flat outputs and their derivatives in order to determine the trajectories. Then, the integrating backstepping approach is used to perform trajectory tracking.

The main objective in the present study is to track the active and reactive power delivered to the grid. In a DFIG, the stator dynamics are very slow and stator fluxes are usually considered constant in modeling. In fact, $\dot{\Psi}_{ds}$ and $\dot{\Psi}_{qs}$ are usually neglected in power system stability studies. These terms represent stator transients and their neglect corresponds to ignoring the dc component in the stator transient currents permitting representation of only fundamental frequency components [59]. Therefore, considering the stator flux as one of the flat outputs is unlikely to lead to desired trajectory tracking for active and reactive power as is desired in this wrok. Thus, the stator dynamics in (5.5) are neglected which results in a 3^{rd} order DFIG

model. In addition, since rotor speed is not controlled directly in the generator control, equation (5.9) is also neglected. We select the rotor flux argument and electrical torque and show these are flat outputs of the reduced system. To prove this, stator and rotor fluxes and voltages are written in exponential forms as

$$\overline{\Psi}_s = \psi_s e^{j\beta} \tag{5.12a}$$

$$\overline{\Psi}_r = \psi_r e^{j\theta} \tag{5.12b}$$

$$\overline{V}_s = v_s e^{j\gamma} \tag{5.12c}$$

$$\overline{V}_r = v_r e^{j\alpha} \tag{5.12d}$$

and denote that $y := (\theta, Te)$ is the flat output. The first derivatives of θ and Te can be expressed as

$$\frac{1}{w_s}\dot{\theta} = (\frac{w_r - w_s}{w_s}) + \frac{v_r sin(\alpha - \theta)}{\psi_r} - \frac{R_r T_e}{\psi_r^2} \tag{5.13}$$

$$\begin{aligned}\frac{1}{w_s}\frac{D}{X_m}\dot{Te} =& \psi_s \psi_r cos(\beta - \theta)(\frac{w_r - w_s}{w_s}) + \psi_s v_r sin(\alpha - \beta) \\ & - \frac{R_r X_s}{X_m} T_e\end{aligned} \tag{5.14}$$

and

$$T_e = \frac{X_m}{D}\psi_s \psi_r sin(\theta - \beta) \tag{5.15}$$

Equation (5.15) indicates that ψ_r can be interpreted in terms of flat outputs and stator states, which are assumed to be constant. On the other hand, v_r and α can be derived from (5.13) and (5.14). Let

$$\begin{aligned}M =& (D^2(\dot{T}_e \sin(\beta - \theta) - T_e \omega_r \cos(\beta - \theta) \\ & + T_e \omega_s \cos(\beta - \theta)) + D R_r T_e X_s \omega_s \sin(\beta - \theta))) \\ & /(D^2(T_e \dot{\theta} + T_e \omega_r - T_e(\omega_r - \omega_s)) \\ & - {Q_s}^2 R_r {X_m}^2 \omega_s \sin(\beta - \theta))\end{aligned} \tag{5.16}$$

Then

$$\alpha = \tan^{-1}\left(\frac{\sin(\beta) + M\sin(\theta)}{\cos(\theta + M\cos(\theta))}\right) \tag{5.17}$$

$$\begin{aligned} v_r = &- (Q_s X_m \sin(\beta - \theta) \\ &(R_r T_e - (D^2 T_e^2 (\dot{\theta}/\omega_s + \frac{(\omega_r - \omega_s)/\omega_s)}{{Q_s}^2 {X_m}^2 \sin(\beta - \theta)^2})) \\ &/ D T_e \sin(\alpha - \theta) \end{aligned} \tag{5.18}$$

Finally $\overline{V}_r$ is transformed to voltage values in q-axis and d-axis using

$$\overline{V}_r = v_{qr} - j v_{dr} \tag{5.19}$$

5.4.2 Trajectory Generation

Supervisory control at the wind farm level sends the reference values for active and reactive power to individual turbines in a wind farm. The overall response of turbines provide the possibility for wind plants to actively participate in grid control tasks in the same way that conventional power plants do. The generated active and reactive power of DFIG are expressed in (5.1), where

$$P_s = v_{ds} i_{ds} + v_{qs} i_{qs} \tag{5.20a}$$

$$P_r = v_{dr} i_{dr} + v_{qr} i_{qr} \tag{5.20b}$$

$$Q_s = v_{qs} i_{ds} - v_{ds} i_{qs} \tag{5.21}$$

Due to the flat systems properties, all system variables can be interpreted as algebraic functions of flat outputs and derivatives up to appropriate order. Therefore, using (5.6) and (5.15), the expressions for P_s and Q_s are found directly in terms of flat outputs, θ and T_e, and no derivative terms appear in this model.

$$P_s = \frac{X_m}{D}\psi_r v_s \cos(\theta - \gamma) - \frac{X_r}{D}\psi_s v_s \cos(\beta - \gamma) \tag{5.22}$$

$$Q_s = \frac{X_m}{D}\psi_r v_s \sin(\theta - \gamma) - \frac{X_r}{D}\psi_s v_s \sin(\beta - \gamma) \tag{5.23}$$

Moreover, assuming rest to rest trajectories, i.e. the reference values for derivative of flat outputs are set to zero, the system input can also be written as an algebraic function of the flat output state variables. These terms are derived by setting $\dot{\theta}$ and $\dot{T}e$ to zero in (5.17) and (5.18). This results in writing P_r and eventually the reference values for P_g and Q_g in terms of θ and T_e and other states that are assumed to be constant.

$$P_{gen}^{ref} = f_{P_g}(\theta^{ref}, {T_e}^{ref}, Q_s, \beta, v_s, \gamma, \omega_r) \tag{5.24}$$

$$Q_{gen}^{ref} = f_{Q_g}(\theta^{ref}, {T_e}^{ref}, Q_s, \beta, v_s, \gamma) \tag{5.25}$$

Given P_{gen}^{ref} and Q_{gen}^{ref} and solving (5.24) and (5.25) for θ^{ref} and T_e^{ref} the desired output references are found. The PI controllers in the traditional DFIG vector control are replaced here with the solution of the above algebraic equations.

5.4.3 Trajectory Tracking

Tracking the desired active and reactive power is guaranteed through tracking the trajectories θ^{ref} and ${T_e}^{ref}$. This can be realized by finding $\dot{\theta}$ and $\dot{T}_e$ through two proportional controls as stated in

$$\dot{\theta} = K_\theta(\theta^{ref} - \theta) \tag{5.26a}$$

$$\dot{T}_e = K_{T_e}({T_e}^{ref} - T_e) \tag{5.26b}$$

Then, the control input is calculated from (5.17) and (5.18). Control block diagram for trajectory tracking is shown in Fig. 5.3. The reference values for flat outputs, θ^{ref}, ${T_e}^{ref}$ are received from trajectory generation. The stator and rotor

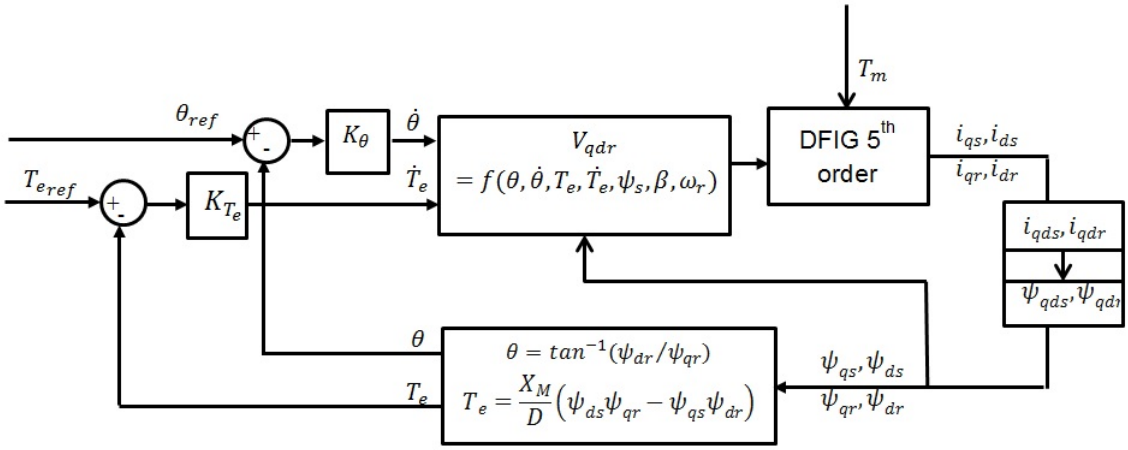

Figure 5.3: Trajectory Tracking Control

output currents of the machine are measured and converted to flux values and then transformed to flat outputs using (5.7) and (5.12). The flat outputs are compared with their reference values and the first derivative of these outputs is obtained by proportional gains.The control inputs v_{qr} and v_{dr}, found using (5.17), (5.18) and (5.19), are applied to DFIG as inputs. It can be observed that the PI controllers used in vector control to follow the current references are also replaced with proportional gains. Additionally, no field orientation and shift-angle transformer is needed. It is worth noting that, since only first derivatives of flat outputs appear in expressing DFIG input in terms of flat outputs, there is no need to measure or estimate the derivation of flat outputs. The overall control block diagram including trajectory generation, pitch control and wind farm supervisory control is shown in Fig. 5.4.

5.5 Simulation Results

The proposed approach is implemented on a wind farm in a 4-bus system as shown in Fig. 5.5. The system data is provided in Appendix for simplicity. It is assumed that the wind farm consists of one wind turbine. Since the supervisory wind farm control sends the reference active and reactive power to each WTG independently, the

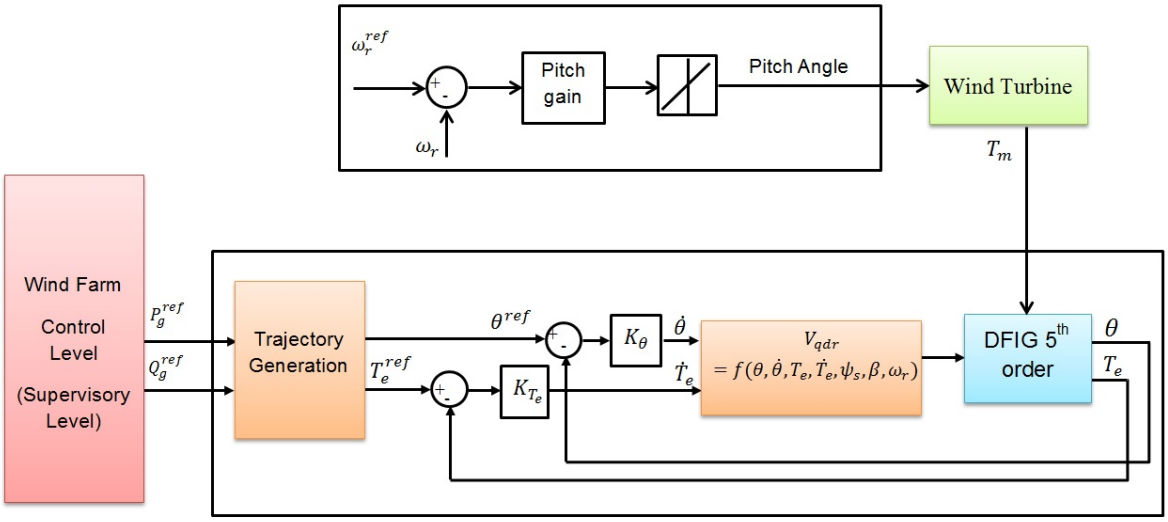

Figure 5.4: Flatness-based DFIG Control Block Diagram

assumption does not effect the performance of the control approach. The aggregated power output of the wind farm is the sum of power output of individual WTGs minus the losses in the farm. A wind speed time series, shown in Fig. 4.19, is randomly generated from a Weibull distribution for the period of $0 - 300\ s$. The approximate mean value of wind speed is $12m/s$ in the first and last 100 seconds and $10m/s$ from $100 - 200s$. The wind turbine is equipped with pitch control and the $C_p - \lambda$ characteristic of the turbine as described in section 5.2.1.

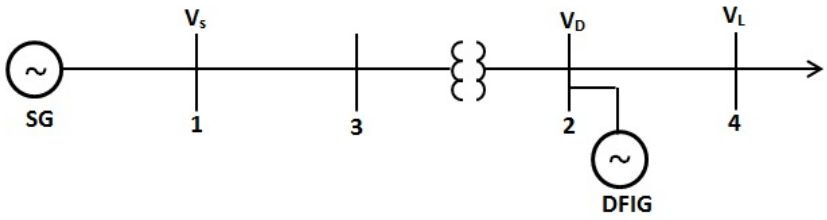

Figure 5.5: 4-bus Test System

As mentioned before, the control objectives are tracking the active and reactive power references. Tracking is achieved through a combination of generation and pitch control. The pitch angle is generally held at zero to achieve maximum C_p at lower to medium wind speed. The electrical power is controlled by adjusting the power

converters. Once the wind speed increases and wind power generation is above the desired reference value or the rotor speed goes beyond a controllable limit, the pitch control increases the pitch angle to shed aerodynamic power.

The simulations are performed in Matlab Simulink and in order to demonstrate the performance of flatness-based DFIG, three scenarios are studied:

1. Maximum Power Point Tracking (MPPT): In this control C_p is kept at maximum to extract the maximum power from wind, considering the converter and rpm limits. The maximum power value, obtained from the one-to-one correspondence between optimal power and rotor speed at a given wind speed using $C_p - \lambda$, is used as the active power reference. The reactive power reference is assumed to be $0\,pu$ in $0 - 140\,s$ and $0.2\,pu$ in $140 - 300\,s$. The approach is compared with the traditional vector control. The results are shown in Figures 5.6 - 5.17. The active power generation consists of components of stator and rotor active powers as mentioned in (5.1) and shown in Figures 5.6-5.8. On the other hand, the synchronous generator connected to bus 1 varies its generation as the slack bus to maintain the generation-load balance as demonstrated in Figure 5.9. The reactive power follows the step change in reference as shown in 5.10. The rotor speed changes in the same direction and the same rate as the wind speed variations to keep the C_p at the maximum value, Figures 5.11 and 5.12. The pitch control increases the pitch angle, shown in Figure 5.13, when wind speed has a high value, around 14 m/sec, which results in reducing the mechanical power and ensuring the rotor speed remains within a controllable limit. Analyzing the stator and rotor fluxes, Figures 5.14 and 5.15, verifies that the active power changes only depend on flux changes in q axis, which is the fact used in vector control. Moreover, variations are mostly observed in ϕ_{qr} due to controlling rotor voltages. Also, variation of ϕ_{dr} results in reactive power changes. Finally, the flat outputs, the rotor flux argument and electrical torque, are shown in Figures 5.16 and 5.17. It is observed that

as the wind speed varies, the electrical torque and rotor flux argument are controlled to provide the desired active and reactive power. Comparing the results shows that the proposed approach leads to nearly identical results as the vector control. However, the proposed control has a far simpler structure, which can be considered an important advantage.

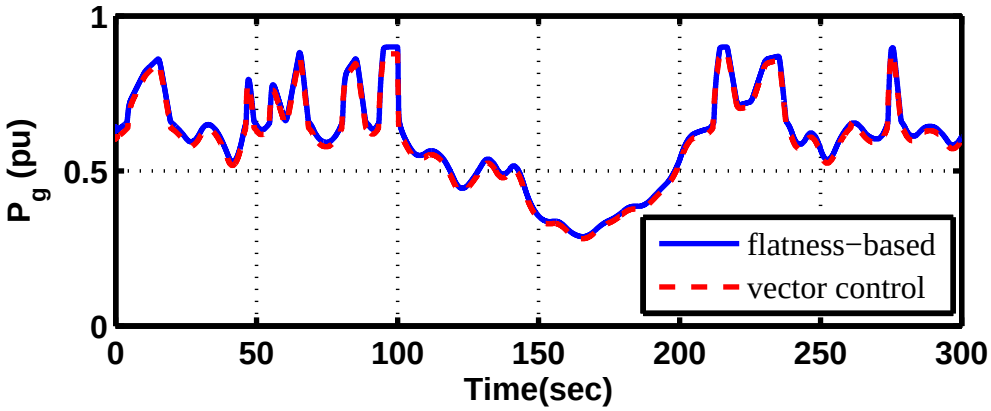

Figure 5.6: Active power for MPPT control

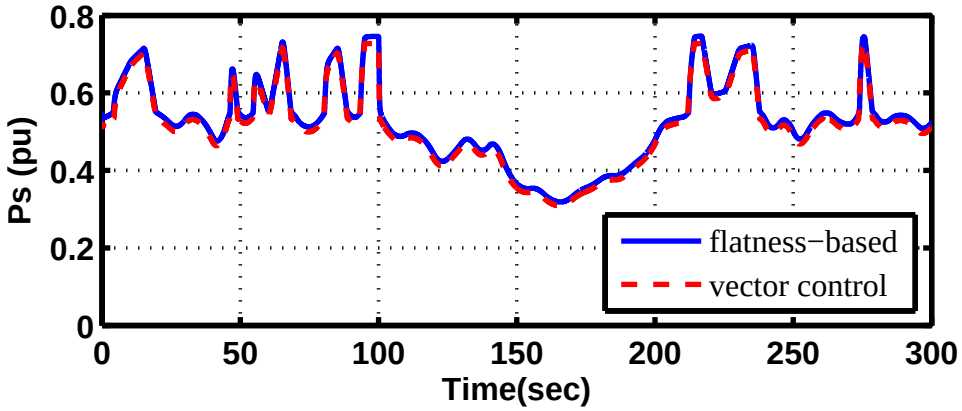

Figure 5.7: Stator active power for MPPT control

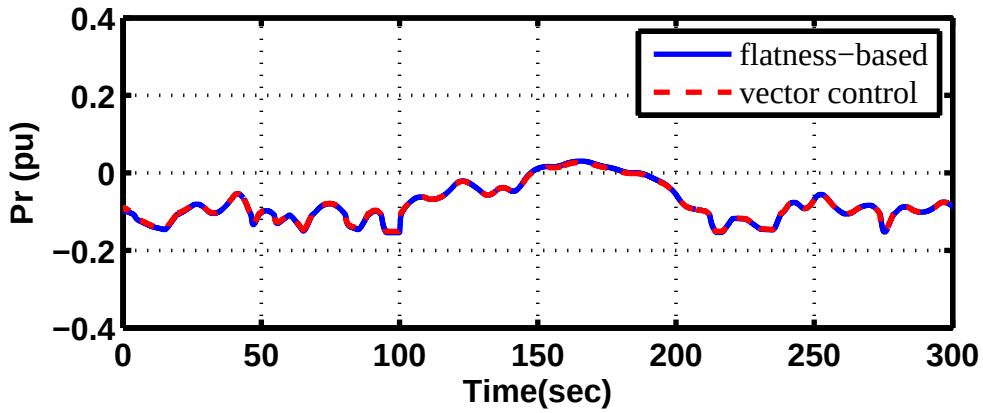

Figure 5.8: Rotor active power for MPPT control

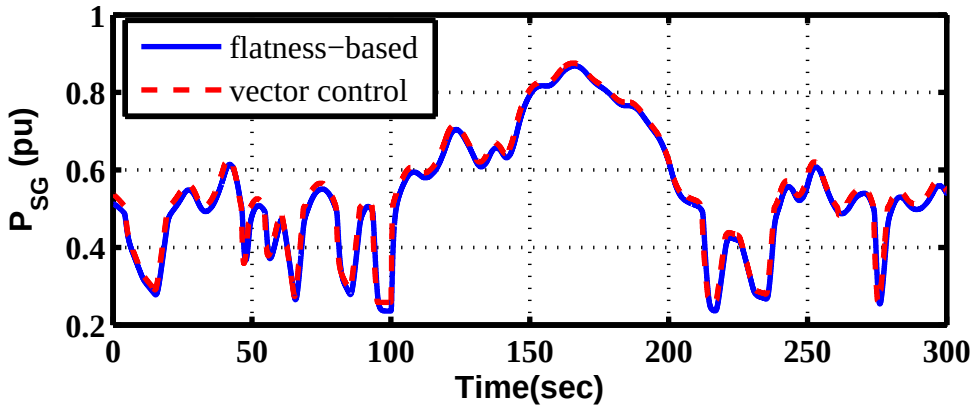

Figure 5.9: Synchronous generator active power for MPPT control

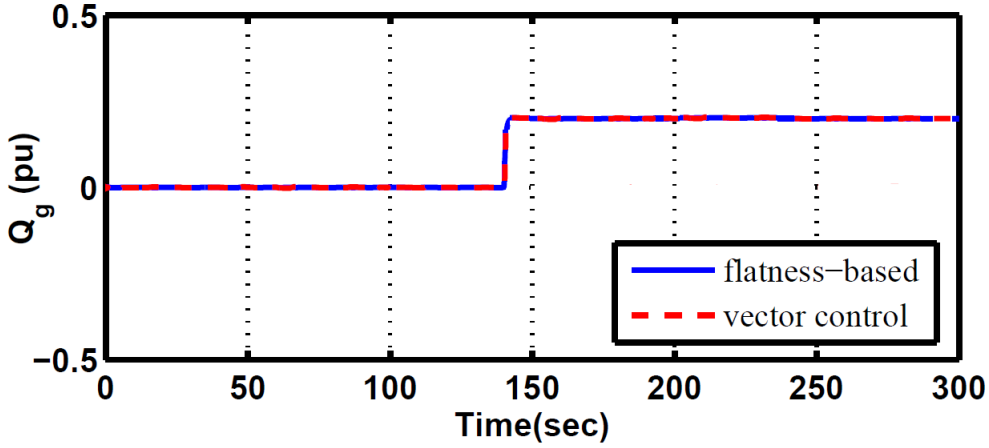

Figure 5.10: Reactive power for MPPT control

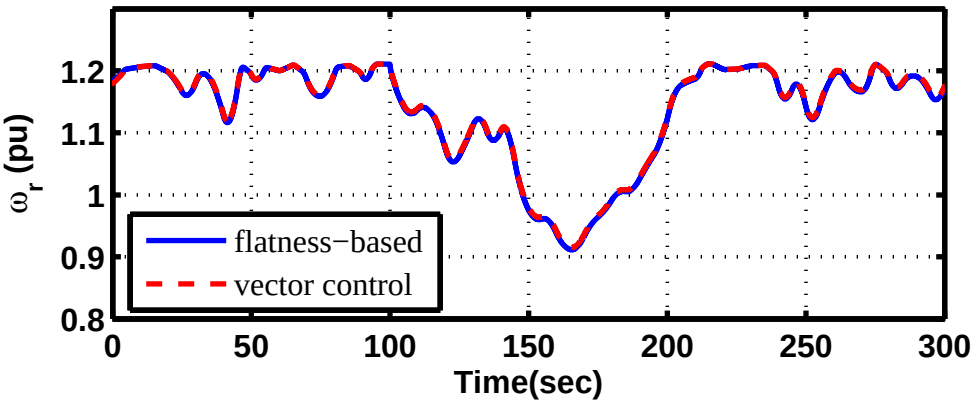

Figure 5.11: Rotor speed for MPPT control

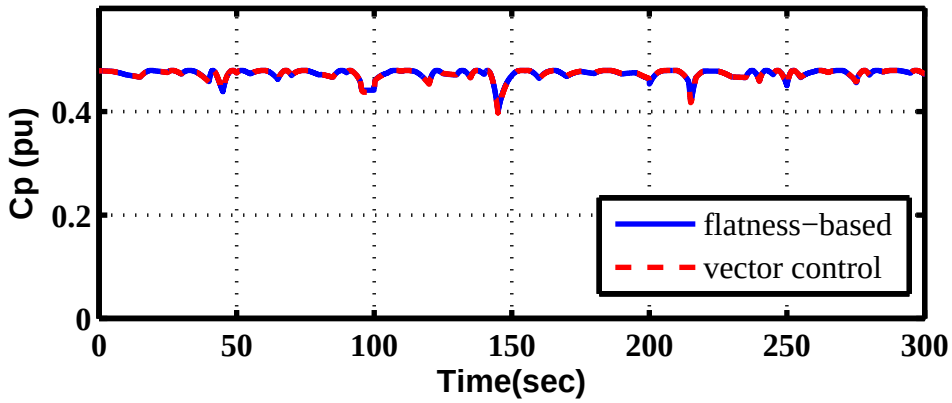

Figure 5.12: Cp for MPPT control

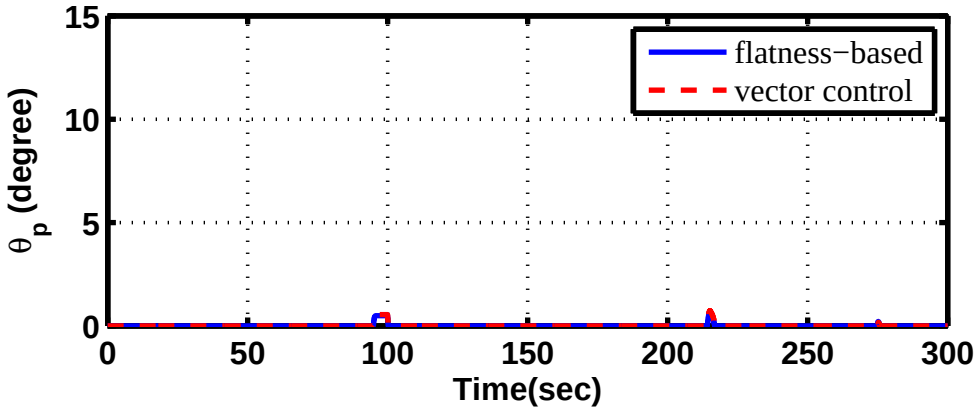

Figure 5.13: Pitch angle for MPPT control

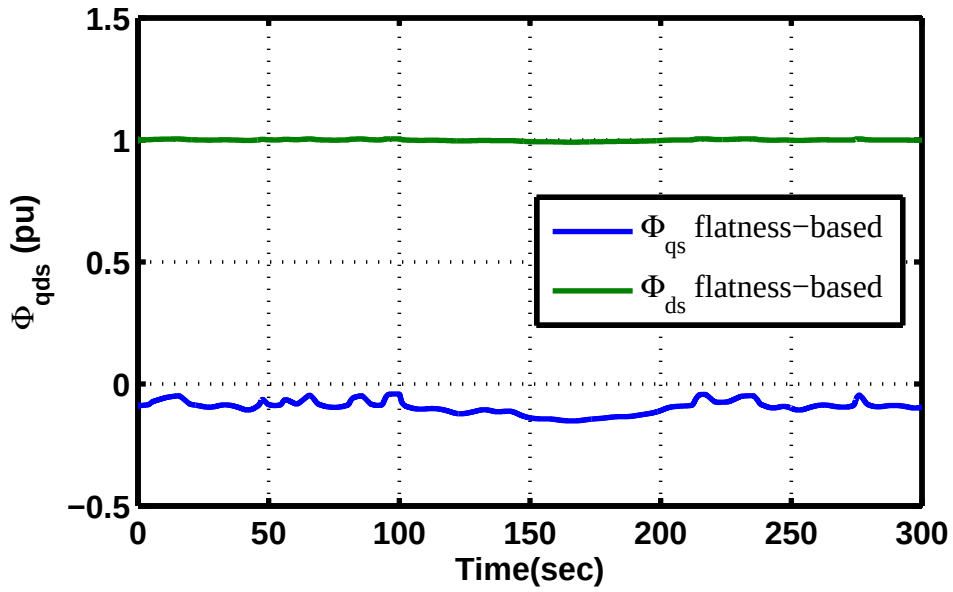

Figure 5.14: Stator fluxes in d and q axises for MPPT

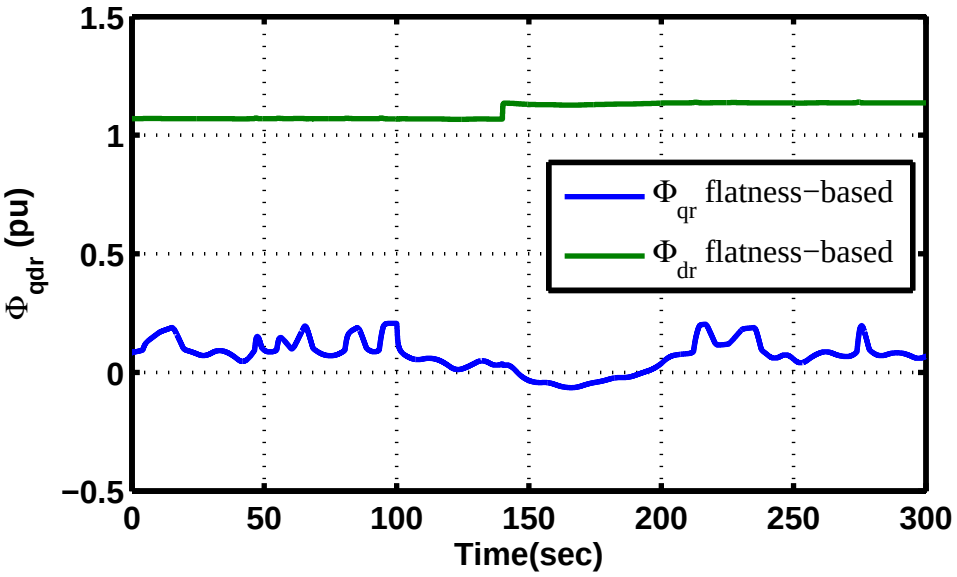

Figure 5.15: Rotor fluxes in d and q axises for MPPT

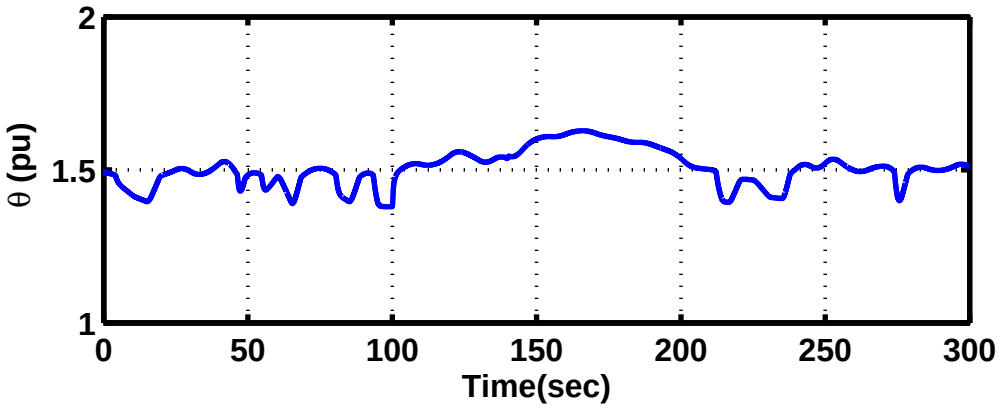

Figure 5.16: Rotor flux argument for MPPT control

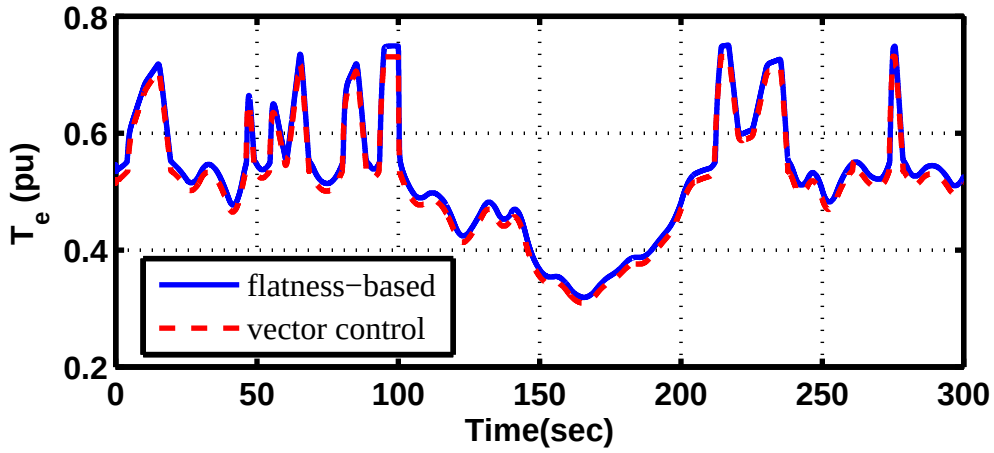

Figure 5.17: Electrical torque for MPPT control

2. Delta Control: In this scenario, the active power is dropped by $0.2pu$ to provide reserve so as to contribute in frequency regulation. The maximum power is calculated using rotor speed, as described in the MPPT scenario. The maximum power minus 0.2 is applied as the reference for active power and two methods are used for pitch control. The first method is similar to MPPT, where pitch is only controlled at high wind speed and when rotor speed exceeds the limit, which is 1.21 pu. In the second method, the WTG is maintained at an optimal λ as suggested in [38]. The reason to keep λ constant is to ensure that the WTG will return to the MPPT operating point instantaneously when the pitch angle is

returned to normal. For this purpose, a control block is added to pitch control to act when rotor speed is not at the optimal value. The generator control adjusts the electrical torque and the rotor flux to follow the new mechanical torque and provide the desired power. The results for this scenario are shown in Fig. 5.18- Fig. 5.26. It is observed that the rotor speed in Fig. 5.23 for the second method is very close to the speed for MPPT control in Fig. 5.11, which makes it possible to return to MPPT when required. The pitch angle variations in Fig. 5.24 shows that more control action is required to maintain λ at optimum value and decrease the C_p to reduce the active power generation. The reactive power, on the other hand, has not changed for the two control methods.

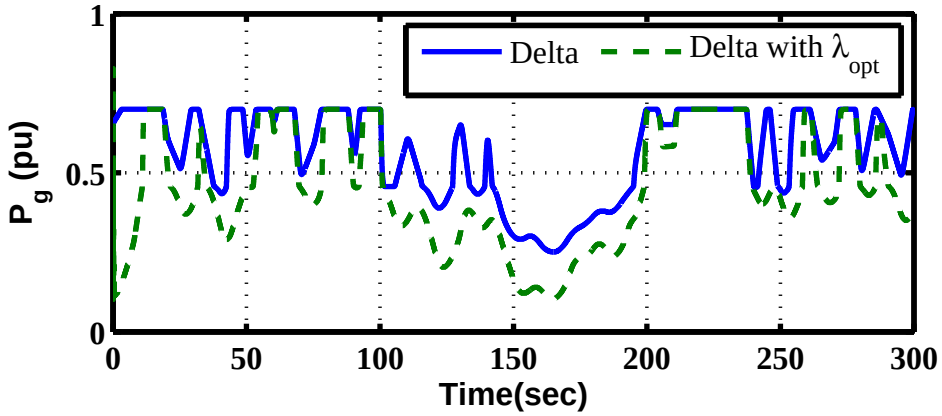

Figure 5.18: Active power for delta control

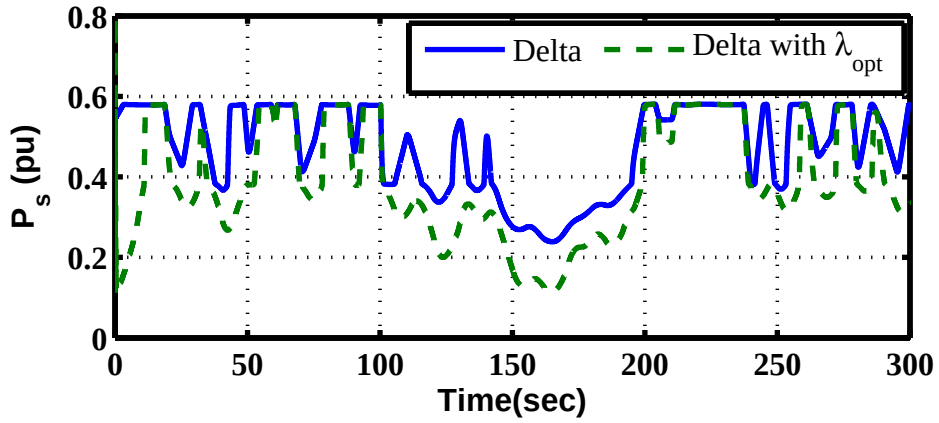

Figure 5.19: Stator active power for delta control

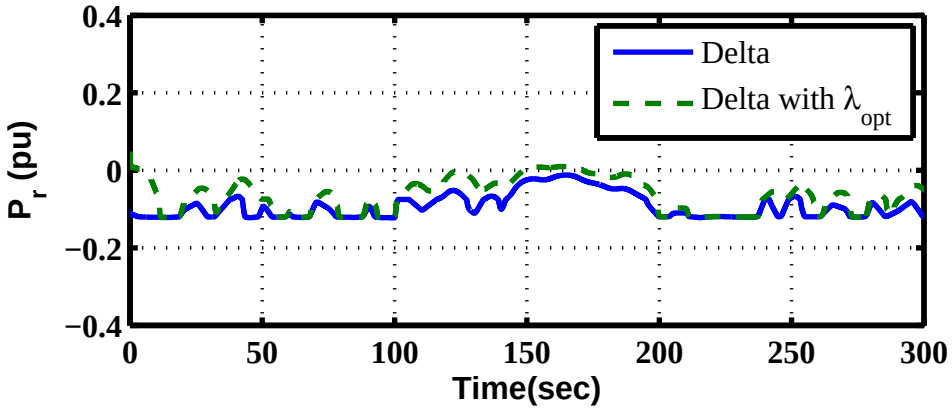

Figure 5.20: Rotor active power for delta control

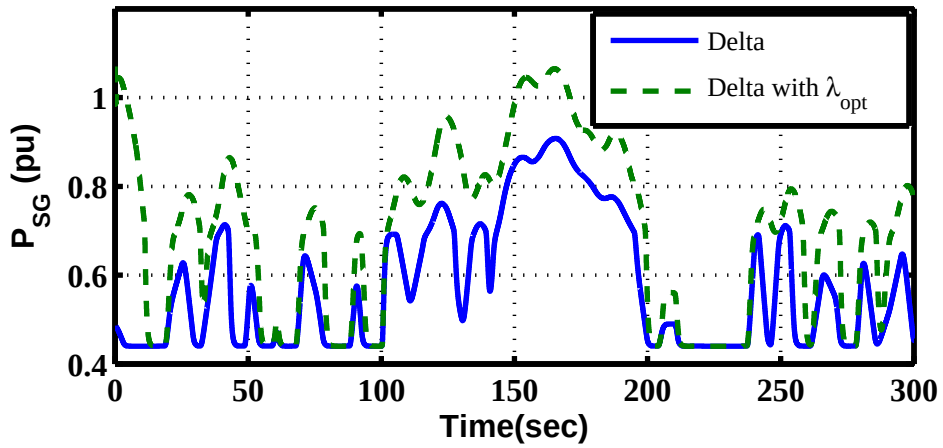

Figure 5.21: Synchronous generator active power for delta control

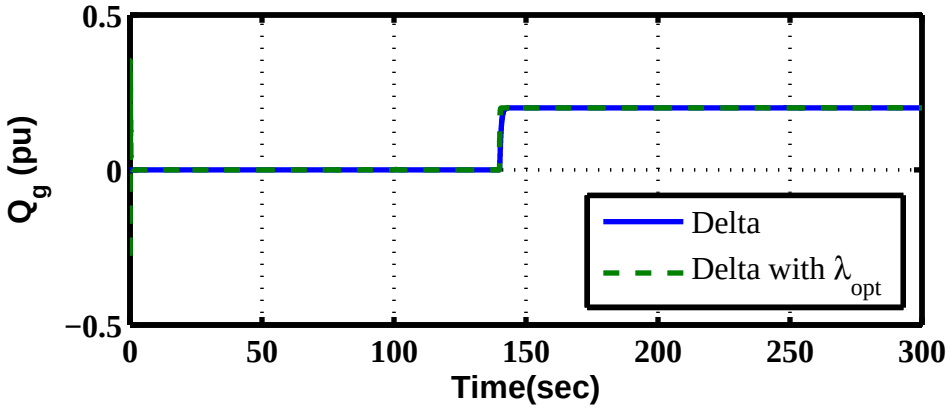

Figure 5.22: Reactive power for delta control

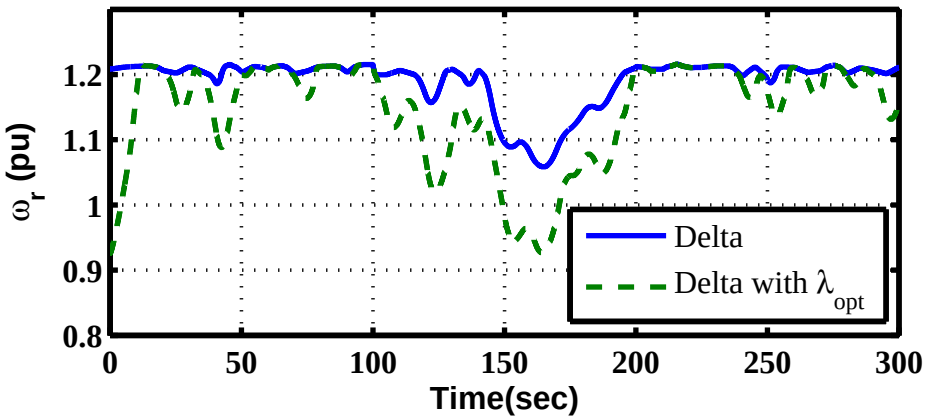

Figure 5.23: Rotor speed for delta control

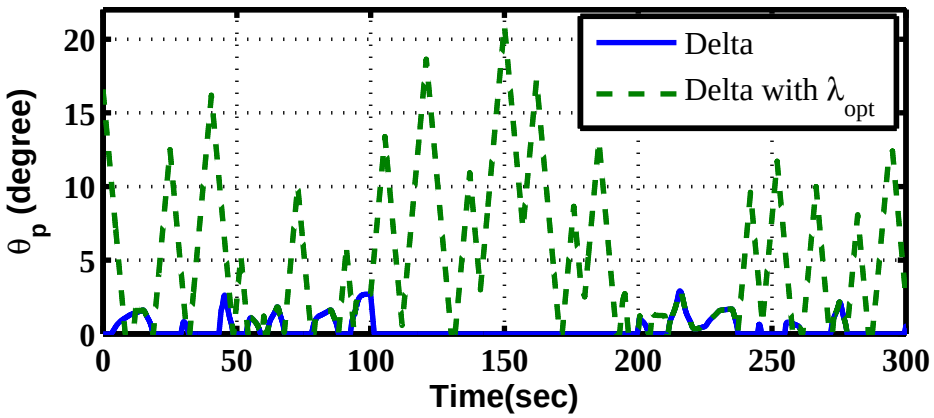

Figure 5.24: Pitch angle for delta control

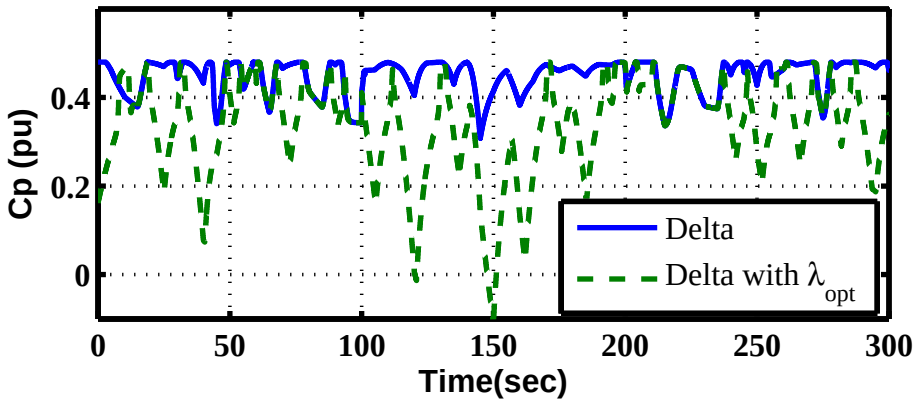

Figure 5.25: Active power for delta control

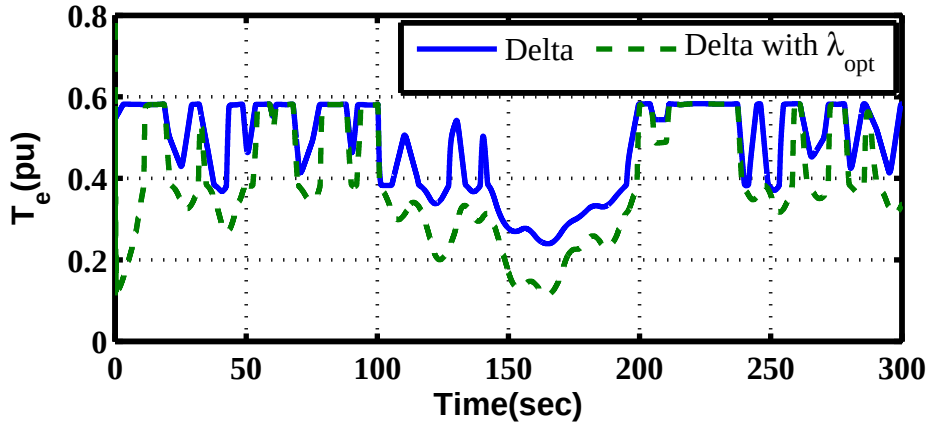

Figure 5.26: Electrical torque for delta control

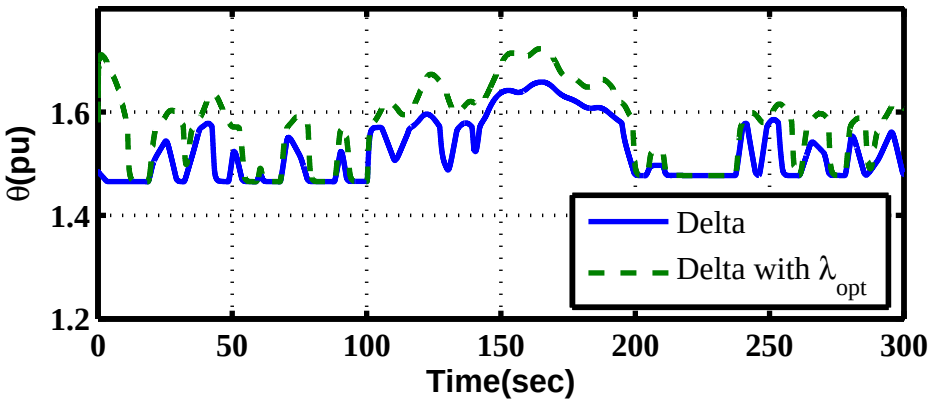

Figure 5.27: Rotor flux argument for delta control

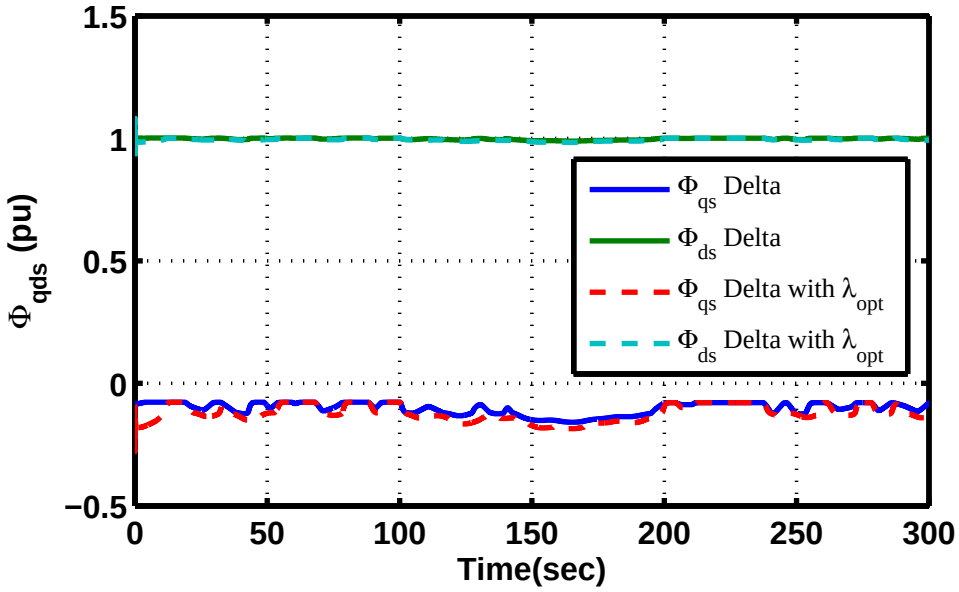

Figure 5.28: Stator fluxes in d and q axises for delta control

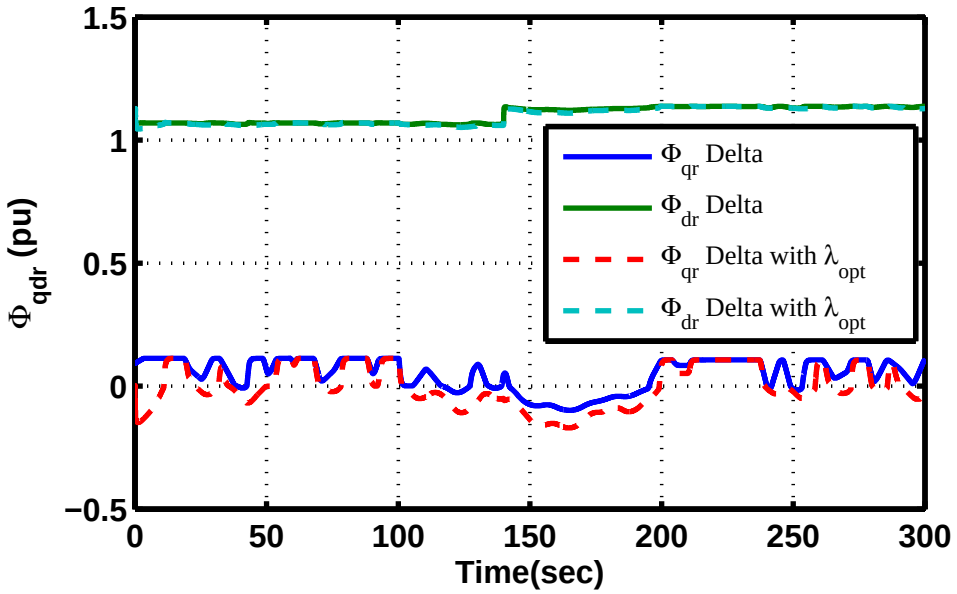

Figure 5.29: Rotor fluxes in d and q axises for delta control

3. Constant Power: In this scenario, the power output is kept at a constant value based on the available wind power. If the desired active power is more than the maximum power available, the maximum power is considered as the reference.

The extra power, which varies as the wind changes, can be considered as a reserve. The reference power is assumed to be $0.6\,pu$ in $0-100\,s$, $0.3\,pu$ in $100-200\,s$ and $0.5\,pu$ in $200-300\,s$. Results are shown in Fig. 5.30- Fig. 5.36. The active power is shown in Fig. 5.30, where the set point is not reached when the maximum available power is less than the reference. This scenario results in less variation in the generated active power of the wind plant and therefore less changes in the synchronous generators to balance the generation and load. Still, economic considerations are necessary to choose which scenario best reflects the system needs at a given moment.

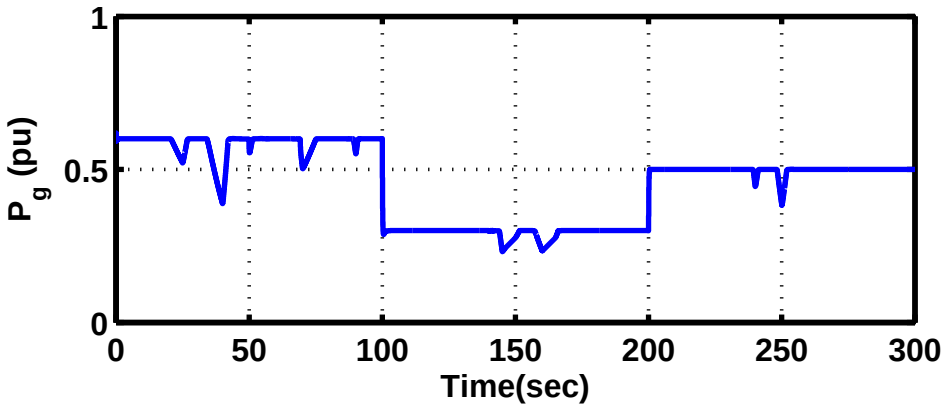

Figure 5.30: Active power for constant power control

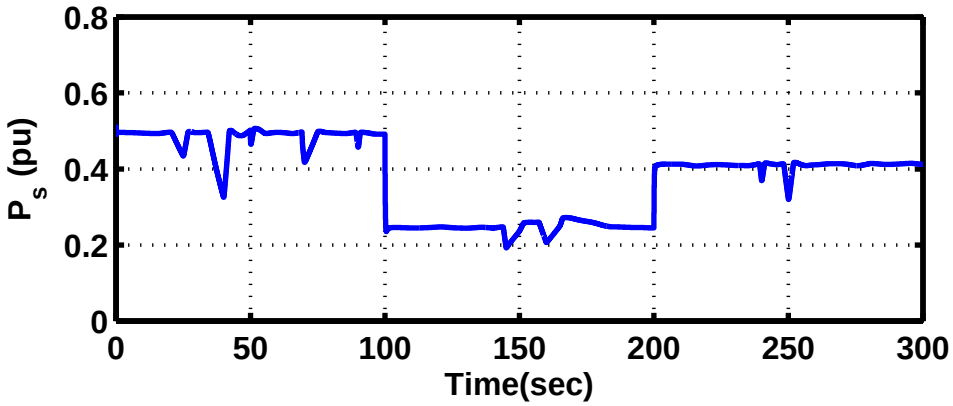

Figure 5.31: Stator active power for constant power control

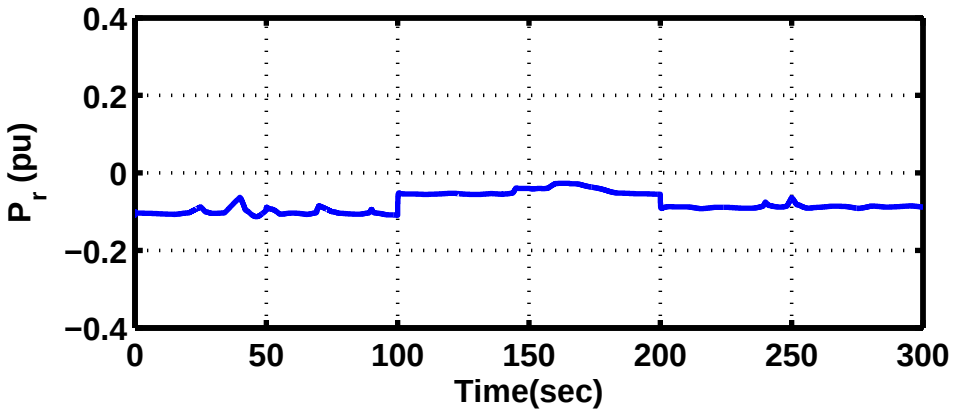

Figure 5.32: Rotor active power for constant power control

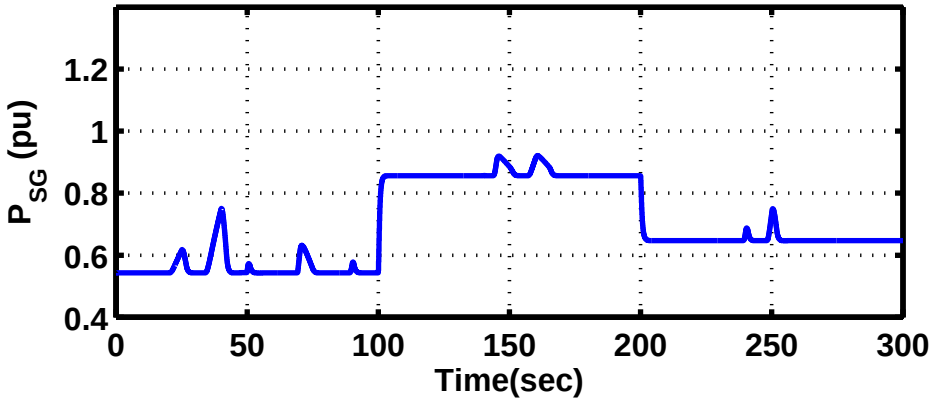

Figure 5.33: Synchronous generator active power for constant power control

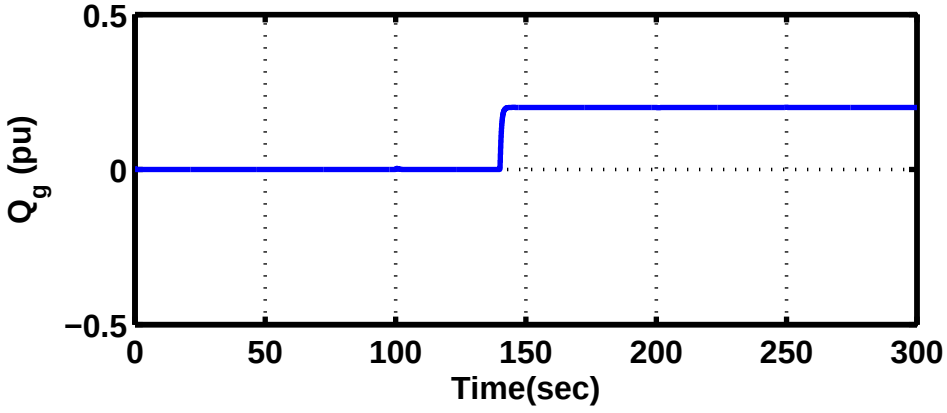

Figure 5.34: Reactive power for constant power control

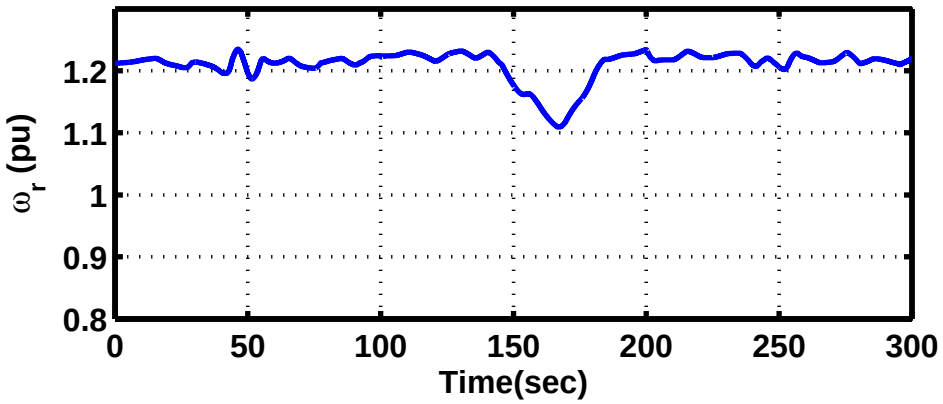

Figure 5.35: Rotor speed for constant power control

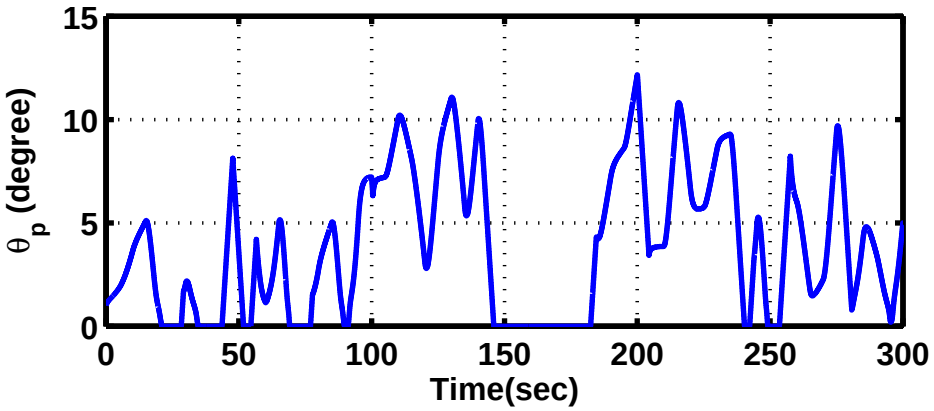

Figure 5.36: Pitch angle for constant power control

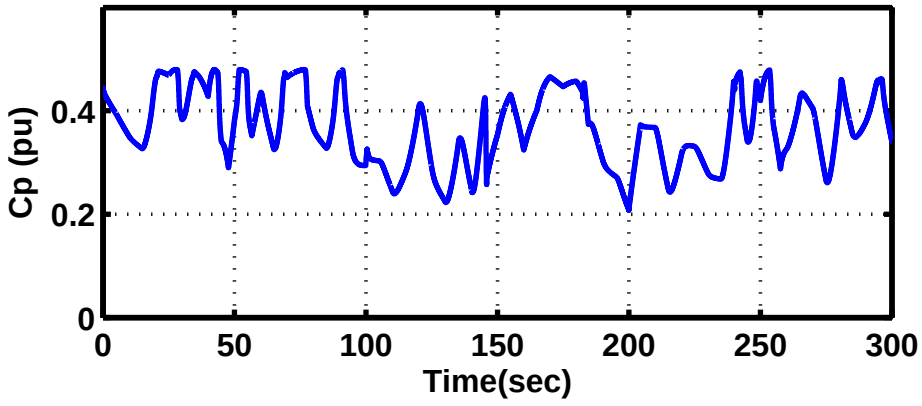

Figure 5.37: Active power for constant power control

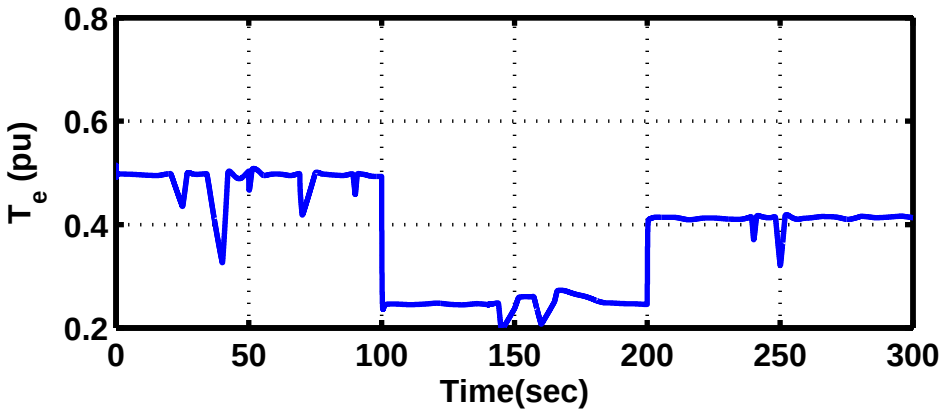

Figure 5.38: Electrical torque for constant power control

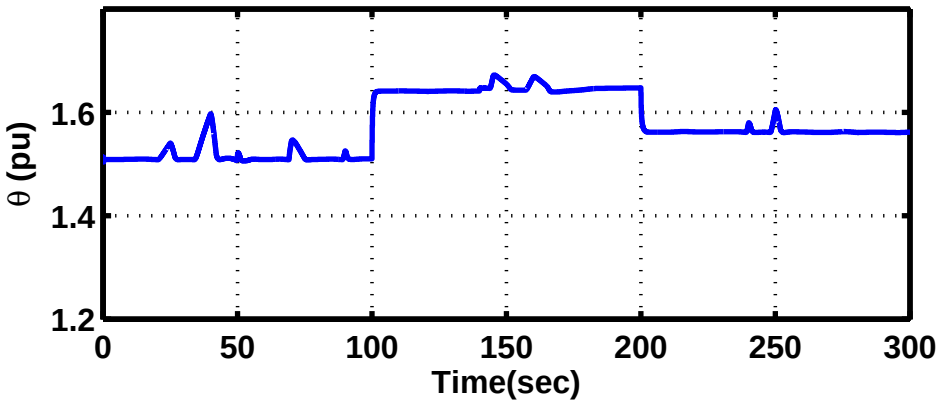

Figure 5.39: Rotor flux argument for constant power control

5.6 Conclusions

This chapter presented a flatness-based method to control systems of DFIG. The two level control consists of trajectory generation and trajectory tracking as a replacement for vector control. An important feature of the proposed approach is that the set of PI controllers to generated the rotor current reference values are replaced with simple algebraic equations to find the rotor flux and electrical torque. Moreover, the set of PI controllers to follow the reference currents are replaced with two simple proportional controllers. The main required measurement is for stator and rotor currents, which

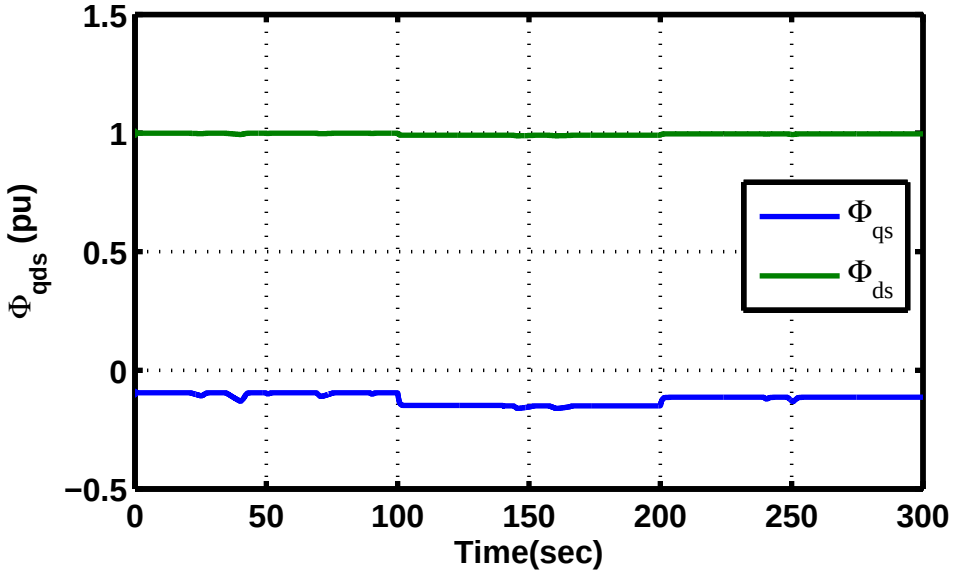

Figure 5.40: Stator fluxes in d and q axises for constant power control

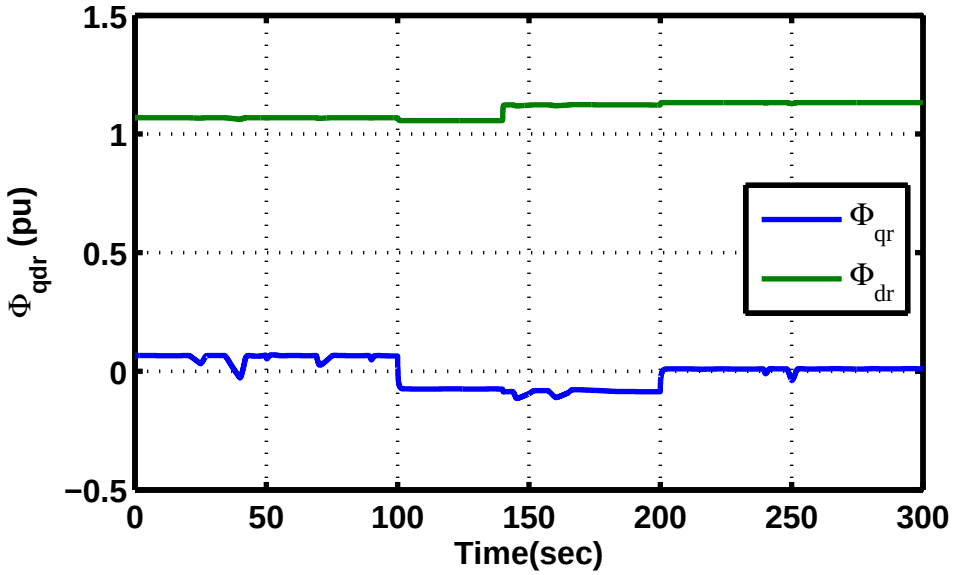

Figure 5.41: Rotor fluxes in d and q axises for constant power control

are available in the DFIG. The proposed control method demonstrates promising performance in a variety of scenarios for active and reactive power control.

Chapter 6

Conclusion

In this dissertation, a two level control structure is proposed to improve performance of a power system with high penetration of wind energy or other variable sources. The main objectives of this work are improving the frequency regulation in such system and following the desired generation of the plants determined by the transmission system operator. For this purpose, a flatness-based control, which is well suited for designing controls in two levels of planning and tracking, is deployed. The control is applied to both conventional generators, synchronous machines, and WTG with DFIG. These generators are controlled to: one, maintain the balance between load and generation in presence of variations in loads, wind generation and sudden outages of generators and as a result keep the system frequency at a constant value; and two, regulate their outputs to the most economic value that is determined by an upper level control.

6.1 Flatness-Based AGC

For conventional generators, this control is known as AGC. In this work, The two level control consisting of trajectory generation and trajectory tracking replaces conventional AGC. As an important feature of the proposed approach, the set of nonlinear equations corresponding to an n-machine system is decoupled into n linear

controllable sub-systems. Therefore, the proposed AGC is easier to design and implement. Local linear controllers are designed for each sub-system to maintain the frequency at nominal value and to keep power flows near scheduled values. The main requirement is the availability of PMU measurements. The flatness-based control method demonstrates promising performance in mitigating frequency and tie-line flow deviations.

The desired set points for generators are determined every 5 minutes through economic dispatch, while these set points need to be updated more frequently due to unpredicted changes in wind speed, load or generation. For this purpose, a method based on PMU measurements is proposed to update the set points by solving a quadratic optimization problem. First the changes in power injection are found through PMU measurements and state estimation. Then using shift factor matrix, the set points for generators contributing in AGC are found to minimize the changes in tie line flows. System constraints including line flow limits and the generation limits of generators on AGC are considered in problem formulation.

To asses the performance of the method on large scale power systems, the approach is implemented on NPCC system with 140 buses and 48 generators. The system model in DSA Tools is used for simulation and a UDM for flatness-based AGC is developed. The UDM uses the local angle and frequency measurements. The approach is also implemented on HTB built in CURENT.

6.2 Flatness-Based DFIG

Next, flatness-based control approch used to control the active and reactive powers in WTGs with DFIG machines. The reference values may be planned such that the machine can contribute to frequency regulation. In this case, the wind plant generation must be curtailed to provide room for an increase in generation. Also, the operator may decide to curtail wind generation to reduce the fluctuations in wind power generation. As a result of applying flatness-based approach, the set of PI

controllers to generate the rotor current reference values are replace with algebraic equations. Moreover, the set of PI controller to track the defined rotor currents are replaced with proportional controllers. Active power control scenarios: MPPT, delta control and constant power control are applied to a test system. The proposed control showed promising performance under different wind speed variations and various control scenarios.

Bibliography

[1] N. Miller, K.Clark, and M.Shao, "Frequency responsive wind plant controls: impacts on grid performance," in *IEEE Power and Energy Society General Meeting*, (Detroit), July 2011. 1, 41

[2] E. Ela, V. Gevorgian, P. Fleming, Y. Zhang, M. Singh, E. Muljadi, A. Scholbrook, J. Aho, A. Buckspan, L. Pao, V. Singhvi, A. Tuohy, P. Pourbeik, D. Brooks, and N. Bhatt, "Active power controls from wind power: Bridging the gaps," tech. rep., National Renewable Energy Laboratory, 2014. 2

[3] "Frequency response and frequency bias setting reliability standard." 2, 10

[4] N. W. Miller, M. Shao, and S. Venkataraman, "Frequency response study," tech. rep., California ISO (CAISO), November 2011. GE Energy. 2

[5] Y. Zhang, V. Gevorgian, E. Ela, V. Singhvi, and P. Pourbeik, "Role of wind power in primary frequency response of an interconnection," tech. rep., National Renewable Energy Laboratory, 2013. 2

[6] J. Undrill, "Power and frequency control as it relates to wind-powered generation," tech. rep., LBNL Report, December 2010. 2

[7] R. A. Walling, L. A. Freeman, and W. P. Lasher, "Regulation requirements with high wind generation penetration in the ERCOT market," in *IEEE PES Power Systems Conference and Exposition, Seattle*, March 2009. 3

[8] L. Xie, L. A. F. M. Ferreira, P. M. S. Carvalho, J. Liu, B. H. Krogh, N. Popli, and M. D. Ilic, "Wind integration in power systems: operational challenges and possible solutions," in *in Proc. of the IEEE*, vol. 99, pp. 214–232, January 2011. 3

[9] C. L. DeMarco, C. A. Baone, Y. Han, and B. Lesieutre, "Primary and secondary control for high penetration renewables," tech. rep., Power Systems Engineering Research Center (PSERC), 2012. 3, 5, 6

[10] N. Jaleeli and L. S. VanSlyck, "NERC's new control performance standards," *IEEE Transactions on Power Systems*, vol. 14, pp. 1092–1099, 1999. 6

[11] V. Vittal, J. McCalley, V. Ajjarapu, and U. V. Shanbhag, "Impact of increased DFIG wind penetration on power systems and markets," tech. rep., 2009. 7, 62

[12] C. A. Baone and C. L. DeMarco, "Observer-based distributed control design to coordinate wind generation and energy storage," in *Proceedings of the 2010 IEEE Conference on Innovative Smart Grid Technologies Europe, Gothenburg*, 2010. 7

[13] R. Doherty, A. Mullane, G. Nolan, D. J. Burke, A. Bryson, and M. O'Malley, "An assessment of the impact of wind generation on system frequency control,," *IEEE Transactions on Power Systems*, vol. 25, pp. 452–460, 2010. 7

[14] J. H. Eto, J. Undrill, P. Mackin, R. Daschmans, B. Williams, B. Haney, R. Hunt, J. Ellis, H. Illian, C. Martinez, M. O'Malley, K. Coughlin, and K. H. LaCommare, "Use of frequency response metrics to assess the planning and operating requirements for reliable integration of variable renewable generation," tech. rep., Ernest Orlando Lawrence Berkeley National Laboratory, 2010. 7, 51

[15] N. Jaleeli, D. N. Ewart, and L. H. Fink, "Understanding automatic generation control," *IEEE Transactions on Power Systems*, vol. 7, pp. 1106–1122, 1992. 10

[16] "Bal-001-1 real power balancing control performance standard background document." 10

[17] N. Jaleeli, L. S. Vanslyck, M. M. Yao, and R. R. Shoults, "Discussion of "AGC logic based on NERC's new control performance standard and disturbance control standard"," *IEEE Transaction on Power Systems*, vol. 15, pp. 852–827, 2000. 10

[18] O. I. Elgerd and C. E. Fosha, "Optimum megawatt-frequency control of multiarea electric energy systems," *IEEE Trans. Power Apparatus and Systems*, vol. PAS-89, pp. 556–563, April 1970. 11

[19] J. Nanda, S. Mishra, P. G. Mishra, and K. V. Sajith, "A novel classical controller for automatic generation control in thermal and hydrothermal systems," in *Power Electronics, Drives and Energy Systems (PEDES) and 2010 Power India, 2010 Joint International Conf.*, pp. 1–6, 2010. 11

[20] G. A. Chown and R. Hartman, "Design and experience with a fuzzy logic controller for automatic generation control (AGC)," *IEEE Transactions on Power Systems*, vol. 13, pp. 965–970, 1998. 11

[21] J. Talaq and F. Al-Basri, "Adaptive fuzzy gain scheduling for load frequency control," *IEEE Transactions on Power Systems*, vol. 14, pp. 145–150, 1999. 11

[22] S. P. Ghoshal and S. K. Goswami, "Application of GA based optimal integral gains in fuzzy based active power-frequency control of nonreheat and reheat thermal generating systems," *Electric Power Systems Research*, vol. 67, pp. 79–88, 2003. 11

[23] T. Yu, B. Zhou, K. Chan, L. Chen, and B. Yang, "Stochastic optimal relaxed automatic generation control in non-markov environment based on multi-step $q(\lambda)$ learning," *IEEE Transactions on Power Systems*, vol. 26, pp. 1272–1282, 2011. 11

[24] H. L. Zeynelgil, A. Demiroren, and N. Sengor, "The application of ann technique to automatic generation control for multi-area power system," *Inrernational Journal of Electricsl Power and Energy Systems*, vol. 24, pp. 345–354, 2002. 11

[25] S. Bhowmik, K. Tomsovic, and A. Bose, "Communication models for third party load frequency control," *IEEE Transaction on Power Systems*, vol. 19, pp. 543–548, 2004. 11

[26] A. Venkat, I. Hiskens, J. Rawlings, and S. Wright, "Distributed MPC strategies with application to power system automatic generation control," *IEEE Transaction on Control Systems Technology*, vol. 16, pp. 1192– 1206, 2008. 11

[27] M. Ilic and Q. Liu, "Toward sensing, communications and control architectures for frequency regulation in systems with highly variable resources," *Control and Optimization Methods for Electric Smart Grids Power Electronics and Power Systems*, vol. 3, pp. 3–33, 2012. 11

[28] T. Ahamed, P. Rao, and P. Sastry, "A reinforcement learning approach to automatic generation control," *Electric Power Systems Research*, vol. 63, pp. 9–26, 2002. 11

[29] A. Keyhani and A. Chatterjee, "Automatic generation control structure for smart power grids," *IEEE Transactions on Smart Grid*, vol. 3, pp. 1310–1316, 2012. 12

[30] H. Bervani, Y. Mitani, and K. Tsuji, "Robust decentralized AGC in a restructured power system," *Energy Conversion and Management*, vol. 45, pp. 2297–2312, 2004. 12

[31] M. Ilic and Q. Liu, "Toward a systematic framework for deploying synchrophasors and their utilization for improving performance of future electric energy systems," tech. rep., Power Systems Engineering Research Center (PSERC), 2012. 12

[32] M. Fliess, J. Levine, P. Martin, and P. Rouchon, "Flatness and defect of nonlinear systems: introductory theory and examples.," *Int. J. Control*, vol. 61, pp. 1327–1361, 1995. 12, 18, 20

[33] E. C. Anene, U. O. Aliyu, J. Levine, and G. K. Venayagamoorthy, "Flatness-based feedback linearization of a synchronous machine model with static excitation and fast turbine valving," in *Power Engineering Society General Meeting*, June 2007. 12

[34] J. Mauricio, "Frequency regulation contribution through variable-speed wind energy conversion systems," *IEEE Trans. Power Systems*, vol. 24, pp. 173–180, February 2009. 13

[35] B. Kirby, "Providing minute-to-minute regulation from wind plants," in *The 9th Annual International Workshop on Large-Scale Integration of Wind Power into Power Systems and Transmission Networks for Offshore Wind Power Plant*, (Qubec, Canada), October 2010. 13, 64

[36] J. L. Rodriguez-Amenedo, S. Arnalte, and J. C. Burgos, "Automatic generation control of a wind farm with variable speed wind turbines," *IEEE Transactions on Energy Conversion*, vol. 17, pp. 279–284, 2002. 13

[37] A. D. Hansen, "Centralised power control of wind farm with doubly fed induction generators," 2006. 14, 15, 69, 70

[38] M. Singh, V. Gevorgian, V. Muljadi, and E. Ela, "Variable-speed wind power plant operating with reserve power capability," in *Energy Conversion Congress and Exposition (ECCE), 2013 IEEE*, pp. 3305–3310, 2013. 14, 84

[39] R. Pena, J. C. Clare, and G. M. Asher, "Doubly fed induction generator using back-to-back PWM converters and its application to variable speed wind-energy generation," in *Electric Power Applications, IEE Proceedings*, 1996. 15

[40] J. M. Mauricio, "An adaptive nonlinear controller for DFIM-based wind energy conversion systems," *IEEE Trans. Energy Conversion*, vol. 23, pp. 1025–1035, December 2008. 15, 64, 65

[41] N. P. Quang, A. Dittrich, and A. Thieme, "Doubly-fed induction machine as generator: control algorithms with decoupling of torque and power factor," *Springer- Verlag*, vol. 80, pp. 325–335, 1997. 15, 65

[42] B. Boukezzar, "Robust sliding mode control of a DFIG variable speed wind turbine for power production optimization," in *16th Mediterranean Conference on Control and Automation*, (Congress Centre, Ajaccio, France), June 2008. 15

[43] B. Boukhezzar, "Nonlinear control with wind estimation of a DFIG variable speed wind turbine for power capture optimization," *Energy Conversion and Management*, vol. 50, pp. 885–892, April 2009. 15, 65

[44] F. Wu, X. P. Zhang, P. Ju, and M. J. H. Sterling, "Decentralized nonlinear control of wind turbine with doubly fed induction generator," *IEEE Trans. Power Systems*, vol. 23, pp. 613–621, May 2008. 15

[45] M. Korkali, "Strategic and robust deployment of synchronized phasor measurement units with restricted channel capacity," Master's thesis, Northeastern University, 2010. 16

[46] A. G. Phadke, J. S. Thorp, and M. G. Adamiak, "New measurement technique for tracking voltage phasor , local system frequency, and rate of change of frequency," *IEEE Transactions on Power Apparatus and Systems*, vol. PAS-102, pp. 1025–1038, 1983. 16

[47] A. Abur and A. G. Exposito, *Power System State Estimation: Theory and Implementation*. CRC Press, 2004. 16

[48] R. Diao, K. Sun, V. Vital, R. O'Keefe, M. Richardson, D. S. N. Bhatt, and S. Sarawgi, "Decision tree-based online voltage security assessment using PMU measurements," *IEEE Transaction on Power Systems*, vol. 24, pp. 832–839, 2009. 16

[49] M. Glavic and T. Cutsem, "Wide-area detection of voltage instability from synchronized phasor measurements. part i: Principle," *IEEE Transaction on Power Systems*, vol. 24, pp. 1408–1416, 2009. 16

[50] M. Glavic and T. Cutsem, "Wide-area detection of voltage instability from synchronized phasor measurements. part ii: Simulation results," *IEEE Transaction on Power Systems*, vol. 24, pp. 1417–1425, 2009. 16

[51] P. Tripathy, S. C. Srivastava, and S. N. Singh, "A divide-by-difference-filter based algorithm for estimation of generator rotor angle utilizing synchrophasor measurements," *IEEE Transactions on Instrumentation and Measurement*, vol. 59, pp. 1562 – 1570, 2009. 16

[52] P. Martin, R. M. Murry, and P. Rouchon, "Flat systems, equivalence and trajectory generation," technical report, Ecole des Mines de Paris, April 2003. 18, 19, 21, 22

[53] H. Sira-Ramirez and S. K. Agrawa, *Differentially Flat Systems*. Marcel Dekker AG, New York, 2004. 20, 21, 72

[54] M. Fliess, J. Levine, P. Martin, and P. Rouchon, "Lie backlund approach to equivalence and flatness of nonlinear systems," *IEEE Trans. Automatic Control*, vol. 44, May 1999. 20

[55] J. Levine, *Analysis and Control of Nonlinear Systems: A Flatness-based Approach*. Springer-Verlag Berlin Heidelberg, 2009. 21, 22, 24, 25

[56] K. Tomsovic and M. Venkatasubramanian, *Electrical Engineering Handbook*, ch. Power system operation and control, pp. 761–778. Elsevier Academic Press, 2005. 26

[57] A. J. Wood and B. F. Wollenberg, *Power Generation Operation and Control*. John Wilely and Sons,Inc., 1996. 27

[58] NERC, "NERC IVGTF task 2.4 report operating practices, procedures, and tools," tech. rep., North American Electric Reliability Corporation (NERC), 2011. 30

[59] P. Kundur, *Power System Stability and Control*. McGraw-Hill, Inc., 1993. 31, 36, 58, 73

[60] A. D. Dominguez-Garcia, *Control and Optimization Methods for Electric Smart Grids*, ch. Models for impact assessment of wind-based power generation on frequency control. Springer-Verlag, Berlin, 2012. 31

[61] P. Sauer and A. Pai, *Power System Dynamics and Stability*. Upper Saddle River, NJ: Prentice Hall, 1998. 31, 32

[62] Y. C. Chen, A. D. Dominguez-Garcia, and P. W. Sauer, "A sparse representation approach to online estimation of power system distribution factors," *IEEE Transactions on Power Systems*, to appear. 37

[63] F. L. Lewis and V. L. Syrmos, *Optimal Control*. J. Wiley, November 1995. 39

[64] B. Singh, N. K. Sharma, A. N. Tiwari, K. S. Verma, and S. N. Singh, "Applications of phasor measurement units (pmus) in electric power system networks incorporated with facts controllers," *International Journal of Engineering, Science and Technology*, vol. 3, no. 3, pp. 64–82, 2011. 40, 41

[65] C. Luo and B. Ooi, "Frequency deviation of thermal power plants due to wind farms," *IEEE Trans. Energy Conversion*, vol. 21, pp. 708–716, September 2006. 41

[66] N. W. Miller, M. Shao, S. Pajic, and R. D'Aquila, "Eastern frequency response study," tech. rep., National Renewable Energy Laboratory, 2013. 51

[67] L. Yang, X. Zhang, Y. Ma, J. Wang, L. Hang, K. Lin, L. M. Tolbert, F. Wang, and K. Tomsovic, "Hardware implementation and control design

of generator emulator in multi-converter system," in *IEEE Applied Power Electronics Conference and Exposition (APEC)*, 2013. 58

[68] J. Wang, L. Yang, X. Zhang, K. Lin, X. Shi, L. Hang, L. M. Tolbert, F. Wang, and K. Tomsovic, "Regenerative power converters representation of grid control and actuation emulator," in *IEEE Energy Conversion Congress and Exposition (ECCE)*, 2012. 58

[69] J. Wang, Y. Ma, L. Yang, L. M. Tolbert, and F. Wang, "Power converter-based three-phase induction motor load emulator," in *IEEE Applied Power Electronics Conference and Exposition (APEC), Ft. Worth, Texas*, 2013. 58

[70] Y. Ma, L. Yang, J. Wang, F. Wang, and L. M. Tolbert, "Full-converter wind turbine emulator in converter based power grid emulation system," in *IEEE Applied Power Electronics Conference and Exposition (APEC), Ft. Worth, Texas*, 2013. 58

[71] W. Cao, Y. Ma, J. Wang, L. Yang, J. Wang, F. Wang, and L. M. Tolbert, "Two-stage PV inverter system emulator in converter based power grid emulation system," in *IEEE Energy Conversion Congress and Exposition (ECCE)*, 2013. 58

[72] W. Cao, Y. Ma, J. Wang, and F. Wang, "Virtual series impedance emulation control for remote PV or wind farms," in *2014 Applied Power Electronics Conference and Exposition (APEC)*, 2013. 58

[73] E. Muljadi, "Understanding inertial and frequency response of wind power plants," 2012. 63, 64

[74] H. Pulgar-Painemal, *Wind Farm Model for Power System Stability Analysis*. PhD thesis, University of Illinois at Urbana-Champaign, 2010. 65, 67, 68, 71

[75] Z. Lubosny, *Wind Turbine Operation in Electric Power Systems*. 2003. 65, 69, 72

[76] P. C. Krause, O. Wasynczuk, and S. D. Sudhoff, *Analysis of Electric Machinery and Drive Systems*. Wiley-IEEE Press, 2002. 67, 68

[77] J. G. Slootwag, "Dynamic modeling of a wind turbine with doubly fed induction generator," in *Power Engineering Society Summer Meeting, 2001*, vol. 1, pp. 644–649, July 2001. 67

[78] M. W. Hansen, R. Josefsson, and H. Mehmedovic, "Frequency controlling wind power modeling of control strategies," tech. rep., Elforsk, 2012. 70

[79] E. Muljadi and C. Butterfield, "Pitch-controlled variable-speed wind turbine generation," 1999. 71

[80] P. Martin and P. Rouchon, "Two remarks on induction motors," July 1996. 72

[81] A. Gensior, T. M. P. Nguyen, J. Rudolph, and H. Guldner, "Flatness-based loss optimization and control of s doubly fed induction generator system," 2011. 73

Appendix

HTB System Data

Generators data in per unit on $900\,MVA$ and $20\,kV$ base

$X_d = 1.8$ $X_q = 1.7$ $x_I = 0.2$ $X'_d = 0.3$ $X'_q = 0.55$
$X''_d = 0.25$ $X''_q = 0.25$ $R_a = 0.0025$ $T'_{do} = 8.0\,s$ $T'_{qo} = 0.4\,s$
$T''_{do} = 0.03\,s$ $T''_{qo} = 0.05\,s$

Transformer data in per unit on $900\,MVA$ and $20/230\,kV$ base

$R_t = 0$ $X_t = 0.15$

Transmission system data in per unit on $100\,MVA$ and $230\,kV$ base

$r = 0.0001pu/km$ $x_L = 0.001pu/km$ $b_c = 0.00175pu/km$

System Generation and Load

	Gen 1	Gen 2	Gen 3	Gen 4	Load 1	Load 2
P (pu)	0.44	0.3	0.1	0.2	0.4	0.83

Four Bus System Data

DFIG:

$R_s = 0.00706$ $R_r = 0.005$ $X_{ls} = 0.171$ $X_{lr} = 0.156$ $X_M = 2.9$
$\omega_s = 120\pi$ $H = 5.04$

Network:

Line 1	$R_1 = 0.03$	$X_1 = 0.1$
Line 2	$R_1 = 0.10$	$X_2 = 0.1$
Transformer	$X_T = 0.07$	
Load	$P_L = 1\,p.u.$	$Q_L = 0.1\,p.u.$

Vita

Maryam Hassani Variani received her B.S. and M.S. from Amirkabir Universrity of Technology, in 2006 and 2009, respectively. She joined University of Tennessee at Knoxville in August 2009 for a PhD degree in Electrical Engineering. Her main research interests include power system control with high penetration of renewable energy systems and optimization methodologies applied to power systems.